BEHAVIOR OF CONCRETE BRIDGE DECKS UNDER COMBINED SHRINKAGE, THERMAL AND LIVE LOADING

by

ANUOLUWA O. ADEDIJI

A Dissertation submitted to the

Graduate School-New Brunswick

Rutgers, The State University of New Jersey

In partial fulfillment of the requirements

For the degree of

Doctor of Philosophy

Graduate Program in Civil and Environmental Engineering

Written under the direction of

Dr. Hani H. Nassif, Ph.D.

And approved by

_____

_____

_____

_____

New Brunswick, New Jersey

May, 2016

ABSTRACT OF THE DISSERTATION

Behavior of Concrete Bridge Decks under Combined Shrinkage, Thermal and Live Loading

By ANUOLUWA O. ADEDIJI

Dissertation Director:

Dr. Hani H. Nassif, Ph.D.

Designers have consistently been concerned with long term deformation of bridges to mitigate unfavorable effects such as excessive movement and cracking. Furthermore, any developed tool of use to a designer must make use of parameters known at the time of design as well as be simplistic in nature as defined in the code. As such, many prediction models for the free shrinkage of a concrete specimen have been developed toward this end. However, structures designed and placed in the field experience shrinkage under restraint. Also, the differences in environmental conditions affect the shrinkage of structures. It is important to understand the restrained shrinkage of structures under field conditions and use this understanding to make improved guidelines on shrinkage from a design standpoint.

In this study, the prediction and modelling of the free shrinkage of small samples under constant conditions were expanded to the prediction and modelling of restrained shrinkage under field conditions of large samples using finite element analysis. A parametric analysis was then performed to derive useful information from a design perspective such as the impact of various design parameters on the performance of a bridge deck. The findings indicated that the use of reinforcement is the preferable method of addressing shrinkage in bridge decks. Furthermore, the efficacy of the amount of reinforcement specified in the AASHTO guidelines to mitigate excessive cracking in bridge decks was discussed. The traditional and empirical methods of bridge deck design were investigated for shrinkage reinforcement. Finally, recommendations were suggested to the reinforcement requirements based on the findings of this study.

ACKNOWLEDGEMENTS

I, first of all, acknowledge God, who brought me here and saw me through. I would also like to acknowledge my advisor, Dr. Hani Nassif for extending this opportunity to me and supporting me throughout my program. To my committee members; Dr. Husam Najm, Dr. Yook-Kong Yong and Dr. Thomas Tsakalakos, I thank you all for your time and critique which was essential in getting this work to a good completion. I would like to thank the New Jersey Turnpike Association, whose funding made this work possible.

I would like to thank all my colleagues, who worked on several projects with me and at many points along the way helped me to make progress: Dr. Dan Su, Peng Lou, Dr. Chaekuk Na, Adi Abu-Obeidah, Miguel Beltran and Dalexander Gonzalez. Also, I acknowledge the undergraduate students who assisted me in my laboratory experiments: Justin Grant, Muhammad Mansour and Giuseppe Liberti. Thank you. To the administrative staff at the civil engineering deparment; Gina Cullari and Linda Szary, I appreciate all your assistance during my time at Rutgers University.

A very special thanks to my mentor, Pastor Fola and his family. Your guidance, love and support over the years have been invaluable. I would like to thank my friends; Roseline Atte, Tosin Ipaye, Ademilolu Ajayi and many others. I could not have done this without your prayers and encouragement. I would also like to thank my family, the Adedijis, and the Ogunkanmis for all their support along the way. I am deeply grateful for your sacrifices which enabled me to finish this program. I would like to specially acknowledge the Adeyemis who have been there for me throughout my entire academic pursuit in the United States. I would also like to thank the Ayenis for their support even from afar. To Mama Yetunde, I am forever indebted to you for your kindness to me and I thank you for

your assistance. Finally, I would like to express my sincere gratitude to my loving husband, Dr. Adeleye Ogunkanmi, who met me halfway and supported me to the end. I am truly blessed to have you. Special thanks to my son, Gbeminiyi Ogunkanmi whose presence lightened my load.

TABLE OF CONTENTS

LIST OF FIGURES

LIST OF TABLES

CHAPTER I

INTRODUCTION

Cracking of concrete bridge decks is a common problem that affects the serviceability of a concrete bridge deck. It occurs when the movement of a bridge is restrained by elements such as the boundary conditions and connections. Shrinkage of concrete, defined as the change in volume due to loss of moisture, is a major contributor to the movement of concrete bridge decks. Attempts have been made to quantify and account for the amount of shrinkage in a concrete specimen. Physical measurements of concrete samples are often collected however such procedures may require more time than is available to a designer. This gave rise to the development of shrinkage prediction models to estimate the shrinkage of a concrete sample under specified conditions, based on data from a database of shrinkage readings. These readings were taken from relatively small samples under constant conditions and as such are not directly transferable to large scale samples under field conditions and under restrained conditions. There is a need to explore shrinkage under restrained and external environmental conditions in order to gain a better understanding of shrinkage under these conditions.

In this study, shrinkage samples were taken from small, medium and large scale samples under various environmental conditions. Laboratory experiments were conducted under constant conditions and the results were compared to samples taken under ambient environmental conditions. Environmental influences observed in the data were separated from true shrinkage using an approximate method. Additionally, data

from samples of various sizes were collected to observe the effect of size on the shrinkage of concrete samples. The shrinkage of small samples was extrapolated to larger samples and a comparison was made to measured results. Finite element models of the samples were built to further facilitate the study of the shrinkage behavior of the concrete samples. Finally, a parametric analysis of design variables was performed using the finite element models to observe and assess the effect of the design variables on the cracking behavior of a bridge deck. The AASHTO LRFD guidelines for the design of concrete bridge decks in the area of shrinkage and temperature reinforcement were re-evaluated based on the findings from the parametric analysis.

1.1. Motivation

Cracking in concrete bridge decks is undesirable as it leads to deterioration as salts and other impurities in the environment accelerate the corrosion of the embedded reinforcement. Shrinkage, known as the deformation of a concrete section predominantly due to loss of moisture, has been identified as a contributor to the development of high strains which lead to the formation of cracks in concrete sections under restraint (Elsafty & Jackson, 2012). Previous studies of shrinkage have allowed for the development of prediction models and consequently design guidelines, with the aim of accounting for and mitigating shrinkage effects on designed structures (Branson & Christiason, 1971; CEB,1993). However, these shrinkage studies were performed using data compiled from small specimens relative to structures in the field as well as specimens undergoing unrestrained shrinkage known as free shrinkage (ACI, 2008). Additionally, these studies were done in laboratories with controlled environments. Structures constructed in the field usually experience some degree of restraint due to boundary conditions, embedded reinforcement and formwork. Furthermore, they are subject to changing environmental conditions such as temperature and relative humidity. It is important to extend the study of shrinkage to restrained shrinkage under field conditions. Knowledge gained can be used to adapt current design guidelines.

1.2. Research Significance

The degree of cracking of a structural element is affected by the amount of shrinkage the element undergoes. An assessment of the serviceability of a structure therefore requires knowledge of the time-dependent strains experienced by the structure. The development

of shrinkage prediction models is in response to this need. However, these models were developed for small samples undergoing free shrinkage under laboratory conditions. Several issues arise in the use of these models directly to larger structures under field conditions. Change in size of specimen and environmental conditions greatly affect the prediction results. Furthermore, the presence of restraint also alters the expected shrinkage.

Although modification factors are provided for adaptation of the prediction model results to varying sizes and environmental conditions, the databank used for the development of these models did not contain data from structures in the field. It is beneficial to study the shrinkage of structures under field conditions. Adaptation of prediction models can be improved based on field data. An improvement of the understanding of shrinkage in the field can facilitate the design of structures in the field to perform better under serviceability conditions. This results in decreased deterioration and reduction in the associated maintenance costs.

1.3. Objectives and Scope

The primary objective of this research is to study restrained shrinkage of concrete bridge decks under field conditions. Toward this end, finite element models of concrete bridges in the field, capable of simulating restrained shrinkage will be developed. Based on this research, modifications to design guidelines for restrained shrinkage of concrete bridges under field conditions will be provided. The relationship between free shrinkage of a small sample and restrained shrinkage of a bridge deck will also be examined.

In this research, shrinkage data for small free shrinkage prisms, medium size concrete slabs and large concrete bridge decks in the field were collected. Finite element models

for all specimen were modeled and a method to incorporate shrinkage was calibrated. Measured data was compared with the finite element analyses, finally, a parametric analysis was performed to assess the effect of design parameters on restrained shrinkage.

1.4. Organization of the thesis

This dissertation comprises of seven chapters. Chapter one provides an introduction to the research problem and outlines the objectives herein.

In chapter two, a literature review of related topics is presented to lay groundwork for the research. A more in depth discussion on bridge deck cracking, its effects and causes was presented. Also, Current design guidelines and shrinkage predictions models were presented. Testing methods for free and restrained shrinkage were outlined.

In Chapter three, details on laboratory experiments performed to facilitate the study of shrinkage under various conditions were outlined. Experiments were initially performed on small free shrinkage prism samples. The first set of testing was performed on small free shrinkage prisms. Shrinkage data was measured from a sample under constant conditions, a sample under controlled fluctuating temperature, a sample under external environmental conditions and a larger sized sample. Furthermore, shrinkage data from a scaled bridge deck sample built in a laboratory were collected from a report for use in the study of shrinkage.

Chapter four presents the field work performed to facilitate the study of shrinkage in this report. Several bridges were instrumented with Vibrating Wire Strain Gages (VWSG) during construction to facilitate the collection of strain data over time. Static

and dynamic tests were also conducted to allow for the validation of models of these bridges during computer analysis. Also, concrete samples were collected during construction to be tested for concrete material properties.

In Chapter five, the results of all the laboratory experiments performed previously are presented. Also, finite element models built for the analysis of shrinkage are discussed. A comparison between measured data and finite element analysis results are presented in this chapter.

In Chapter six, results of a parametric analysis performed using the developed finite element models are presented. The influence of various design variables on the cracking behavior of the bridges is discussed. The AASHTO LRFD guidelines for shrinkage and temperature reinforcement are re-evaluated based on the results of the parametric analysis. Recommendations based on the results of the study are also given.

Chapter seven summarizes the findings and conclusions of this study.

CHAPTER 2

LITERATURE REVIEW

2.1. Bridge Deck Cracking and Deterioration

Cracking in bridge decks is a common problem experienced by many bridge owners (Krauss and Rogalla, 1996). Early references of concrete cracking date back to the 1960s where cracking was identified as a problem with concrete bridge decks that leads to further deterioration of the decks and often occurs before any live loads are applied or soon after (Banks, 1986; Tam & Scanlon,1984). Banks (1986) found a huge occurrence of cracking in the state of Texas and recommended that changes be made to the design, material and construction methods being used. Design recommendations included an increase in the deck thickness from 6 in to a minimum of 7 in as well as an increase in the concrete clear cover from 1.5 in to 2 in. Material modifications included the use of class S concrete with 3600 psi strength and construction modifications included a mandatory use of moist curing and the requirement of entrained air.

Over the years, the problem of bridge deck cracking has persisted. A report by Babaei and Purvis (1995) mentioned that cracking in newly constructed bridges remains a concern in the state of Pennsylvania, with transverse cracking being the prevalent type of cracking. A separate report by French, Eppers, Le and Hajjar (1999) expressed similar concerns of early age transverse cracking observed in the state of Minnesota. Numerous

other studies have been performed by bridge owners and researchers with the aim of addressing the problem of cracking in concrete decks. Frosch, Bice, & Erickson (2003) stated that transverse cracking has been observed at early ages when volumetric changes in a deck due to shrinkage or thermal effects are restrained by the girders. Rahim, Jansen & Abo-Shadi (2006) stated that concrete bridge deck cracking is the most common issue with concrete bridge decks throughout the United States and performed research on the use of sealants to retrofit bridge decks with extensive cracking in order to prevent further deterioration. Curtis (2007) published a report for the New York State Department of Transportation (NYSDOT) after High Performance Concrete (HPC) bridge decks were found to undergo premature cracking before any load was applied due to concrete shrinkage and temperature loads. Subramaniam & Agrawal (2009) performed research on the influence of local materials on concrete cracking and provided recommendations relating to temperature gradient limits, good aggregate use and addition of admixtures. Ganapuram, Adams & Patnaik (2012) performed a study to quantify the problem of cracking in the state of Ohio by performing visual inspection of bridges and calculating crack densities of the corresponding bridges.

The use of High Performance Concrete (HPC) has increased in the last decade owing to its superior characteristics such as increased strength and improved workability which have allowed concrete to be used for capabilities that where hitherto challenging (Wang, 2013). However a study by Chaunsali, Li, Mondal, Foutch, Richardson, Tung and Hindi (2013) stated that the use of HPC may exacerbate the problem of bridge deck cracking

because it tends to have a lower water-cement (w/c) ratio and has been found to be more susceptible to shrinkage, which is a major cause of cracking in bridge decks.

Bride deck cracking is of significant concern because it leads to further deterioration of the bridge deck, thereby reducing its normal service life (Rahim et al., 2006) and increasing maintenance costs (Ganapuram et al., 2012). Several issues associated with bridge deck cracking include corrosion of the embedded reinforcement as chlorides and carbon dioxide penetrate through the cracks into the concrete and to the reinforcing steel (Elsafty & Jackson, 2012), Spalling of concrete when corroded rebar expands in volume and applies a stress to the concrete (Krauss & Rogalla, 1996) and loosening of the bond between the concrete and the reinforcement as the corrosion process forms a powdery coating between the rebar and the concrete and thereby causing reinforcement slip. Cracking also affects the degradation of bridge decks by reducing the benefits which come from air entrainment in concrete. To tackle freeze/thaw cycles, it is common practice to make use of air-entrained concrete. These air pockets allow the concrete pore water to expand when the bridge is exposed to freezing temperatures. When cracks occur in the concrete, water penetration can saturate the concrete and hamper the effect of the air entrainment. The expanding water, having no room for volume increase, exerts stresses on the concrete and enhances the cracking process further (Krauss and Rogalla, 1996).

Bridge deck cracking is a relevant problem affecting bridge owners today. Causes of bridge deck cracking and methods of mitigation from previous research will be discussed in detail below.

2.2. Causes of Bridge Deck Cracking

Many studies have been performed to uncover the causes of bridge deck cracking. A state of the art review pertaining to cracking of concrete bridge decks by Hadidi and Saadeghvaziri (2005) highlighted that cracks in bridge decks occur when concrete undergoing volumetric changes, is restrained. Other studies performed more recently also support this finding with the predominant cause of volume changes in concrete being shrinkage and temperature loads (Elsafty & Jackson, 2012; Chaunsali et al., 2013). As a result, cracks form on bridge decks when the concrete develops tensile stresses greater than the tensile capacity of the concrete. A large number of factors and processes can cause or affect the degree of volumetric changes and restraint which cause tensile stresses on a bridge deck. These causes can be broken into three distinct areas which are design, material properties and construction practices.

Design factors affect cracking in concrete because the extent of restraint in a bridge is usually determined during design. The design process dictates the boundary conditions to be used, size and spacing of reinforcement and shear studs as well as connection methods, which are all factors that determine the amount of restraint on a bridge deck. Bridge decks with more restraint show greater occurrences of cracking than those with less restraint. A study by Schmitt and Darwin (1995) evaluated forty bridges to ascertain the cause of cracking. Field surveys were performed to compile information on crack

densities and subsequently, compared with construction documents, weather logs and other field books to identify correlations. It was found that fixed ended girders exhibited more cracking than pin-ended girders because of the additional restraint. Ramey et al. (1997) stated that although durability is of utmost importance in highway maintenance, little consideration is given to this during bridge design and bridge deck cracking is a major factor affecting the durability of bridge deck. Saadeghvaziri and Hadidi (2005) also added that research on the effect of structural design factors on bridge deck cracking has received less focus than in the other areas of concern such as materials and construction practices. They performed a study to evaluate the effect of design factors on deck cracking and recommended that uniform reinforcement meshes and more flexible superstructures be employed. A study by Nielson, Schmeckpeper, Shiner and Blanford (2010) was also performed to assess the effectiveness of current AASHTO design methods in controlling bridge deck cracking. The proposed reinforcement ratios were found to be inadequate and recommendations were made to reduce reinforcement spacing and increase bar size, factors which are decided upon in the design process.

The material properties of the concrete are also another significant factor affecting cracking of concrete bridge decks. Properties such as the modulus of elasticity and thermal expansion coefficient affect the reaction of the concrete to applied strains and external temperature variations. Also, all concrete mixes exhibit a behavior known as shrinkage. This is the natural tendency for the concrete to reduce in volume as chemical reactions occur and water gradually evaporates from the mix. This behavior causes tensile stresses when the volumetric changes are restrained on the bridge deck. The survey responses collected by the NCHRP determined that majority of all bridge deck

cracking is attributed primarily to shrinkage and thermal stresses (Krauss and Rogalla, 1996). Folliard (2003) performed a study to evaluate methods for controlling cracking in concrete from a material perspective by optimizing concrete mixes and using innovative materials. The use of Shrinkage Reducing Admixtures (SRAs) and fibers were encouraged to reduce the shrinkage of a concrete mix. Tia, Submaranian, Brown and Broward (2005) researched effective laboratory tests for evaluating the shrinkage potential of a concrete mix. It was found that an embedded strain gage in a concrete specimen was adequate for measuring shrinkage potential. Optimization of concrete mixes was also performed and the use of fly ash and SRAs were found to mitigate shrinkage. Ray, Gong, Davalos and Kar (2012) compared different HPC mixes to develop a threshold for cracking potential. Chaunsali et al. (2013) performed a study on type K and type G shrinkage compensating concretes as a technique to counteract concrete shrinkage. During small scale tests, the concrete mixes expanded which produced a compressive strain in the concrete. As such, the tensile stresses produced were lessened when the concrete began to shrink. Wang (2013) also performed research to address high shrinkage strains often found in HPC. The influence of additives such as slag and fly ash was analyzed.

Construction practices also affect the degree of cracking that occurs on a bridge deck. The method of curing as well as length of time which the concrete is cured for impact the amount and rate of moisture loss that affects concrete shrinkage. Xi, Shing, Abu-Hejleh, Asiz, Suwito, Xie and Ababneh (2003) performed analyses on 72 bridges in the state of Colorado. A report was issued on recommendations to mitigate bridge deck cracking which included construction practices such as a temperature limit between 45º F and 80º

F at the time of deck casting and a minimum of seven days continuous wet curing. Darwin, Browning, Lindquist, McLeod, Yuan, Toledo & Reynolds (2010) began a six year study to develop methods across design, materials and construction practices to produce Low Cracking High Performance Concrete bridge decks (LC-HPC). To accomplish this, strict guidelines were given in all three areas of concern. Construction recommendations included wet curing for fourteen days and a narrower temperature range of 55º F to 70º F. Also, concretes which are placed on days with high temperature ranges have been found to exhibit a high degree of cracking (French et al., 1999; Curtis, 2007). The time at which construction loads are first applied to the bridge deck also affects the occurrence of cracks. Bridge decks which are loaded before the concrete has attained adequate strength are likely to suffer from early age cracking.

2.3. Means and methods of studying bridge deck cracking

The approach to studying the problem of bridge deck cracking has evolved over the years. Earlier research made use of visual inspections and bridge surveys to correlate incidences of cracking with several variables in order to identify the causes of cracking and make recommendations. However, these methods are more qualitative in nature. As experimental methods became available, laboratory tests were conducted to learn more about concrete cracking and develop solutions. These tests include the ASTM free shrinkage test (ASTM, 2008) and retrained shrinkage ring tests by AASHTO and ASTM and are discussed in greater detail in a later section. Although these tests prove useful, laboratory conditions may not be adequately representative of field conditions where

temperature and humidity influence bridge deck cracking. Also, it is challenging to quantify and replicate the level of restraint of a bridge in the field. Furthermore, the time taken to conduct a test and procure relevant information may not be conducive to the development timeline of a bridge. This has improved with the development of prediction models such as the ACI 209 prediction equation (ACI, 2008). Finally, the use of sensors in bridge decks and finite element methods to perform analyses on bridge deck cracking has been increasing in recent times. Instrumentation of bridges with sensors such as Vibrating Wire Strain Gages (VWSG) and Accelerometers provide data on the performance of a bridge under field conditions in real time. Shortcomings of this method are that sensors cannot be placed in every part of the bridge deck and it is difficult to predict where cracking may occur. The use of Finite Element (FE) methods is beneficial because field information can be used to produce a more global result. FE models can also be used to simulate various analyses that may be difficult or time consuming to conduct physically. Using a combination of these tools, design criteria for restrained shrinkage which were developed based on empirical methods can be improved by analytical means.

Over the years, the use of finite element methods to study shrinkage in concrete bridge decks has increased. Tang (2000) conducted a study to understand the process of cracking in concrete overlays on a segmental box-girder bridge using finite element methods after severe cracking and delamination were found shortly after construction. Saadeghvaziri and Hadidi (2002) also performed research to study the factors contributing to cracking in concrete bridge decks. The study employed FE analysis in addition to traditional methods such as bridge surveys and physical inspection. A study

was performed by Lange et al. (2003) to analyze the behavior of HPC in regards to cracking with a focus on creep and shrinkage. Several other studies have been performed over the years using FE modeling to analyze shrinkage such as Frosch et al. (2003), Eldhose (2006) and Minnetyan (2011).

2.4. Shrinkage experimental testing

As previously discussed, concrete undergoes volume changes due to chemical reactions and loss of water. When the concrete is free to expand and contract, no tensile forces occur and as such no cracking occurs. This change in length under unrestrained conditions is referred to as the free shrinkage of concrete. However, when concrete is placed, there are usually many components which prevent the concrete from freely changing in volume. Some of these components include embedded reinforcement, formwork, boundary conditions and shear studs. The corresponding change in length under restrained conditions is referred to as restrained shrinkage. Experimental procedures exist for the determination of both free and restrained shrinkage properties of a concrete sample.

2.4.1. Free shrinkage experimental testing

There are several methods for measuring free shrinkage. This report makes use of the standard ASTM C-157 test (ASTM, 2008). In this test, the concrete is placed in a rectangular prism with gage studs at the end. A mechanical dial gage length comparator or an embedded strain gage is then used to measure the change in length over time

a)

b)

Figure 1: Free shrinkage testing equipment a) using length comparator b) using embedded vibrating wire strain gage

2.4.2. Restrained shrinkage experimental testing

There are several methods for testing the restrained shrinkage of a concrete sample. The most popular experimental method is the ring test. In this test, a concrete sample is cast around a steel ring which serves as a restraint to the concrete's change in length. As the concrete shrinks, it exerts a compressive stress on the steel ring, which in turn exerts a tensile stress on the concrete. If the tensile stress in the concrete exceeds the tensile strength of the concrete, a crack will form in the concrete. Strain gauges can be used to measure the time and strain at which the crack occurred. Both ASTM and AASHTO have adopted versions of this ring test with slight variations.

Figure 2: Retrained shrinkage testing equipment

Free shrinkage tests are used more often than restrained shrinkage tests in determining the shrinkage potential of a concrete sample because the free shrinkage test is easier to perform than the restrained shrinkage test. A study performed by Nassif et al. (2007) showed a correlation between the free and restrained shrinkage performance of a concrete sample.

2.5. Design code guidelines for shrinkage

The development of codes has been useful in providing design standards for infrastructure. Code specifications are central to the design of bridges today as they provide minimum standards that designers can reference. Guidelines from the AASHTO and the ACI design codes relating to concrete shrinkage will be discussed in the sections below.

2.5.1. AASHTO

In the United States, the American Association of State Transportation and Highway Officials (AASHTO) publishes guidelines for the design of bridges. Krauss and Rogalla (1996) stated that 92% of US agencies design based on AASHTO specifications. Much

of the specifications given are based on past research which is beneficial to the design community at large. However, in the area of concrete shrinkage, the guidelines given are based on empirical methods and are applicable for the case of unrestrained shrinkage. For the case of restrained shrinkage, the code indicates that the effect of temperature and shrinkage loads should be considered but gives no further guidance (AASHTO, 2010). Concerns exist on the ability of the given guidelines to mitigate restrained shrinkage cracks. Nielson et al. (2010) expressed that although the Idaho Department of Transportation (IDOT) allows bridge decks to be designed using the AASHTO empirical method, there is a perceived inability of the code to control bridge deck cracking evidenced by the cracking problem of bridge decks in Idaho. Current guidelines for the treatment of shrinkage and temperature loads in bridge decks will be discussed below.

The AASHTO LRFD Bridge Design Specifications is the primary design code used to design concrete bridges within the United States. Although, some states have additional provisions, the AASHTO specifications serve as the backbone for bridge design in the US. Two methods are provided by the code for the design of bridge decks which are the empirical method and the traditional method. The code considers cracking in concrete decks as a serviceability issue and not a strength issue. This means that cracking in concrete bridge decks does not directly cause a failure in the bridge but rather reduces the service live and user comfort of the structure as well as causes increased maintenance costs. Hence, the deck design methods were developed primarily to meet strength requirements.

The empirical method is based on internal arching action and stipulates a set of design criteria that must be met in order for the specified reinforcement to be used. Four layers of reinforcement are provided with a minimum reinforcement amount of 0.27 in^2/ft of steel for each bottom layer and 0.18 in^2/ft of steel for each top layer. Spacing shall not exceed 18 in and reinforcing steel shall be grade 60 or better (AASHTO, 2010). The commentary indicates that 0.2 % reinforcement in each of the four layers satisfies strength requirements as shown by testing. However, a conservative value of 0.3 % of the gross area which corresponds to 0.27 in^2/ft for a 7.5 in slab is specified for better crack control (AASHTO, 2010). The code does not expatiate on the effectiveness of a 0.3 % reinforcement criterion for the control of cracking.

The traditional method is based on flexural behavior between beams and provides four layers of rebar provided that the slab meets certain design requirements. The transverse reinforcements are designed for flexure. The top transverse reinforcement is designed for negative flexure while the bottom transverse reinforcement is designed for positive flexure. The bottom longitudinal reinforcement is designed as a percentage of the positive flexure reinforcing steel. The top longitudinal reinforcement is designed as temperature and shrinkage reinforcement (AASHTO, 2010). The area of reinforcement per foot on each face and in each direction is to satisfy the following criteria

$$A_s \geq \frac{1.30bh}{2(b+h)f_y}$$

$$0.11 \leq A_s \leq 0.60$$

Where A_s = area of reinforcement (in^2/ft)

b = least width of component section

h = least thickness of component section

f_y = specified yield strength of reinforcing bars (must be ≤ 75 ksi)

Other limitations apply for components with dimensions that vary across the length, for components 6 inches or less and in cases where prestressed concrete is used.

The AASHTO code commentary indicates that these guidelines are derived from the ACI 207.2R and ACI 318 reports.

2.5.2. ACI

The American Concrete Institute (ACI) publishes guidelines pertaining to the use of concrete. The ACI 318 building code (ACI, 2008) gives directions on the use of shrinkage and temperature reinforcement in section 7.12 which are summarized below.

Shrinkage and temperature reinforcement shall be provided with a minimum reinforcement to gross concrete area of the following but not less than 0.0014

a) Slabs where grade 40 or 50 deformed bars are used…….. 0.0020
b) Slabs where grade 60 deformed bars or welded wire fabric are used….0.0018
c) Slabs where reinforcement with yield stress exceeding 60,000 psi measured at yield strain of 0.35 percent is used……..…$\frac{0.0018 \times 60000}{f_y}$

> Shrinkage and temperature reinforcement shall not be spaced further apart than 18 in or five times the slab thickness.

Furthermore, the code adds that in cases of restrained shrinkage, consideration should be given to the effects of shrinkage and temperature changes. However, the code does not give further guidelines on the matter.

The commentary on the code adds that these provisions are satisfactory in the case of unrestrained shrinkage and that it may be necessary to increase the reinforcement in cases where the movement due to shrinkage or temperature is significantly restrained but does not give provisions on how much reinforcement is adequate.

The commentary on the equation from the AASHTO code states that the coefficient is derived from the ACI provision by using a reinforcement ratio of 0.0018 and grade 60 bars for a one foot slab section. However, the ACI code explains that this is inadequate in cases with significant restraint such as exists in a bridge deck.

2.6. Drying shrinkage prediction methods

Several methods have been developed for the prediction of unrestrained shrinkage. A database of free shrinkage measurements for various concrete specimen under various conditions was assembled. Researchers then developed models to fit this databank within certain guidelines. The American Association of State and Highway Transportation Officials (AASHTO) developed a model as well as the American Concrete Institute (ACI) and Euro-International Concrete Committee/International Federation of Prestressing (CEB-FIP). Additional models for the prediction of drying shrinkage exist such as the Bazant B3 (Bazant & Baweja, 2000), Sakata (Sakata, 1993) and

Gardner/Lockman (Gardner & Lockman, 2001) equations. These methods are described in the sections following.

2.6.1. AASHTO

The AASHTO method for calculating shrinkage strains is shown in the equation below.

$$\boldsymbol{\varepsilon_{sh} = k_s k_{hs} k_f k_{st} 0.48 * 10^{-3}}$$

In which

$$K_{hs} = 2 - 0.0014H$$

Where

K_{hs} = humidity factor for shrinkage

2.6.2. ACI model

The ACI method is detailed in ACI report 209 (ACI, 1997) and is given.

$$\boldsymbol{(\varepsilon_{sh})_t = \frac{t}{35+t}(\varepsilon_{sh})_u}$$

Where,

$(\varepsilon_{sh})_t$ = shrinkage at time t after curing

t = time after curing

$(\varepsilon_{sh})_u$ = ultimate shrinkage coefficient

The default value of the ultimate shrinkage coefficient is 780 x 10^{-6} με. This equation is valid for shrinkage after 7 days under moist curing conditions as well as other standards conditions detailed in the report. To use this equation for other non-standard conditions, correction factors are provided in the report.

2.6.3. CEB-FIP model

The CEB-FIP 90 model for predicting shrinkage strains is given in the equation below

$$\boldsymbol{\varepsilon_{cs}(t - t_s)} = \varepsilon_{\boldsymbol{cso}}\boldsymbol{\beta(t - t_s)}$$

In which

$$\varepsilon_{cso} = \varepsilon_s(f_{cm})\beta_{RH}$$

$$\beta_{RH} = -1.55\left[1 - \left(\frac{RH}{100}\right)^3\right]$$

$$\varepsilon_{cs}(f_{cm}) = \left[160 + 10\beta_{sc}\left(9 - \frac{f_{cm}}{1450}\right)\right] * 10^{-6}$$

$$\beta_s(t - t_o) = \sqrt{\frac{t - t_s}{350\left(\frac{h}{4}\right)^2 + (t - t_s)}}$$

Where

β_{sc} is a factor accounting for cement type with 4 for slow hardening concrete, 5 for normal/rapid hardening concrete and 8 for rapid hardening high strength cement.

2.6.4. Bazant B3 model

The Bazant B3 model by Bazant and Baweja (2000) was developed at northwestern university. It is recommended for complex structures of structures that require very accurate prediction values. The method is summarized below.

$$\varepsilon_{sh}\,(t, t_0) = -\varepsilon_{sh\infty} K_h S(t)$$

$$\varepsilon_{sh\infty} = -\alpha_1 \alpha_2 (26(w)^{2.1}(f_c')^{-0.28} + 270)10^{-6}$$

$$K_h = 1 - h^3$$

$$S(t) = \tanh \sqrt{\frac{t - t_0}{T_{sh}}}$$

Where,

$\varepsilon_{sh}(t,t_0)$ = shrinkage strain (in/in)

$\varepsilon_{sh\infty}$ = ultimate shrinkage strain (in/in)

$\alpha_1 = 1$, $\alpha_2 = 1$

w= water content of concrete (lb/ft^3)

K_h = cross section shape factor

h = relative humidity (%)

t = age of concrete (days)

t_0 = age of concrete at beginning of shrinkage

S(t) = time function for shrinkage

2.6.5. Gardner/Lockman model

A model was developed by Gardner and Lockman (2001). The method can be used for concretes with chemical admixtures and can account for various curing procedures. This method is summarized below.

$$\varepsilon_{sh} = \varepsilon_{sh}\,\beta(h)\beta(t)$$

$$\varepsilon_{shu} = 1000K\left(\frac{4350}{f'_{cm28}}\right)^{\frac{1}{2}}\,10^{-6}$$

$$\beta(h) = 1 - 1.18h^4$$

$$\beta(h) = \left(\frac{t - t_c}{t - t_c + 97\,(V/S)^{\frac{1}{2}}}\right)10^{-6}$$

ε_{sh} = shrinkage strain (in/in)

ε_{shu} = ultimate shrinkage strain (in/in)

β(h) = correction term for effect of humidity on shrinkage

β(h) = correction term for effect of time on shrinkage

h = humidity

t_c = age drying commenced (days)

t = age of concrete (days)

2.6.6. Sakata Model

This model was developed by Sakata (1993). The method is summarized below.

$$\varepsilon_{sh}\,(t, t_0) = \varepsilon_{sh\infty}[1 - exp\{-0.108(t - t_0)^{0.56}\}]$$

$$\varepsilon_{sh\infty} = -50 + 78\left(1 - exp\left(\frac{RH}{100}\right) + 38\,(\ln(w)) - 5\left(\frac{ln\left(\frac{V}{S}\right)}{10}\right)^2\ 10^{-5}\right)$$

Where,

$\varepsilon_{sh}(t,t_0)$ = predicted shrinkage strain (in/in)

$\varepsilon_{sh\infty}$ = ultimate shrinkage strain (in/in)

w = water content of the concrete (kg/m^3)

RH = relative humidity (%)

V/S = volume to surface area ratio

t = time (days)

t_0 = time drying started (days)

2.7. Adaptation of prediction models

Several factors affect the free shrinkage of a concrete sample. As such, the prediction models developed above are given in generalized forms. Modification factors are then provided so to adapt the equations to a wider array of scenarios. These modification factors include size factors, environmental factors and concrete material factors. The process by which these factors have been accounted for is detailed in the sections below.

2.7.1. Sample size factor

The free shrinkage of a concrete specimen changes with the sample size. This effect has been considered in two ways which are the ultimate shrinkage and the rate of shrinkage. Over the years, a general consensus has emerged on the effect of sample size on the rate of shrinkage. Several early research projects such as the work by Hansen and Mattock (1966) and Almudaiheem and Hansen (1987) present results indicating that the rate of shrinkage reduces as specimen size increases. Furthermore, more recent studies such as Al-Saleh and Al-Zaid (2004), Bissonnette, Pierre and Pigeon (2009) and Jayakumar, Upadhyah and Bhandari (2013) support these earlier findings. Hence, smaller concrete samples are expected to shrink at a faster rate than their corresponding larger samples.

There is no general agreement on the effect of specimen size on the ultimate shrinkage. The study by Hansen and Mattock (1966) stated that the ultimate shrinkage of a concrete sample decreases with specimen size and is widely cited by proponents of this conclusion. In this study, samples of various sizes were monitored for a period of four years. This work forms part of the basis for the ACI code position that specimen size affects the ultimate shrinkage of a sample (ACI, 2008). A more recent publication by

Mingfang, Chunxiang and Hui (2013) also supports this conclusion. Conversely, studies by Almudaiheem and Hansen (1987), Al-Saleh and Al-Zaid (2004), and Bissonnette, Pierre and Pigeon (2009) conclude that specimen size does not affect the ultimate shrinkage. The CEB code (CEB, 1991) agrees with this finding and cites that the conclusion of the study by Hansen and Mattock (1966) on ultimate shrinkage is a result of insufficient time for which measurements were observed.

The length of time for which the experimental measurements were taken and the point at which samples were considered to have reached ultimate shrinkage is an important factor in this debate. As it is generally agreed that smaller samples shrink faster, it then follows that at any given point in time, smaller samples will record higher values of shrinkage than larger samples because they are further along in the shrinkage process. A study by Sener, Sener and Koc (2009) presented results collected for 70 days that indicated that smaller samples had higher values of shrinkage than larger samples. However, since results were not measured for a significant period of time, the samples were dried in an oven to expedite moisture loss. It was found that larger specimens lost about 70% more moisture while smaller samples only lost 20% more moisture. This would indicate that while the smaller specimens were closer to reaching ultimate shrinkage, the larger specimens were still far away. Hence, over time the ultimate shrinkage values may approach the same value. Studies by Almudaiheem and Hansen (1987) and Jayakumar, Upadhyah and Bhandari (2013) stated that while the difference in the shrinkage of small and large samples was significant curing early measurements, the values appeared to be converging over time. The methods adopted by the ACI and the CEB for modifying shrinkage for size are given below.

2.7.1.1. ACI size modification

The ACI 209 equation for predicting concrete shrinkage indicates that the effect of shape/size can be taken into consideration with or without adjusting ultimate values and leaves the decision up to judgement of the user. The general form of the ACI 209 prediction model is reiterated below.

$$(\varepsilon_{sh})_t = \frac{t}{f+t}(\varepsilon_{sh})_u$$

f is the shrinkage half time of the concrete sample taken as 35 and 55 for 7 days moist curing and 1-3 days steam curing respectively. To modify the rate of shrinkage, the time ratio portion of the ACI equation is modified by adjusting f as follows

$f = 26.0e^{(1.42 \times 10\text{^-}2(v/s))}$ in S.I. units

$f = 26.0e^{(0.36(v/s))}$ in.-lb units

To modify the ultimate shrinkage value for size, it is multiplied by the the size factor $\gamma_{sh,vs}$. $\gamma_{sh,vs}$ can be derived from the volume to surface ratio (v/s) or from the average thickness of the member.

For volume/surface ratio

$\gamma_{sh,vs} = 1.2e^{(-0.00472(v/s))}$ in S.I. units

$\gamma_{sh,vs} = 1.2e^{(-0.12(v/s))}$ in in.-lb units

For average thickness

$\gamma_{sh,d}$ = 1.17-0.00114d in S.I. units

$\gamma_{sh,d}$ = 1.17 – 0.029d in in.-lb units

2.7.1.2. CEB size modification

The CEB MC90 equation accounts for specimen size in the time development component of the equation only not on the notional (ultimate) shrinkage in accordance with their views on the available research. The time function accounting for the size factor is reiterated below.

$$\beta_s(t-t_o) = \sqrt{\frac{t-t_s}{350\left(\frac{v/s}{v/s0}\right)^2 + (t-t_s)}}$$

where v/s is the volume to surface ratio of the concrete specimen.

2.7.2. Environmental factor

Environmental factors such as relative humidity as well as temperature have an effect on the shrinkage of a concrete sample. Samples stored in higher relative humidity environments give lower shrinkage values than samples stored in lower relative humidity environments. Since shrinkage is related to a loss of water, it follows that samples stored in drier environments will lose moisture more rapidly than samples stored in moist environments. A study by Barr, Hoseinian and Beygi (2003) supported this finding.

Additionally, both the ACI and the CEB code include parameters that adjust shrinkage values in this manner. An interesting study stipulated that a sample under cyclic RH conditions does not produce different results from a sample under the average of those conditions (Bazant and Wang, 1985).

The effect of temperature on the shrinkage of a concrete sample is similar to the effect of relative humidity. Concrete samples stored under high temperature conditions give higher shrinkage values than samples stored in lower temperature conditions. Additionally, samples under cyclic temperature variations give similar results to samples stored under the average of the cyclic condition.

2.7.2.1. ACI environmental modification

The ACI code accounts for relative humidity on the ultimate shrinkage using a multiplier described below.

$$\gamma_{sh,RH} = 1.40 - 1.02h \qquad \text{for } 0.4 < h < 0.80$$

$$\gamma_{sh,RH} = 3 - 3h \qquad \text{for } 0.8 < h < 1$$

The ACI code does not give any modification factors for temperature. The standard conditions specified for use of the prediction model stipulates a temperature value of 73.4°F.

2.7.2.2. CEB environmental modification

The CEB MC90 provides an adjustment to the predicted notional (ultimate) shrinkage based on relative humidity. The formulas are reiterated below.

$$\beta_{RH}(h) = -1.55\left[1 - \left(\frac{h}{h_0}\right)^3\right] \qquad \text{for } 0.4 \leq h \leq 0.99$$

$$\beta_{RH}(h) = 0.25 \qquad \text{for } h \geq 0.99$$

The CEB considers the effect of temperature on both the time development and the ultimate shrinkage for sustained temperatures above 86°F. The formulas provided by the CEB code for temperature adjustment are also shown below.

Notional shrinkage

$$\beta_{RH,T} = \beta_{RH}(h)\left[1 + \left(\frac{0.08}{1.03 - \frac{h}{h_0}}\right)\left(\frac{18.778 * \frac{T}{T_0} - 37.778}{40}\right)\right]$$

Time development

$$\beta_{s,T}(t - t_c) = \left[\frac{\frac{t - t_c}{t_1}}{350\left[\frac{\frac{v}{s}}{\frac{v}{s_0}}\right]^2 exp\left[-0.06\left(18.778\frac{T}{T_0} - 37.778\right)\right] + \left(\frac{t - t_c}{t_1}\right)}\right]^{0.5}$$

Where,

h= ambient relative humidity

$h_0 = 1$

T= ambient temperature

T_0 = 1°C (33.8°F)

2.8. Summary

Cracking in concrete bridge decks is a problem affecting bridges throughout the United States (Ganapuram et al., 2012). It leads to further deterioration of bridge decks as corrosive chlorides seep into the bridge deck (Rahim et al., 2006). Some examples of degradation closely linked with concrete cracking are corrosion of reinforcement and concrete spalling (Elsafty & Jackson, 2012). These issues are of critical importance in maintaining the integrity of bridge decks over their service life.

Cracking in concrete occurs when tensile stresses in the concrete exceed the tensile strength of the concrete (Hadidi and Saadeghvaziri, 2005) Tensile stresses develop in concrete when the concrete is connected to other permanent fixtures that prevent it from freely undergoing volumetric changes. Temperature changes and concrete shrinkage are factors responsible to volumetric changes in concrete (Chaunsali et al, 2013).

Concrete shrinkage is a serviceability issue and is therefore not designed for directly. However, the AASHTO LRFD Bridge Design Code specifies reinforcement to be included in bridge decks for the purpose of mitigating concrete cracking due to shrinkage and temperature loads (AASHTO, 2010). These provisions are derived from the ACI 318 code (ACI, 2008) and were developed by empirical methods. Furthermore, the ACI code

indicates that the provisions are applicable for the case of unrestrained shrinkage and restrained shrinkage cases should be considered although no guidelines are provided.

Previous attempts to study restrained shrinkage have been performed using analytical methods such as finite element modelling and field instrumentation of bridges (Frosch et al., 2003; Lange et al., 2003). Past research can be improved by modelling of shrinkage as a time dependent load and comparing shrinkage results with data collected from instrumented bridges under field conditions. Using these techniques and validated models, parametric analyses can be performed and observations can be made on the response of concrete bridge decks to shrinkage under field conditions.

CHAPTER 3

LABORATORY SETUP

Several laboratory experiments were conducted to aid in the study of shrinkage. These experiments were simplified cases of shrinkage performed under controlled conditions. Experiments were initially performed on small free shrinkage prism samples. Subsequently, data from experiments conducted on larger laboratory specimen was collected and used to further the study of shrinkage under more controlled conditions than in the field. This section details the laboratory experiments performed towards the end of modelling shrinkage.

3.1. Shrinkage prism experiments

Previously conducted free shrinkage tests were collected and additional free shrinkage tests were performed to study the occurrence of shrinkage under varying conditions and develop a suitable shrinkage model to aid in the study of concrete shrinkage. Details of data collected and setup of various experiments are detailed below.

3.1.1. Experiment 1

In the first experiment, a sample was cast under controlled environmental conditions in the laboratory. A free shrinkage prism sample measuring 3” x 3” x 10” was cast in the laboratory. Figure **3** below shows the shrinkage prism.

Figure 3: Free shrinkage prism

The prisms were cast in a steel mold and wrapped in plastic wrap for 24 hours until the concrete set. Afterwards, the samples were demolded and stored under constant conditions in an environmental chamber to prevent strains due to changes in temperature and other environmental effects. The free shrinkage prism was cured for 14 days using wet burlap. Strain readings were measured at regular intervals using a length comparator for up to 56 days.

Furthermore, cylinders measuring 4 x 8 in were also collected during casting so that the concrete material strength could be measured. The 28 day compressive strength of the mix was found to be 10589 psi. The strength of the concrete mix was high because a high early strength mix was used.

3.1.2. Experiment 2

Another experiment was performed to observe the shrinkage of a concrete prism sample with the addition of restraint. Restraint was applied to the free shrinkage prism in the form of reinforcement bars. Three #4 reinforcement bars were embedded in a shrinkage prism during casting with the configuration shown below.

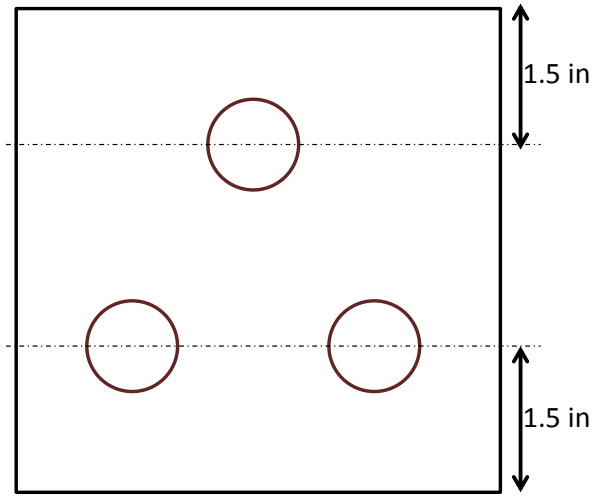

Figure 4: Configuration of prism with reinforcement restraint

A control free shrinkage prism from the same concrete batch was also cast for direct comparison. Strain gages were embedded in the concrete during batching to facilitate the collection of data in more frequent intervals. The samples were also wrapped in plastic wrap for 24 hours and demolded afterwards. Both samples were stored in the environmental chamber so that the effect of reinforcement could be observed without influence from other factors such as temperature or humidity. The environmental chamber was held at 25°C and 50 % relative humidity. The samples were cured for 14

days and readings were taken for up to 56 days. The 28-day material strength of the concrete used was measured as 6791 psi.

3.1.3. Experiment 3

The third laboratory setup was expanded to include more parameters than the previous two setups. An experiment was performed in the lab to compare the results of a free shrinkage sample under constant conditions with a free shrinkage sample under a controlled temperature fluctuation. Furthermore, multiple prism sizes were also used to observe the effect of sample size on the free shrinkage of a sample. The free shrinkage samples were all taken from the same batch to ensure uniform material properties.

Six free shrinkage prisms were cast with VWSG embedded in the samples to measure strain and temperature over time. Four of these samples were cast in free shrinkage prism molds measuring 3 x 3 x 10 in while the other two samples were cast using larger molds measuring 6 x 6 x 20 in to highlight the effect of sample size. The samples were all cast on the same day and wrapped in plastic wrap for 24 hours. Afterwards, the samples were demolded. Two small samples and one large sample were kept in an environmental chamber with constant relative humidity and temperature. The rest of the samples were stored under a heat blanket where the temperature could be controlled manually. The figure below shows the experimental setup while the table gives details on the samples.

Figure 5: a) Free shrinkage prism mold with embedded VWSG b) Concrete prisms stored in environmental chamber c) Concrete prisms connected to datalogger d) Concrete prism stored under heat blanket (top left to bottom right)

Table 1: Sensor label and description for experiment 3

Label	Description
Strain1	Small sample, constant temperature
Strain3	Large sample, constant temperature
Strain4	Small sample, under heat blanket
Strain5	Small sample under heat blanket
Strain6	Large sample, under heat blanket

The heat blanket was turned on and off intermittently to simulate temperature fluctuation. Strain readings form the samples were collected over time. Readings from Sensor 2 were

unavailable as the sensor malfunctioned after placement. Temperatures under the heat blanket as well as in the environmental chamber were also recorded over time.

The environmental chamber maintains a temperature of 18ºC ± 2. The samples under the heat blanket were heated to 30ºC ± 2 during the day for approximately eight hours after which the blanket was switched off and the samples cooled down to match the environmental chamber. The samples were cured using wet burlap for 14 days. Cylinders were also cast along with the shrinkage prisms to allow for the compressive strength of the concrete to be tested. The 28 day compressive strength of the concrete was measured as 4844 psi.

3.1.4. Experiment 4

A final experiment was conducted in the lab to compare shrinkage under controlled temperature and humidity with external environmental conditions which are more variable than conditions controlled by a heat blanket. Four samples were cast using molds measuring 6 x 6 x 20 in and shrinkage sensors were embedded in the samples as shown in the figure below. Furthermore, two of the samples were embedded with reinforcement bars while the other samples were cast without reinforcement. The samples were wrapped in plastic wrap for 24 hours and demolded afterwards. The figure below shows the setup of the molds.

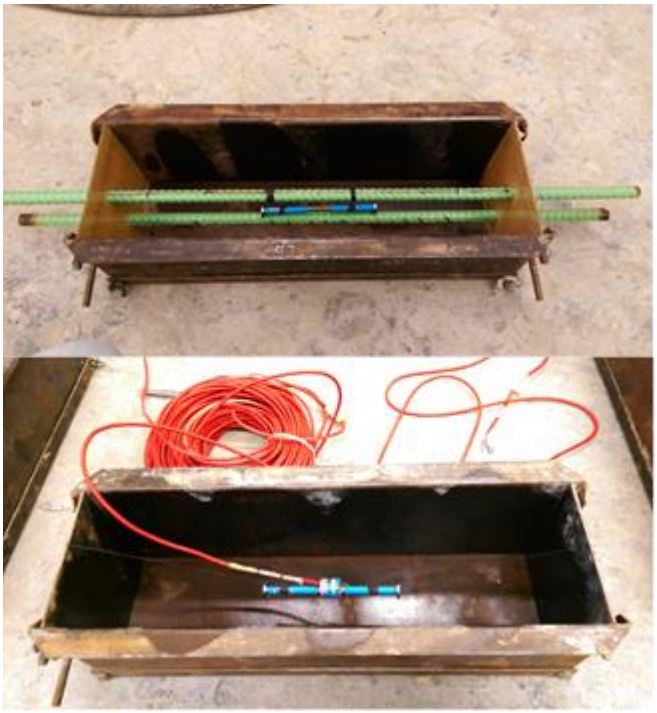

Figure 6: a) Mold with reinforcement b) mold without reinforcement used for experimental setup 4

One sample with reinforcement and one sample without reinforcement were stored in an environmental chamber under constant temperature and humidity. The other two samples were stored outdoors and exposed to environmental conditions. The experimental setup is shown in the figure below.

Figure 7: Concrete samples for experimental setup 4 stored in chamber and outdoors

The samples were cured for 14 days using a wet burlap. VWSG were embedded in the samples to measure strain as well as temperature of the samples. The strain gages were connected to a datalogger to collect the data every five minutes. The temperature in the environmental chamber and outdoors where samples were stored, was also measured using a thermocouple connected to the datalogger. Furthermore, samples were collected during the pouring of the concrete to test for the concrete material strength. The concrete material strength was measured found to be 6500 psi.

Data from all these experiments were compiled and used to study shrinkage using finite element analysis. The results of these studies are discussed in the FE modelling section.

3.2. Slab experiment

Following the collection of experimental shrinkage data for small samples, data was collected for a larger and more complex sample. This mid-scale model used was a slab segment built in a laboratory under more controlled conditions. The laboratory model was a closer representation of bridges in the field than the free shrinkage prism and as such data collected from the model provided a more accurate representation of the behavior of the shrinkage in a full scale bridge.

Data for the analysis of the laboratory model was acquired from a study performed by Frosch et. al (2006). In this study, a slab segment was built by Blackman (2002) and shrinkage data was measured over time. The segment was 33 in wide, 44 in long and 8 in thick. It was built using wooden forms and aluminum tape to create a sealing effect at the bottom of the slab. No reinforcement was included in the setup. Hence the results were considered to be free shrinkage.

Afterwards, a similar laboratory model was built by Radabaugh (2001). The slab was a scaled down segment of an existing bridge deck built using wood forms and measured 9 ft x 9 ft x 8in. The slab was cast on two W12 x 65 girders with 78 in between the girders. The experimental setup is shown in Figure 8 below.

Figure 8: Restrained shrinkage slab segment (Radabaugh, 2001)

Shear studs were used to promote composite behavior between the slab and the concrete deck as is done in full scale field bridges. A steel deck pan was also used to build the form work for the slab. Reinforcement was included as shown in the figure below.

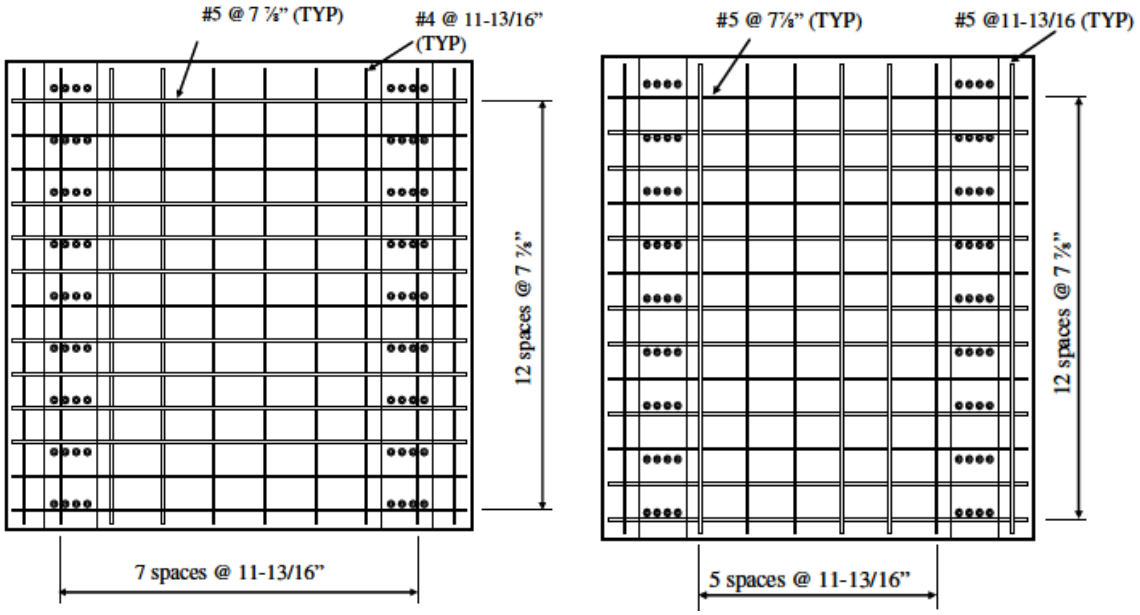

Figure 9: (a) Top reinforcement and (b) Bottom reinforcement in restrained shrinkage specimen for medium scale slab experiment (Frosch, 2006)

The results derived using this specimen were considered restrained shrinkage since the use of shear studs, reinforcement and the form work introduced restraint in the concrete slab. The concrete mixes and slab dimensions used by Blackman (2002) and Radabaugh (2001) were found to be similar which allowed for their results to be compared reasonably. Data for the concrete material input as well as the steel beam was derived from the study. Radabaugh (2001) did not perform any compressive strength tests for the concrete and so the compressive strength from Blackman (2002) was used. The available compressive strength measurements were limited to 21 days. Consequently a value for the 28 day strength was extrapolated and taken as 5750 psi. The plot showing the development of compressive strength with time is shown in Figure 10.

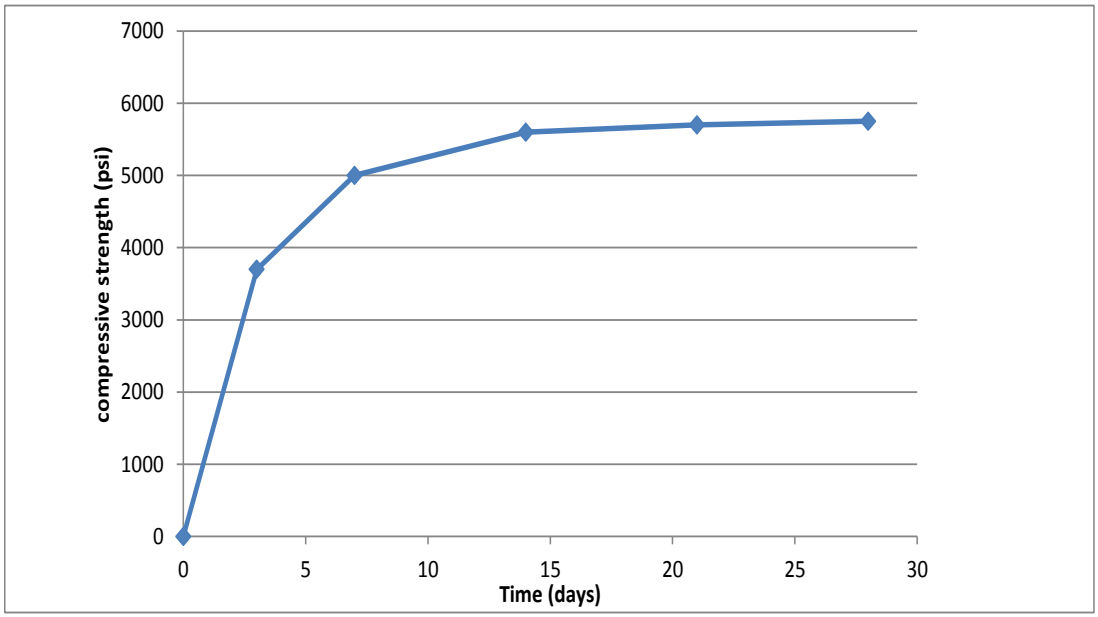

Figure 10: Development of compressive strength with time

There were a total of three functioning sensors in the slab. One sensor was installed in the center of the slab on the bottom rebar. The other two sensors were installed at 30.5 in

north from the center as indicated in the figure below, with one on the top rebar and another on the bottom rebar.

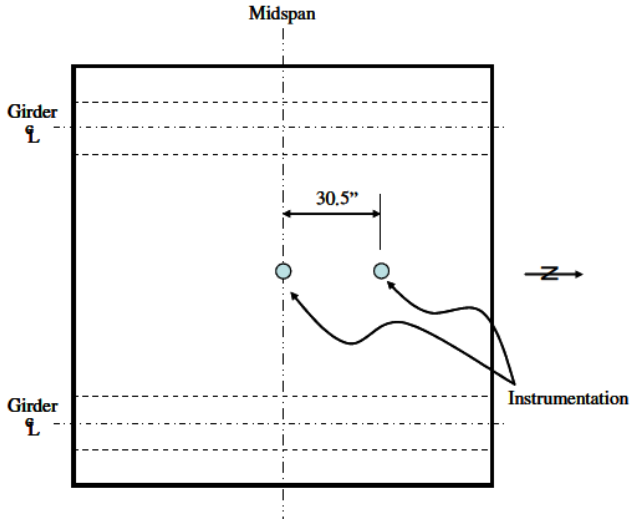

Figure 11: Sensor locations on restrained shrinkage slab (Frosch, 2006)

The top reinforcement was a distance of 2.5 in from the top of the slab while the bottom reinforcement was a distance of 1 in from the bottom of the slab. Readings were collected for a period of 21 days, during which the slab was cured for the first four days. These results were used to facilitate the study of shrinkage using FE modelling.

3.3. Summary

The section above discussed details of experiments performed and experimental data collected under controlled conditions in a laboratory. These studies are instrumental in understanding the behavior of shrinkage under controlled conditions and to verify the validity of any modelling procedure. Reinforcement, sample size and environmental conditions were taken into consideration in the experiments described above. These

results will be used in the finite element modelling section to assess the performance of the developed shrinkage model.

CHAPTER 4

FIELD TESTING

This section discusses field testing performed to facilitate the modelling of shrinkage. Previously, shrinkage data had been procured from small samples in controlled laboratory conditions. In this section, free shrinkage tests were performed and collected during the construction of bridges under field conditions to provide data under actual conditions. Strain gages were placed in the bridge decks to facilitate the collection of long term strain data. This chapter discusses the details of the bridges used to study shrinkage.

4.1. Bridge database

Available bridges as well as relevant data for the study of restrained shrinkage in each bridge were compiled. The input required to perform the shrinkage analysis for all bridges included geometric data as gotten from bridge plans and concrete material properties from field samples so that finite element models of the bridges could be built. The details of the input data for each bridge are discussed in the sections following.

4.1.1. Patcong Creek Bridge

The Patcong Creek Bridge is a five span continuous for live load bridge with two simply supported portions at the ends, and a 3 span continuous section in the middle. The slab thickness of the deck was 9 inches. The bridge is located along the Garden State Parkway (GSP) between exit 31 and 36. Figure 12 and Figure 13 below show the dimensions of the bridge.

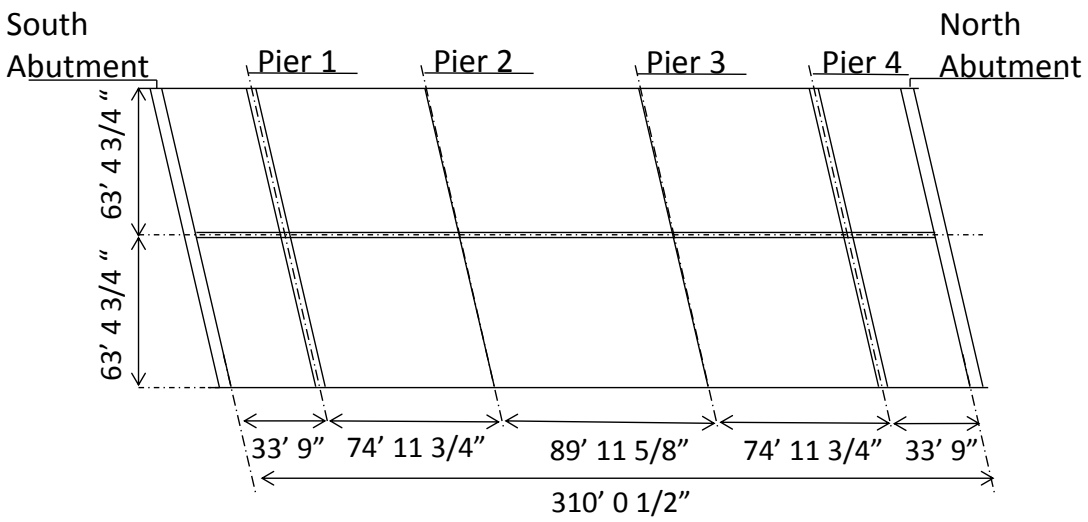

Figure 12: Plan of Patcong Creek Bridge

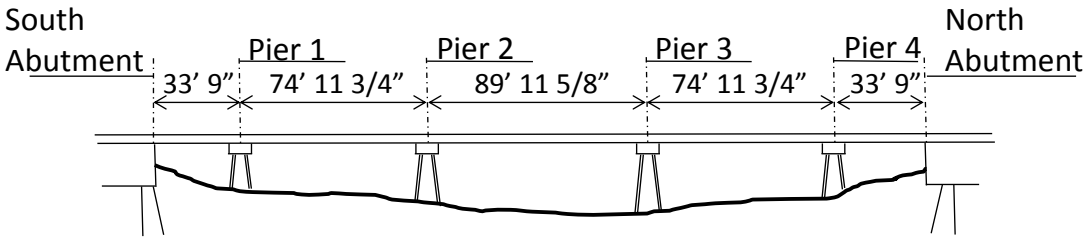

Figure 13: Elevation of Patcong Creek Bridge

During the re-decking of this bridge, a total of 15 Vibrating Wire Strain Gages (VWSGs) were embedded in the northbound half of the concrete deck. Figure 14 below shows the locations of the sensors.

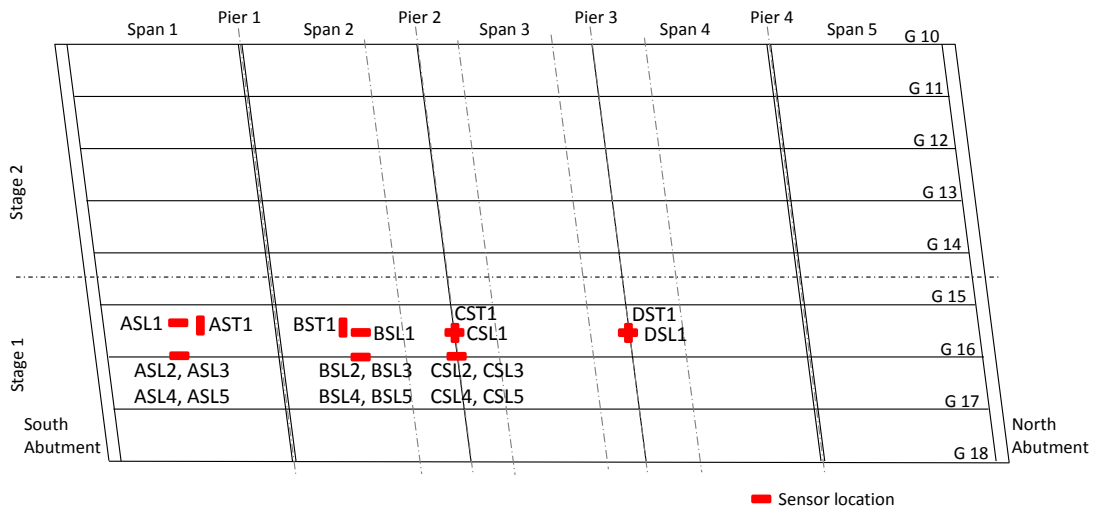

Figure 14: Plan view of VWSG sensor location of Patcong Creek Bridge

More information on the location of the sensors labeled in Figure 14 above is given in Table 2 below.

Table 2: Location of VWSG on Patcong Creek Bridge

Sensor	Orientation	Location along span	Location across span	Location below top of deck
ASL1	Longitudinal	16’ 2” from south abutment	4 ‘ from G 15	8.5”
AST1	Transverse	16 ‘ 8 “ from south abutment	4’ 4 “ from G 15	8.5”
ASL2	Longitudinal	16’ 2” from south abutment	Above G 16	2”

ASL3	Longitudinal	16’ 2” from south abutment	Above G 16	4”
ASL4	Longitudinal	16’ 2” from south abutment	Above G 16	5.5”
ASL5	Longitudinal	16’ 2” from south abutment	Above G 16	8.5”
BSL1	Longitudinal	25 ‘ from pier 1	2’ 10” from G 15	8.5 ”
BST1	Transverse	24 ‘ 9” from pier 1	3’ from G 15	1.5 ”
BSL2	Longitudinal	25 ‘ from pier 1	Above G 16	1.5 ”
BSL3	Longitudinal	25 ‘ from pier 1	Above G 16	3.25”
BSL4	Longitudinal	25 ‘ from pier 1	Above G 16	5”
BSL5	Longitudinal	25 ‘ from pier 1	Above G 16	8.5”
CSL1	Longitudinal	At pier 2	4’ 6” from G 15	8.5 ”
CST1	Transverse	At pier 2	4’ 6” from G 15	1.5 ”
CSL2	Longitudinal	At pier 2	Above G 16	1.5 ”
CSL3	Longitudinal	At pier 2	Above G 16	3.25”
CSL4	Longitudinal	At pier 2	Above G 16	5”
DSL1	Longitudinal	At pier 3	Above G 16	8.5 ”
DST1	Transverse	At pier 3	Above G 16	1.5 ”

The concrete for the bridge deck was poured in stages. Consequently, the material properties for different stages were tested separately and varied slightly. The pouring schedule is shown below in Figure 15.

Figure 15: Concrete pour staging of Patcong Creek Bridge

Cylinder samples were collected during the pouring of the concrete deck. These samples were tested for compressive strength. The average value across the days of pouring was used and is shown below in Table 3.

Table 3: Concrete compressive strength of Patcong Creek Bridge

Age (days)	Average Compressive Strength (psi)
14	3670
21	4128
28	7747

Furthermore, free shrinkage samples were collected during the pouring of the concrete. The free shrinkage properties of the concrete samples collected at each pouring stage are shown in Figure 16 below.

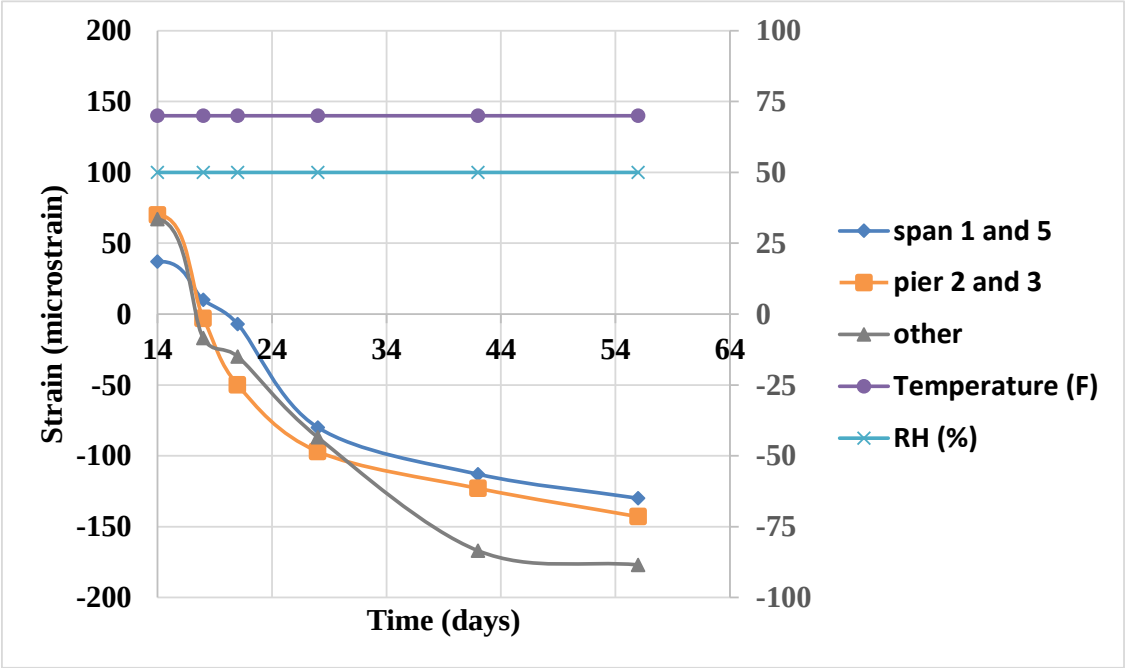

Figure 16: Free shrinkage of Patcong Creek Bridge

Data was collected to validate the structural behavior of this bridge for use in the finite element modelling. The segments of the bridge were separated to appropriately capture the behavior of the bridge. The bridge is conceptualized as a continuous for live load bridge with a continuous concrete pour and discontinuous steel girders however, it was found that the bridge behaves more closely like three separate parts owing to the presence of expansion joints above pier 1 and pier 4 where the simply supported spans meet the continuous span. This assumption was later checked and found to be valid using results from the strain transducers installed to validate the bridge model by a static analysis.

Dynamic and static tests were performed to validate the structural behavior of the FE model of the bridge. In this test, STS strain transducers were attached to the girders on the bridge as shown in Figure 17 below.

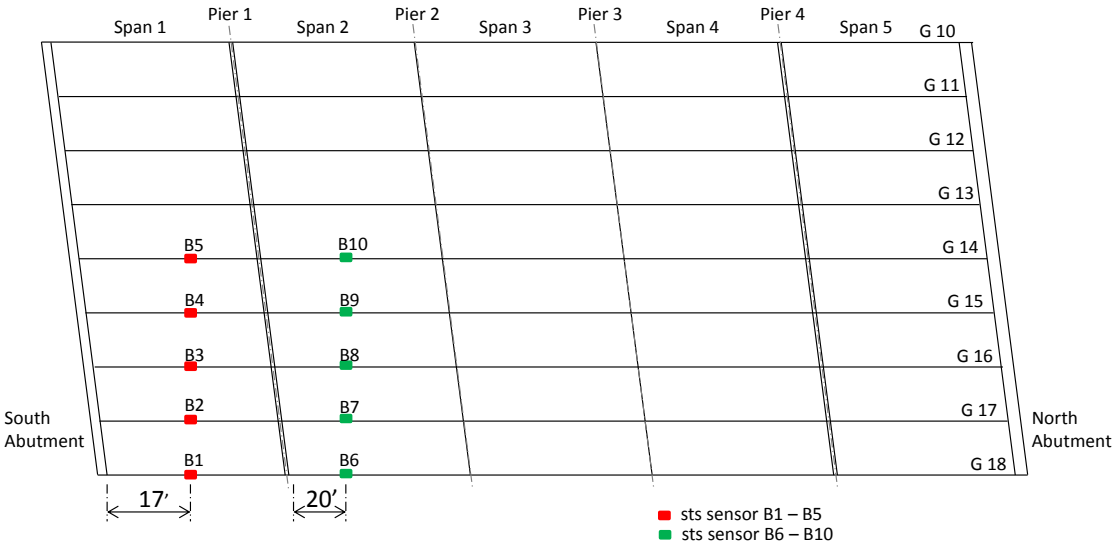

Figure 17: Plan view of STS sensors for Patcong Creek Bridge validation

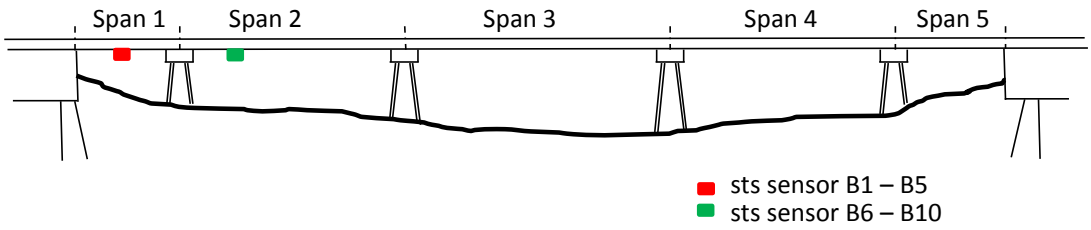

Figure 18: Elevation view of STS sensors for Patcong Creek Bridge validation

10 strain transducer sensors (STS) which measure short term strain were installed on the bridge girders. The sensors were located at about the midspan of span 1 and span 2 to capture the maximum strain readings.

As previously mentioned, the analysis for this bridge was performed using separate segments to capture the behavior of the bridge. This is because the concrete deck and the steel girders of the bridge are discontinuous at pier 1 and pier 4. Therefore, it is expected that minimal strains will be propagated from one simple supported span to the continuous span and vice versa. Two major static tests were performed on the bridge. In the first static test, the truck is positioned at the midspan of span 1 as shown in Figure 19 to maximize the strain readings of the sensors on span 1 that are located directly below the truck.

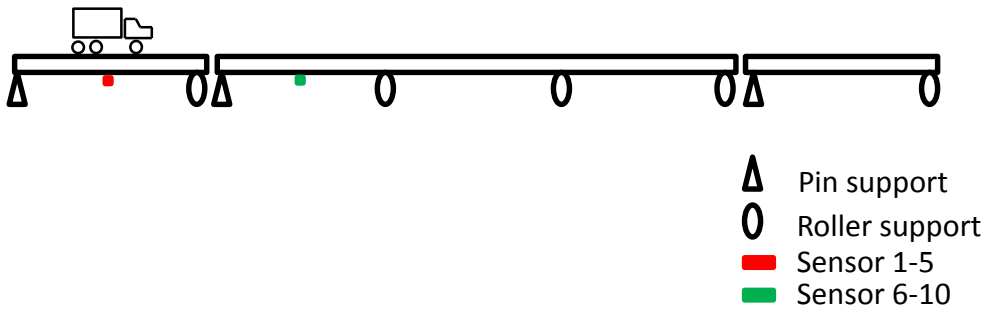

Figure 19: Truck and sensor location for static test 1

The validity of the assumption made can be seen from results of the strain gage results derived from the static testing as shown in the Figure 20 below. From the results of the static tests, it was observed that the sensors on span 2 recorded little or no strains as a result of the maximum loading scenario of span 1. The strains recorded at sensor B6 and B7 are less than five microstrains and are negligible.

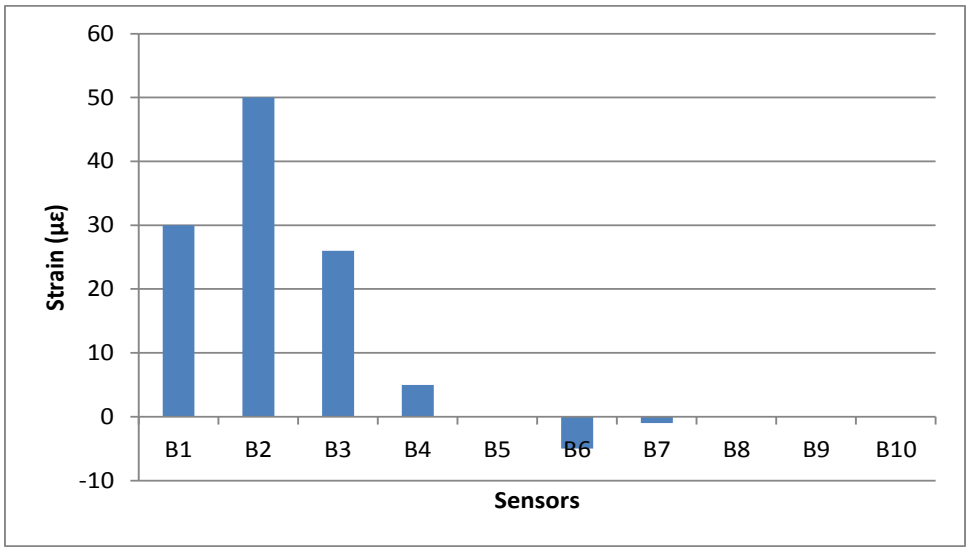

Figure 20: Patcong Creek Bridge span 1 static test results

In the second static test, the truck is positioned above span 2 to maximize the strain readings on sensor 6-10 located directly below the truck in the transverse direction.

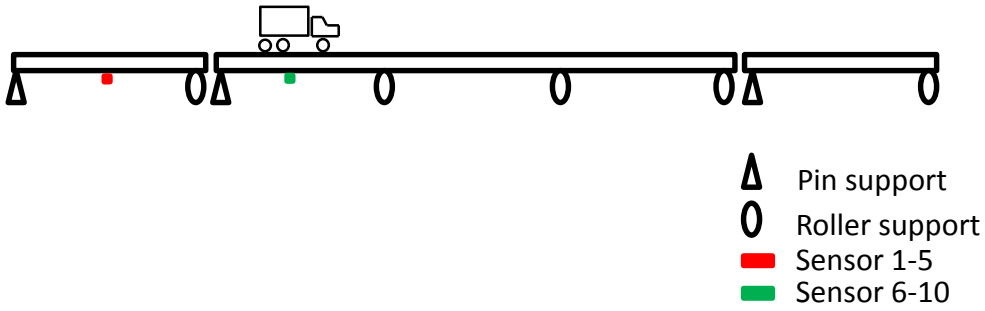

Figure 21: Truck and sensor location for static test 2

Figure 22 below shows that minimal strains are transferred from span 2 to the simply supported span during the maximum loading scenario as shown in Figure 21. The strains recorded by the sensors located on span 1 are all less than 5 microstrains and are negligible. This may be due to the presence of the parapet and other minor components which connect all the spans together.

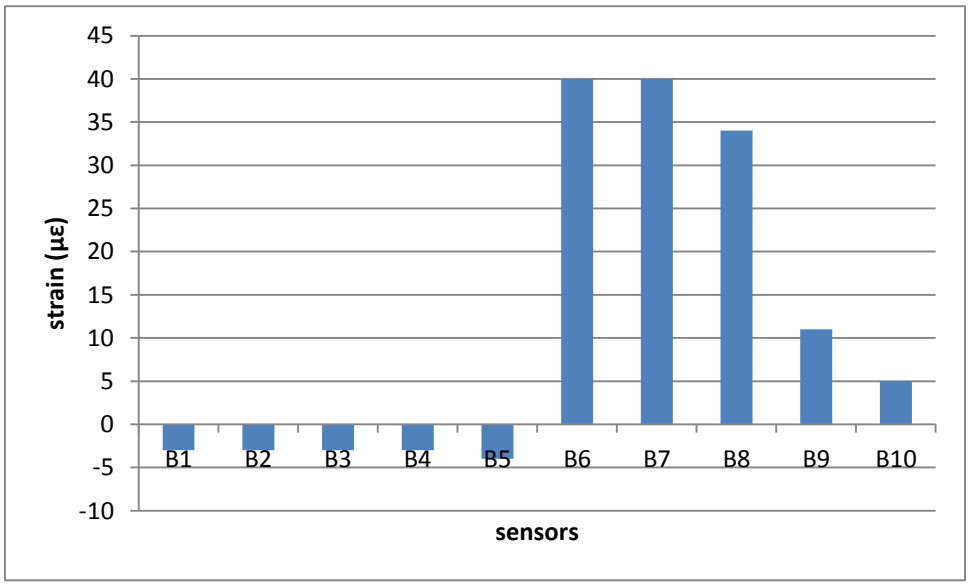

Figure 22: Patcong Creek Bridge span 2 static test results

Additionally, the results from the dynamic test were used to confirm this assumption. In the dynamic test, the truck was driven across the bridge from one end to the other and strain readings from each sensor were recorded throughout the duration of the test. From previous knowledge of structural analysis, the maximum strain reading for each sensor is expected to occur when the load is directly located above each sensor. Also, tools such as influence lines allow for the shape of a moving truck load along a bridge span to be appropriately predicted. The relevant information is shown in Figure 23 below for the associated dynamic test.

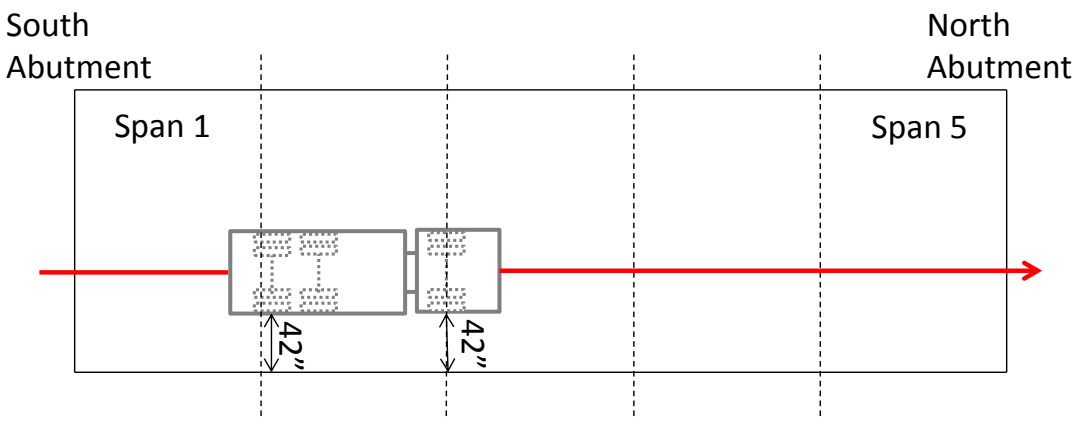

Figure 23: Truck location for Dynamic test on Patcong Creek Bridge

The result of the dynamic test is shown in Figure 24 for span 1 while the results for span 2 are shown in Figure 25 below.

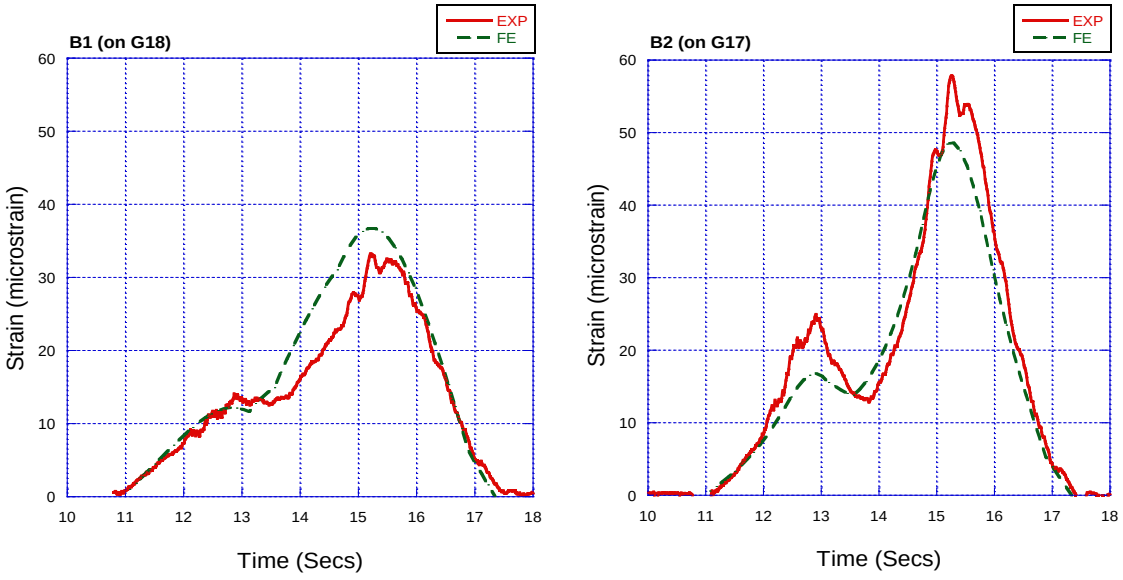

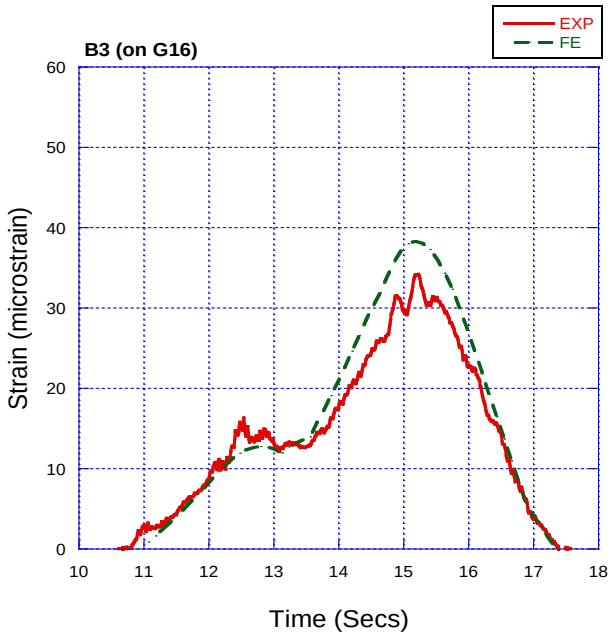

Figure 24: Dynamic test result for span 1

From the results of the dynamic test performed on span 1 of the bridge, it is observed that there is one maximum reading point for each sensor, where the truck load is directly overhead the strain gages. The results of the test performed using the simply supported model match the shape of the experimental results collected from the field.

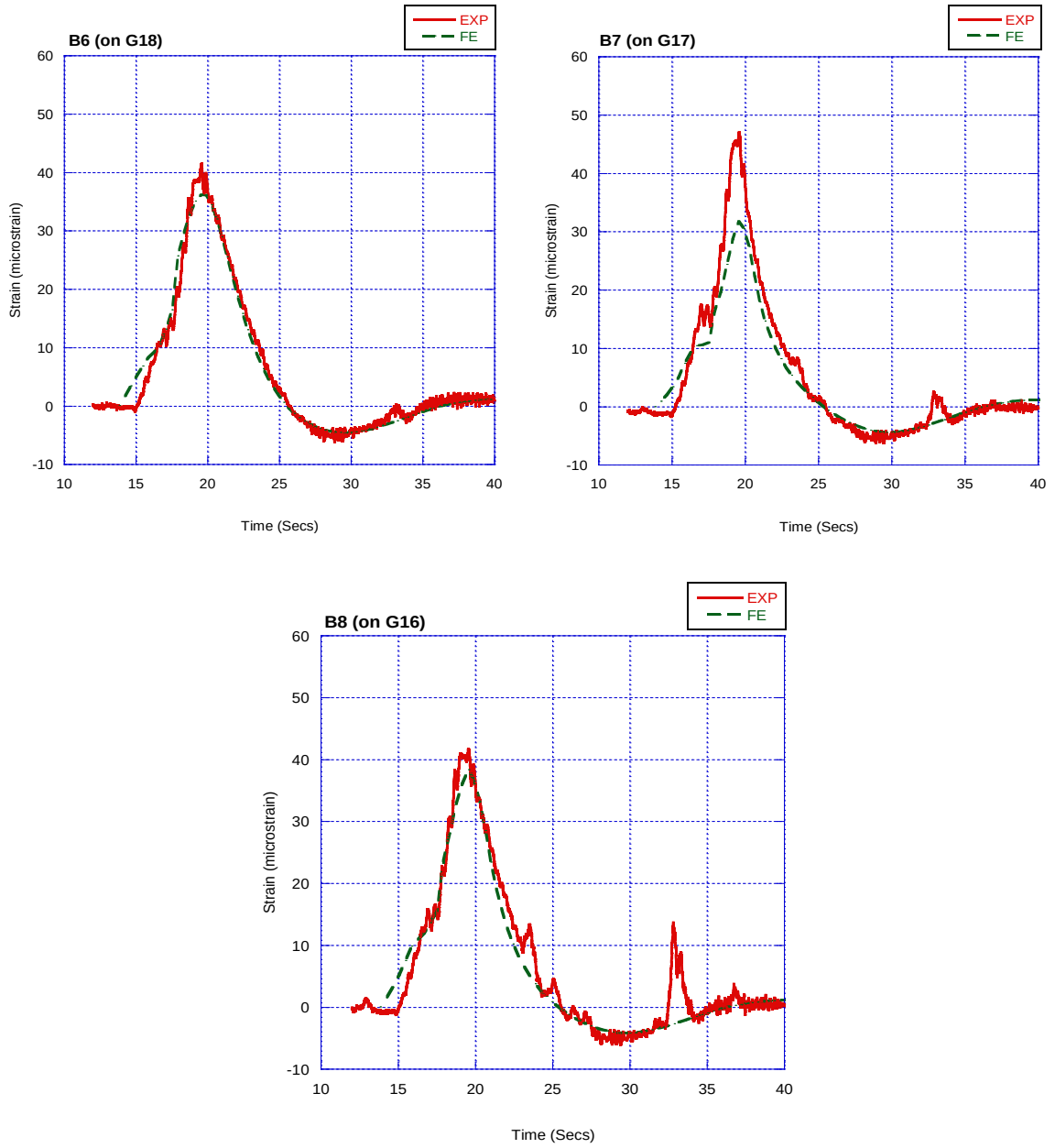

Figure 25: Dynamic test results of span 2

Figure 25 shows the results of the dynamic test performed on span 2 of the bridge. It was observed that there is one maximum reading point for each sensor, where the truck load is directly over the location of the strain transducers. It is also observed that span two (first

span of the continuous segment) goes into reverse curvature when the truck load moves to span three (second span of the continuous segment) and causes the negative strains in span two. This behavior is expected of a continuous bridge under a moving load.

To validate the bridges, the results of the dynamic test collected from the field were compared to the results of similar tests performed using the FE model and the comparisons are shown in Figure 24 and Figure 25. The results of the FE models closely follow the results of the experimental tests and appropriately capture the behavior of the bridge.

The developed FE model was found to be satisfactory for structural behavior. Along with the data collected, this model was used to study shrinkage.

4.1.2. Garden State Parkway Interchange 67

The Garden State Parkway Interchange 67 is an overpass located along the NJ Garden State Parkway in Barnegat Township, NJ. It spans a southbound section of the New Jersey Turnpike at exit 67 on the parkway. The bridge is a simply supported bridge spanning 90 ft. The bridge deck has a thickness of 8.5 in. The figure below shows greater detail on the geometry of the bridge.

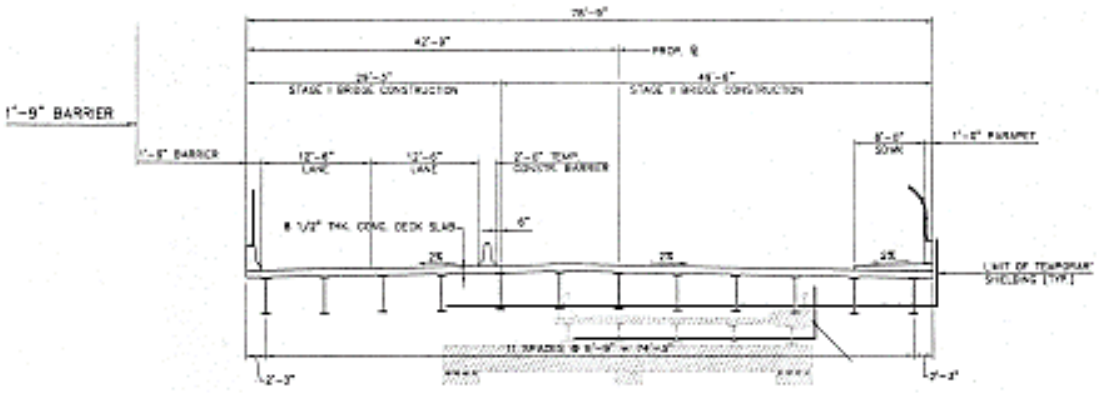

Figure 26: Elevation view of I-67

Sensors were installed on the bridge to measure strain over time. The locations of these sensors are shown in Figure 27 below and further details are given in Table 4.

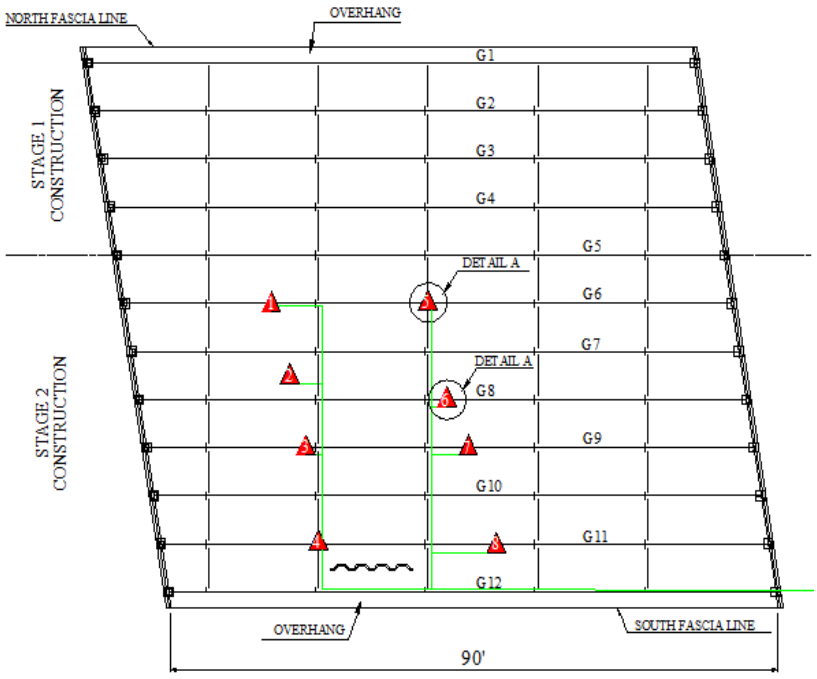

Figure 27: Sensor location on Interchange-67 Bridge

Table 4: sensor label details

Sensor Label	Location
Sensor 2	G10, Midspan, longitudinal, top
Sensor 3	G10, Midspan, longitudinal, top
Sensor 4	G10, Midspan, longitudinal, top
Sensor 6	G10, Midspan, longitudinal, top
Sensor 7	G10, Midspan, longitudinal, top
Sensor 10	G10, Midspan, longitudinal, top
Sensor 12	G10, Midspan, longitudinal, top
Sensor 14	G10, Midspan, longitudinal, top

Samples were also collected during the pouring of the concrete for this bridge to measure the compressive strength as well as the free shrinkage. Compressive strength and free shrinkage tests were performed on the samples and the results are shown in Table 5 and Figure 28 below.

Table 5: Compressive strength of concrete of I-67 Bridge

Time	Strength (psi)
0	0
3	4634
7	5609
14	6026
28	6929
56	7637

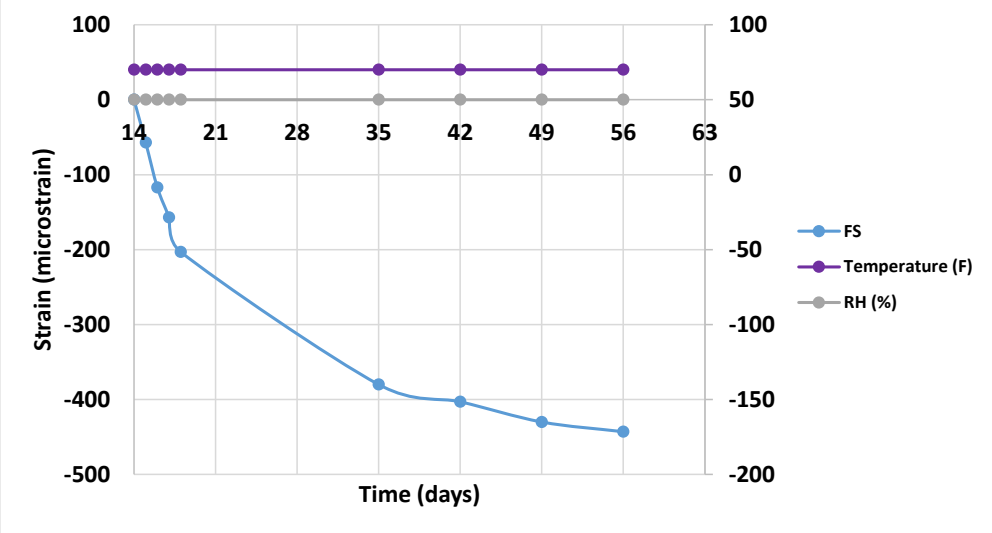

Figure 28: Free shrinkage of concrete for I-67 Bridge

The FE model for I-67 was validated by comparing the girder strains under a truck load to a simulation performed using the FE model. The truck weigh was not measured during the testing, therefore the FE model was analyzed using an iterative procedure. The comparison of the steels train is shown in the table below. The results were found to be satisfactory.

Table 6: Comparison of steel strain for validation of I-67 FE model

	Girder 3	Girder 4	Girder 5
FE model strain	0.000075	0.00006	0.000041
Field strain	0.000078	0.000066	0.000044

4.2. Summary

This section details the field work performed on full scale bridges and data collected for the study of shrinkage under field conditions. This data included concrete strength and free shrinkage data. Furthermore, the field bridges were instrumented and validated using data collected from the bridges. Results from this section are presented in the finite element modelling section and comparisons are made to validate the developed shrinkage model.

CHAPTER 5

FE MODELLING

This chapter details the finite element (FE) modelling of the laboratory experiments and field testing discussed in the previous chapters. Shrinkage data was incorporated into FE models of the samples to simulate the time development of shrinkage. The methodology employed in this study was developed by Eldhose (2006) as discussed in the literature review section. The FE software used does not come readily programmed to simulate concrete shrinkage however it allows the user to create user specified functions known as user subroutines which can be tailored to specialized uses as required by the user. A user subroutine was used to simulate the shrinkage process and is discussed in greater detail in the sections following. The general process of FE modelling of shrinkage in this study began with the simulation of shrinkage in the small free shrinkage specimens. The output of this analysis was checked against laboratory results. Consequently, the methodology was transferred to a larger scale laboratory specimen. In this case, the small slab built in a laboratory was modeled and the results were compared with the available laboratory data. Finally, the analysis was applied to a model of an existing full scale bridge and compared with results collected over time. This process is detailed below beginning with the development of the user subroutine used to model concrete shrinkage behavior.

5.1. Shrinkage modelling

To perform the finite element analyses and simulate concrete shrinkage, a software package known as ABAQUS was used. This software has no function tailored

specifically towards modeling concrete shrinkage however it allows for certain functions to either be used as-built or to be modified to a user defined function otherwise known as a user subroutine. These user subroutines are written in FORTRAN and then linked to ABAQUS. Whenever an analysis requiring the use of a defined subroutine is run, ABAQUS calls the FORTRAN file and runs the embedded code for every instance where the defined subroutine is called.

To model the effect of shrinkage, a user subroutine known as UEXPAN was used as done by Eldhose (2006). This UEXPAN subroutine is the designated user specified function used to define a material's expansion behavior. By default, the material expansion feature in ABAQUS functions as a thermal expansion component which calculates thermal strain ε as:

$$\boldsymbol{\varepsilon = \alpha \Delta T}$$

Where,

ε = thermal strain

α = coefficient of thermal expansion

ΔT = change in temperature

To make use of the default material expansion, the user need only provide the coefficient of thermal expansion and temperature changes as input during the modeling process. No FORTRAN coding is necessary in this case.

The shrinkage model was built by modifying the material expansion function to apply a negative strain to the modeled specimen equivalent to the concrete free shrinkage

laboratory test results over a specified period of time. The test results are written in the FORTAN file as an equation which ABAQUS can use to calculate the shrinkage strain at a specific point in time and apply the corresponding strain to the finite element model. In this analysis, the CEB equation and the ACI equation were both used to model the laboratory free shrinkage results in the FORTRAN file. The prediction results from these equations were modified to fit laboratory measured free shrinkage results to increase accuracy and improve their long term prediction. Consequently, the effect of the user subroutine is to create a contraction or 'shrinkage' which matches the measured concrete shrinkage behavior over time. The free shrinkage strain may also be approximated directly from the predictive equations where laboratory tests are unavailable however this will directly reflect the accuracy of the chosen equation and affect the final results. The models were set to simulate specified time periods during which the strain in the model was calculated incrementally by the finite element program.

5.2. Laboratory free shrinkage prisms

Details on the laboratory experiments performed on free shrinkage prisms under laboratory conditions were discussed in the laboratory setup section. This section discusses the results of the FE analysis of the samples and provides a comparison with the laboratory measurements.

5.2.1. Experiment 1 results

In experiment 1, measurements were taken from a free shrinkage prism under constant temperature and humidity as discussed in chapter three. The Figure below shows the finite element model of the sample.

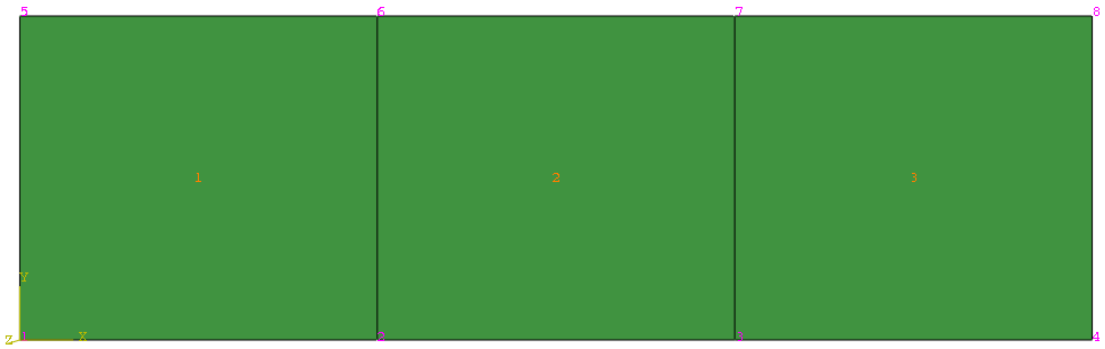

Figure 29: Finite element model of prism

The model was created using a course mesh consisting of only 3 elements and was free to move in the longitudinal direction. All points in the model had a roller-type boundary condition so that they were free to translate in the longitudinal direction. The midpoint had a pin-type connection. This point was not free to translate in any direction to avoid rigid body motion of the model which would cause errors and early termination of the analysis. Additionally, holding the midpoint allowed the model to shrink symmetrically. The free shrinkage prism was cured for 14 days during which shrinkage was nearly zero. Readings were then collected up to 56 days. Consequently, the finite element model was programmed for 56 days during which the shrinkage was delayed until after the first 14 days.

The input strain used in the FE model was a best fit of available free shrinkage prediction models to the experimental measurements. In this case, the best fit was produced by the CEB equation and so the input used in the FE model was the CEB equation calibrated to experimentally measured results.

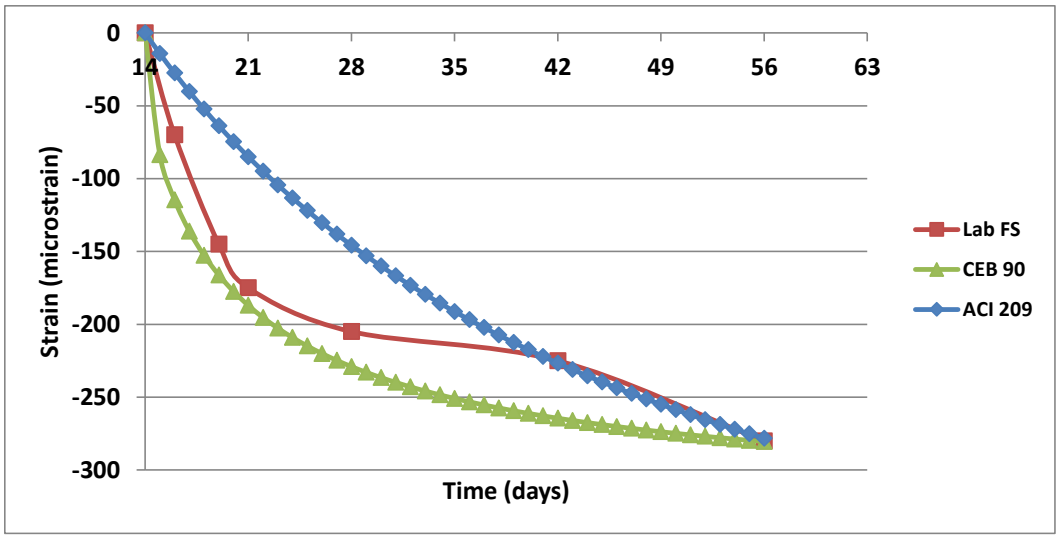

Figure 30: Fit of prediction models to laboratory free shrinkage prism data

The CEB equation produces a better match during the first 2 weeks of measurement while the ACI 209 equation underestimates the shrinkage. However, the ACI 209 model produced a better match during the last two weeks of measurement. The error of the ACI equation exceeded that of the CEB equation overall and so the CEB equation was used. Details on the calculated errors are given in the table below.

Table 7: Comparison of measured results and adapted prediction model for free shrinkage prism

Day	21	28	42	56	Average Error
ACI (Error)	85 (51)	145 (29)	226 (0.4)	278 (0.7)	20.27
CEB	187	229	264	280	8.95

(Error)	(6.8)	(11.7)	(17.3)	(0)	
LAB FS	175	205	225	280	

From the calculated errors in the table above, it can be seen that the CEB model produced a better match in this case with an average error of 8.95 % compared to an error of 20.27 for the ACI model. Consequently, the CEB model was used to incorporate shrinkage into the finite element model of the shrinkage prism. The figure below shows the comparison between the experimentally measured free shrinkage strains, and the results from the finite element model.

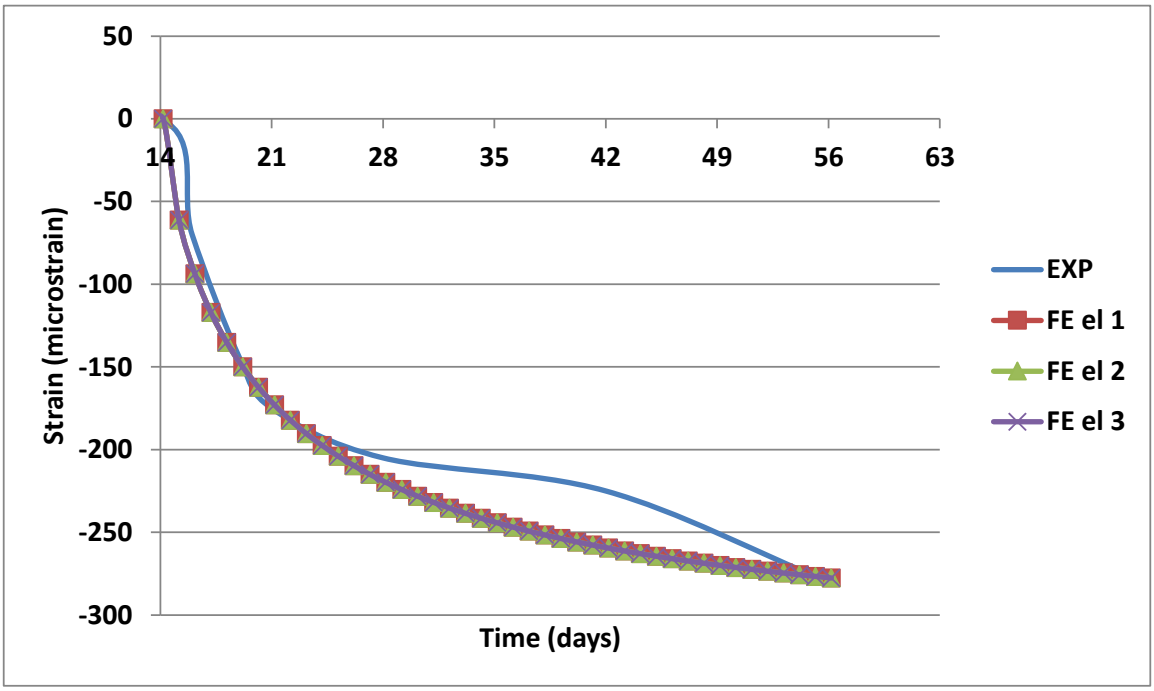

Figure 31: Comparison of experimental free shrinkage and FE results of prism

The results showed that the model adequately simulates the shrinkage behavior of the prism under unrestrained conditions. The average error between the free shrinkage

measurement and the finite element output is about 9%. This error is the same as that between the adapted CEB and the true free shrinkage. Therefore the model produces the same results as the input. This is reasonable as the sample is free to shrink and therefore no significant reduction in shrinkage is expected. Furthermore, this indicates that during this analysis, the model introduces no additional error. A more refined model was built using C3D8 solid elements as shown in the figure below.

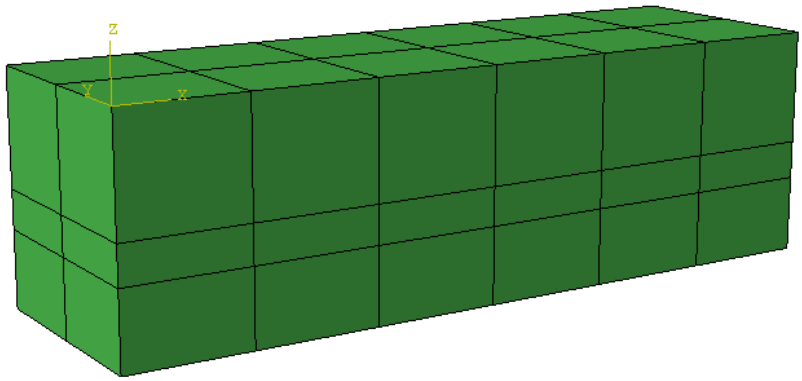

Figure 32: FE solid model of concrete prism

The shrinkage of the model was uniform and also correlated well with the input data as shown in the figure below. There was no observed mesh sensitivity in the results of the refined model.

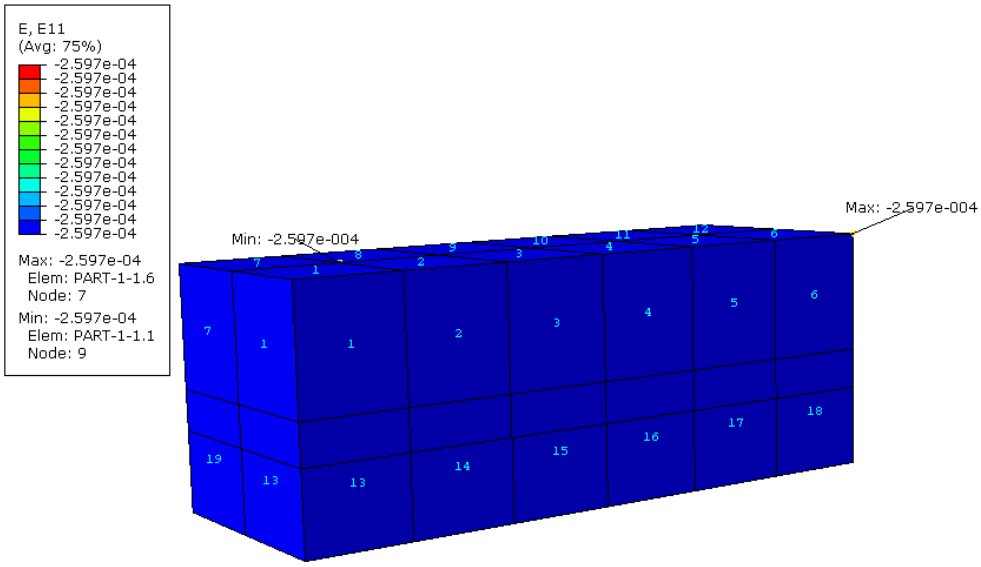

Figure 33: Longitudinal strain in FE solid model of concrete prism

The performance of the model was considered acceptable in capturing the shrinkage behavior of the prism and the modelling of other laboratory setups was continued.

5.2.2. Experiment 2 results

In the second setup described in the laboratory experiment section, reinforcement was added to test the response of the model when restraint of this nature was applied as discussed in the laboratory setup. A more refined model of the free shrinkage prism was built using C3D8 brick elements. The reinforcement was modeled as a rebar layer within a surface element. The surface element was then embedded into the solid element. The FE model is shown in the figure below.

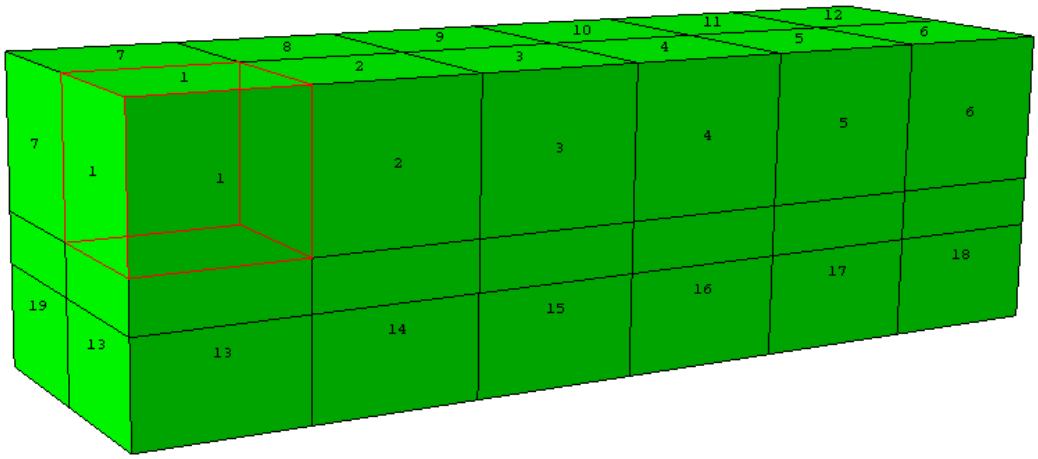

Figure 34: FE model of shrinkage prism using brick elements

The measured free shrinkage results of the concrete prism with embedded reinforcement as well as a control sample with no rebar are shown in the figure below.

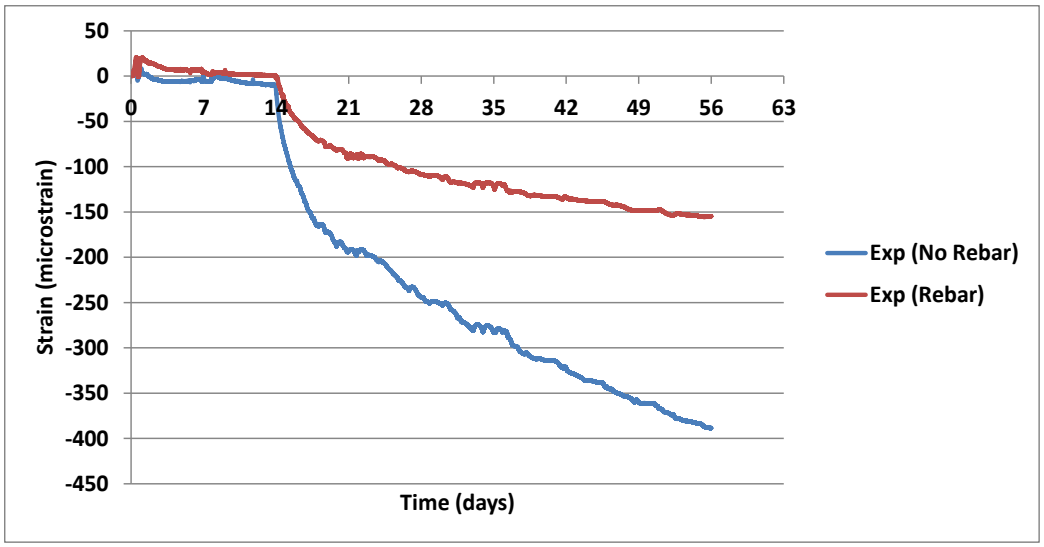

Figure 35: Shrinkage of prism with reinforcement restraint and control prism

The samples were initially cured for 14 days using wet burlap. It was observed that no shrinkage occurred during this period. Less strain was recorded in the sample with reinforcement than the sample without reinforcement as the reinforcement introduces restraint to the movement of the sample. Furthermore, as done previously, the input for the FE model was derived by adapting a prediction model to the measured data from the sample without reinforcement. This data was then applied to the FE model with reinforcement. A shrinkage analysis was performed and the comparison between the measured data from the sample with rebar and the FE model output is shown in the figure below.

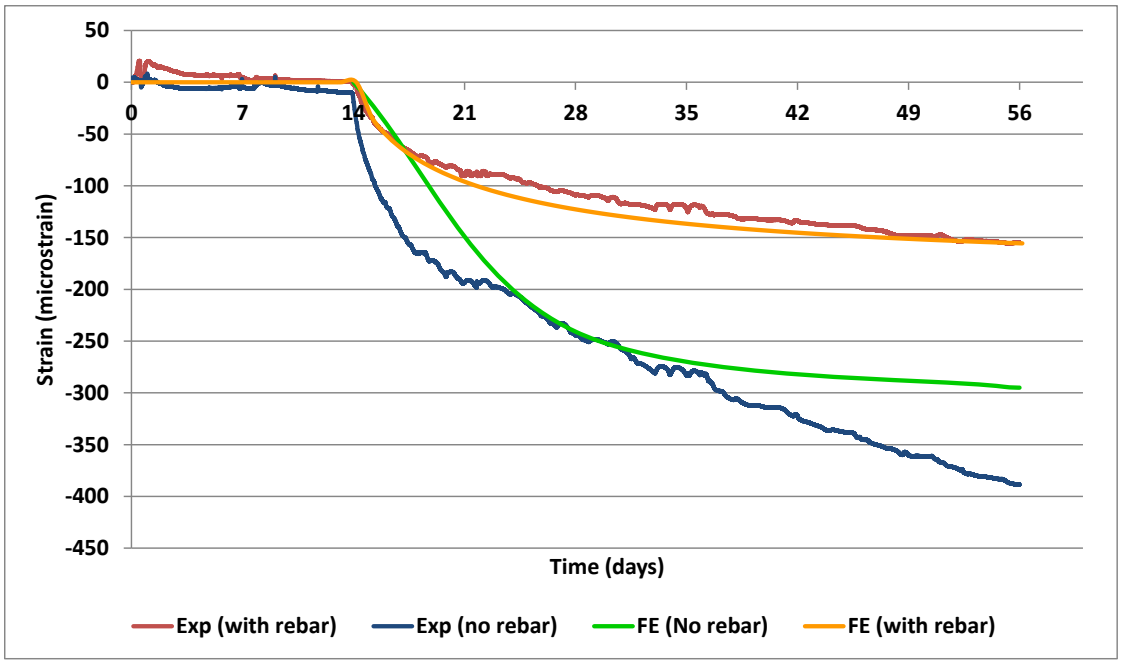

Figure 36: Comparison of experimental and FE results of prism with reinforcement

It was observed that the initial measured strain results and the shrinkage input used in the FE model did not match completely. However, the result showed a close agreement between the measured data and the FE model. This indicates that the model is capable of accounting for the presence of reinforcement in the concrete sample as is the case in full scale bridge decks. Other data were checked to verify the accuracy of the model. Since the section was uncracked, strain compatibility was expected between the concrete and the reinforcement. The strain results at the level of the reinforcement were extracted and compared in the table below.

Table 8: Strain compatibility in FE model of concrete prism

$\varepsilon_{concrete}$	ε_{rebar}
-0.000159	-0.000157

The strain in the concrete at the level of the rebar and the strain in the rebar show close agreement which indicates that there was strain compatibility in the model.

Furthermore, the stress in the concrete was observed as shown in the figure below.

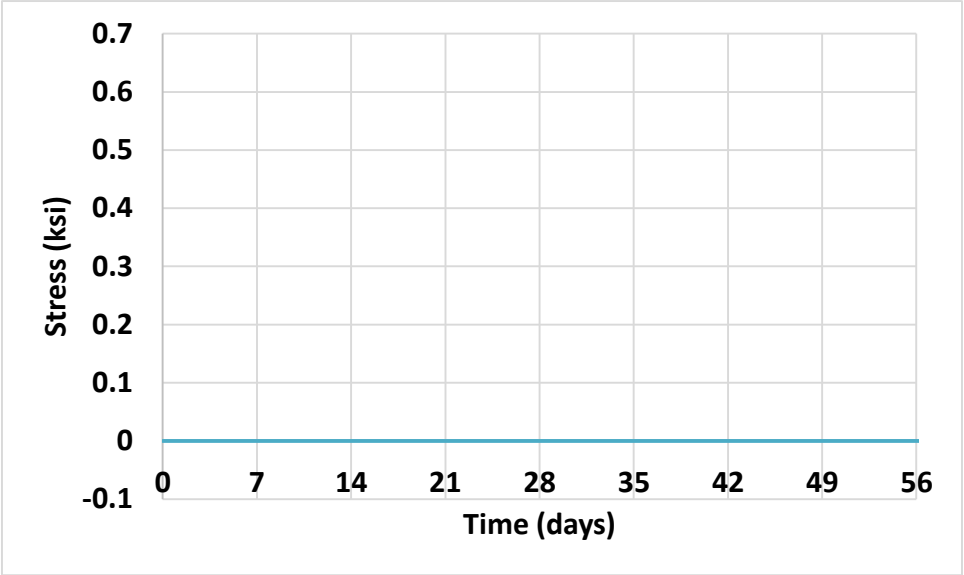

The stress in the concrete was approximately zero which is in agreement with a concrete sample with little or no restraint. The analysis model was modified to include boundary restraints as shown in the figure below.

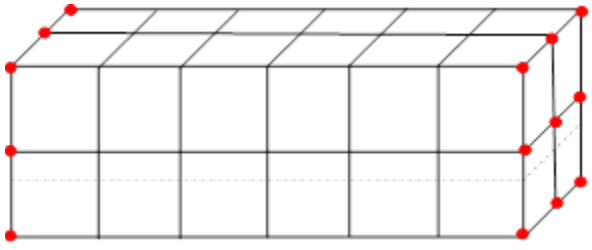

Figure 37: Restraint applied to FE concrete prism model

Although no experiment was performed to simulate this case, useful observations were made from the results as shown in the figure below.

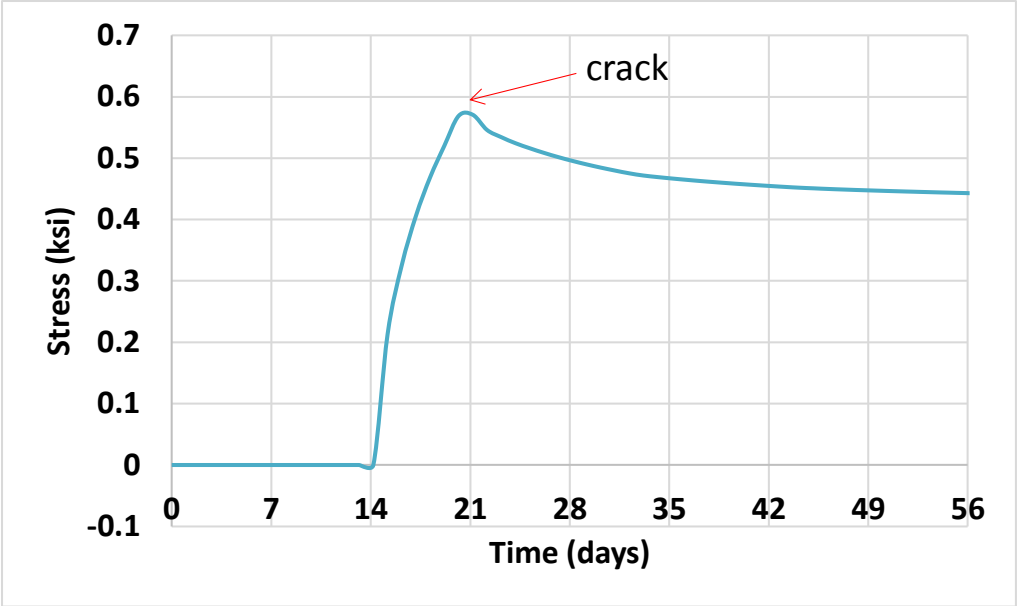

The concrete was modeled to include inelastic behavior and had a strength of 5 ksi. The tensile strength used in the FE model was approximately 0.55 ksi. The stress in the concrete increases steadily and then the concrete fails. A kink was observed in the plot above at approximately .57 ksi indicating a crack in the concrete prism. This agrees with the known tensile capacity of the concrete indicating that the model correctly simulates the cracking behavior of the concrete.

The behavior of the model was considered acceptable and the analysis was continued.

5.2.3. Experiment 3 results

Furthermore, free shrinkage samples were cast and stored under varying temperature conditions controlled by a heat blanket as discussed in experiment three of the laboratory setup section. This was done to study the effect of fluctuating environmental conditions as commonly observed in the field and to develop a method by which temperature data could be separated from strain data in samples collected under these conditions. The temperature under the heat blanket was regulated to 31°C for a period of 8 hours and reduced to 17°C for a period of 16 hours intermittently. The results are shown and discussed below.

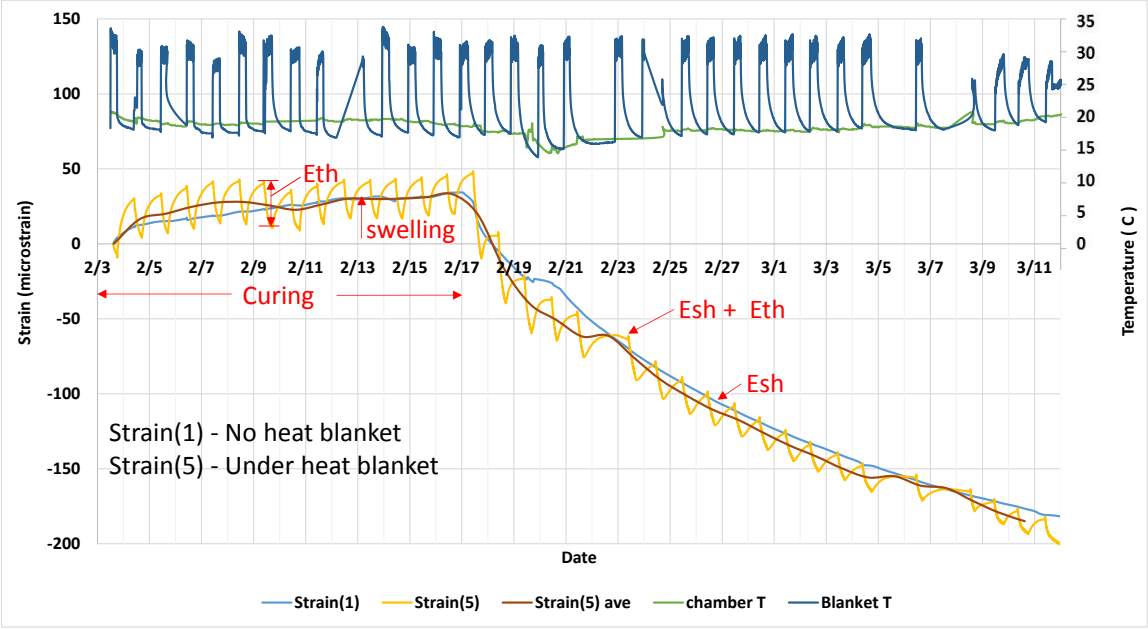

Figure 38: Results of experimental setup 3

Strain(1) represents the sample which was stored in an environmental chamber while strain(5) represents the sample which was stored under a heat blanket with daily temperature variation. The result gotten from the strain(1) sample shows a smooth and

gradually increasing curve which indicates pure shrinkage. However, the result gotten from the strain(5) sample shows a gradually increasing strain curve with daily fluctuations. This indicates a combination of shrinkage and temperature strain due to the change in temperature between day and night.

To isolate the shrinkage effect in strain(5), the average of the daily high and low strain readings were taken. The results of this is shown in the plot above as strain(5) ave. From the plot, it was observed that strain(1) and strain(5) ave show close agreement. This indicates that if the average temperature of a sample stored under fluctuating temperature conditions is equal to the temperature of a sample stored under constant temperature conditions, the average of the strain of the sample under fluctuating conditions should equal the strain of the sample stored under constant conditions. It is noted that in this case the weighted average temperature of the fluctuating sample is 22°C while the temperature of the sample stored under constant conditions is 18°C. Hence, the average curve for strain(5) differs slightly from strain(1). This difference in shrinkage under different average temperatures also appears to be due to the difference in the average temperature. The daily change in shrinkage due to the change in temperature was used to estimate the coefficient of thermal expansion for the sample. This value was found to be between 1.8 to 2.2 °C/microstrain. This value approximately equals the difference between the coefficient of thermal expansion of the steel gage and the concrete which are 12.2 and 10 °C/microstrain respectively. Because the concrete prism is free to move, only the difference between the response of the concrete and the response of the steel to temperature changes was recorded by the strain gage. This effect was discussed in greater detail in the literature review section. When this value is multiplied by the difference in

the average temperatures which was 3°C, a difference in strain of 5 to 7 microstrains is expected between the 2 lines. The results in figure 6 above indicate this to be the case as the average difference between the two curves is approximately 7 microstrains.

This was also confirmed using the finite element model. The strain(5) curve was derived by combining the known applied thermal load and the measured isolated shrinkage data. The figure below shows the thermal strain from the finite element model based on the applied fluctuating temperature.

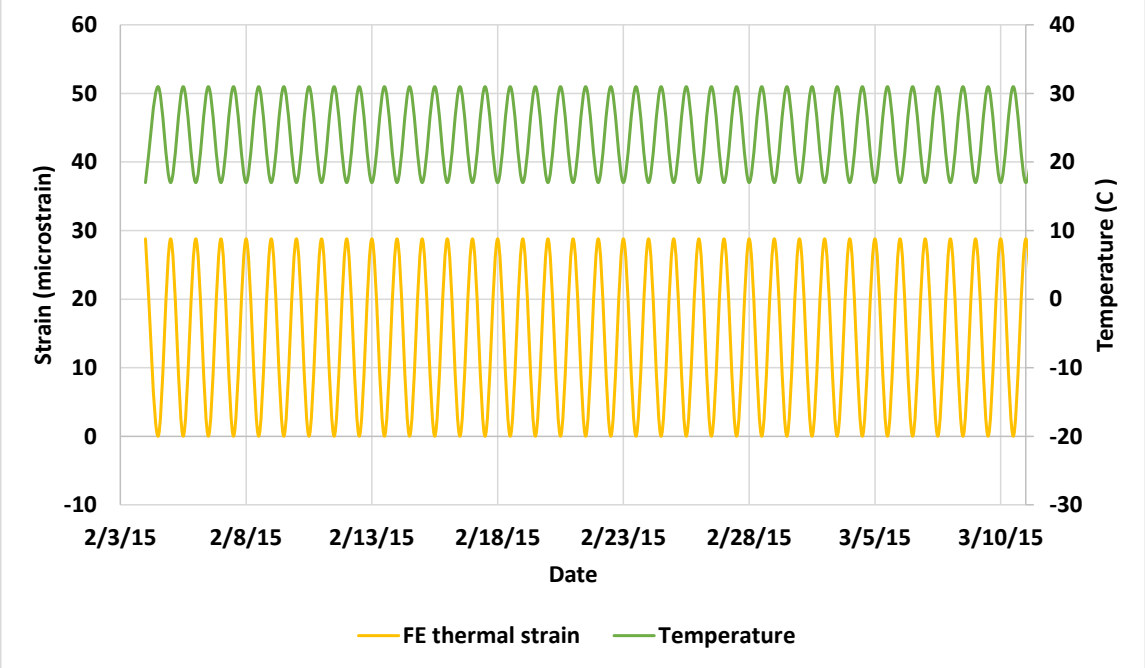

Figure 39: FE result of thermal strain

The thermal strain due to the increase in temperature was found to be 28.8 microstrains. This was close to the thermal strain gotten by subtracting the daily minimum strain from the daily maximum strain which was found to range from 22 to 26 microstrains. The

shrinkage strain was then derived by subtracting the calculated thermal strain from the measured strain (5). The plot below shows the result of the shrinkage isolation.

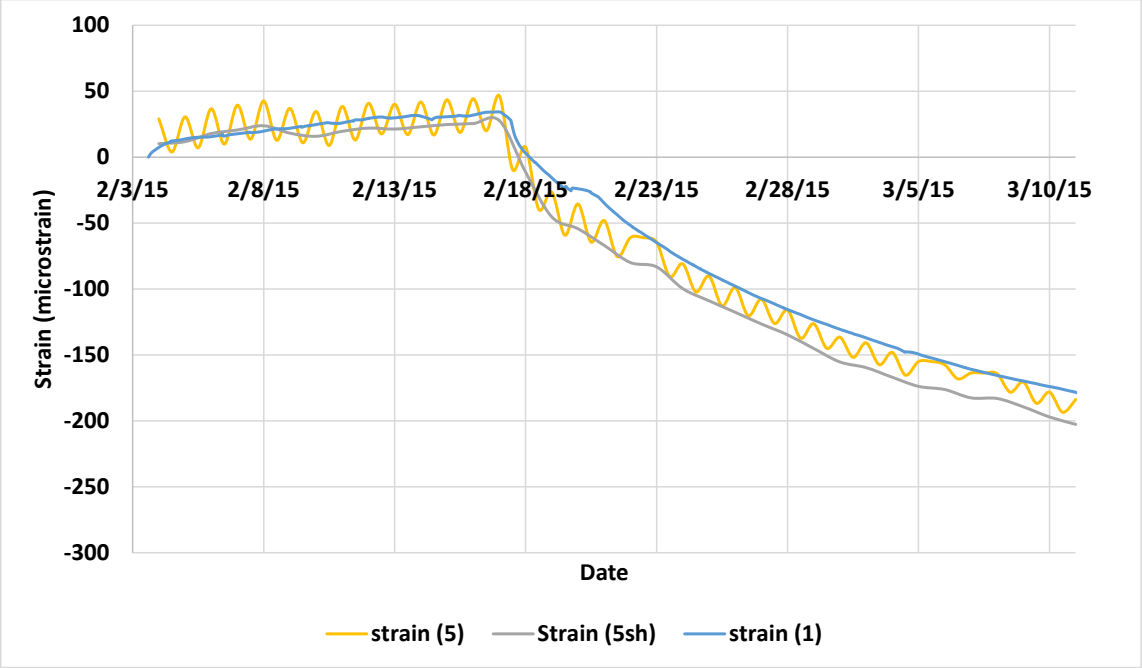

Figure 40: Strain isolation using FE results

Strain (5sh) is the isolated shrinkage curve derived by subtracting the FE results directly from strain (5). The coefficient of thermal expansion was calculated at several points and it was observed that this value increased over time. However, only one value of thermal coefficient was used in the finite element model for the duration of the analysis. Hence, it was observed that the results produced a closer match during the early periods than towards the end. The method of taking daily averages proves viable as an approximate method in removing the temperature effect.

The results of laboratory experiment three were also used to investigate the effect of size. As discussed in the laboratory setup section, two different sample sizes were cast during

the experimental setup. One prism measured 3 in x 3 in x 10 in and is labeled as strain(1) in the figure below while the other measured 6 in x 6 in x 20 in and is labeled as strain(3). The free shrinkage results under constant conditions are shown in the figure below.

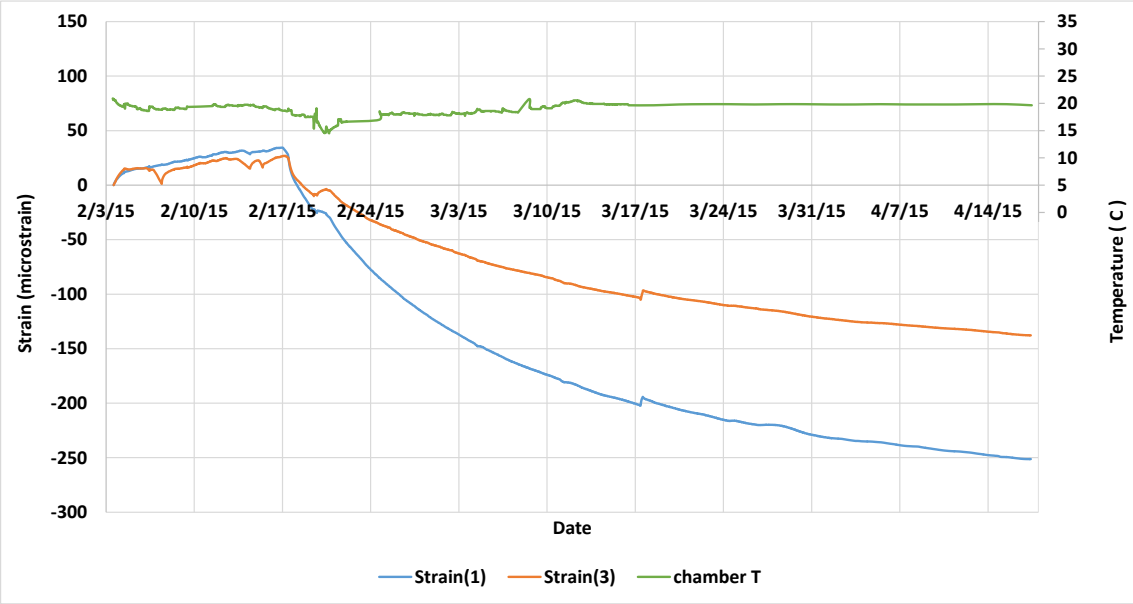

Figure 41: Laboratory setup 3 showing size effect

From Figure 41, it was observed that the shrinkage of the strain(1) sample was greater than the shrinkage of strain(3) for the time period shown. This indicates that larger samples undergo a reduced shrinkage. Furthermore, based on this observation alone, it appears that the ultimate shrinkage of the larger sample would be less than that of the smaller sample provided that the rate of shrinkage of the two samples remain the same over the measured period of time or if the rates of shrinkage slowed down at the same pace. The rates of shrinkage of the samples were therefore plotted to further determine the behavior of shrinkage of the samples as shown in Figure 42 below.

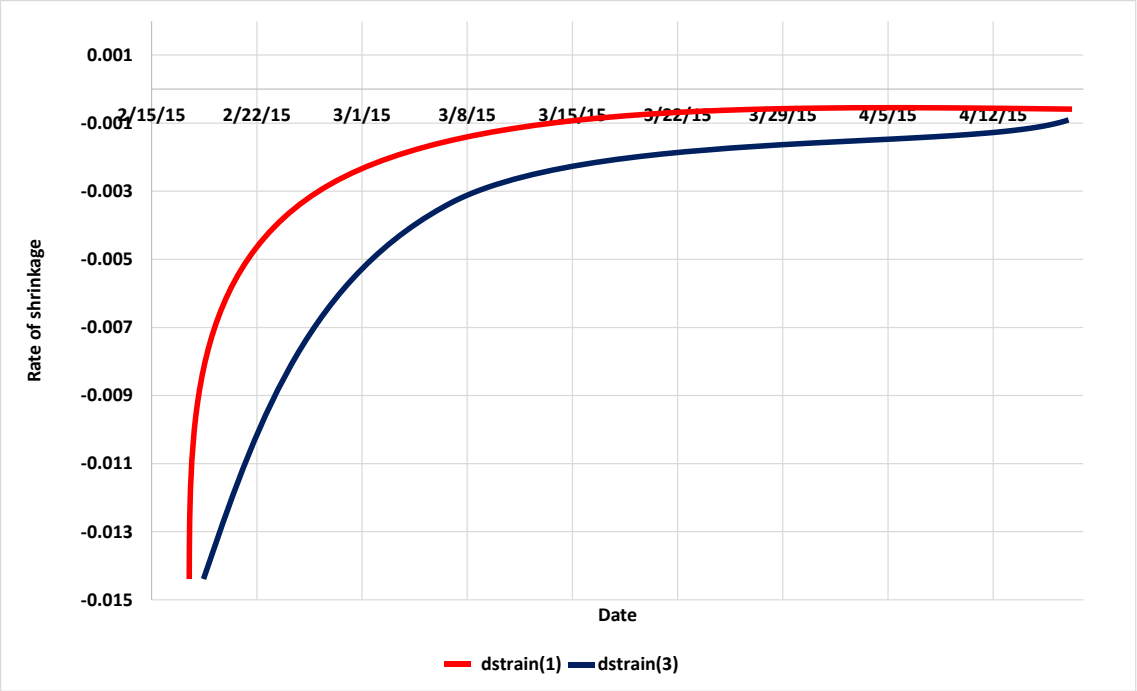

Figure 42: Laboratory 3 setup results showing rate of shrinkage

The rate of shrinkage for the smaller sample slows down quicker than the rate of shrinkage for the larger sample. Therefore although the smaller sample has a larger overall shrinkage, the increase in shrinkage slows while the larger sample continues to increase. This behavior of the rate of shrinkage indicates that the two samples may approach the same value while taking different time frames to do so. In this study, the ultimate shrinkage of a concrete sample was taken to be the same independent of sample size in agreement with the CEB recommendation. Consequently, the ultimate shrinkage derived for smaller samples was used to predict drying shrinkage of larger samples.

The efficacy of this method was analyzed. The figure below shows the results of the use of volume to surface ratio in the CEB model to adapt the shrinkage from a small sample to a larger sample using the results of the experimental data from experiment 3.

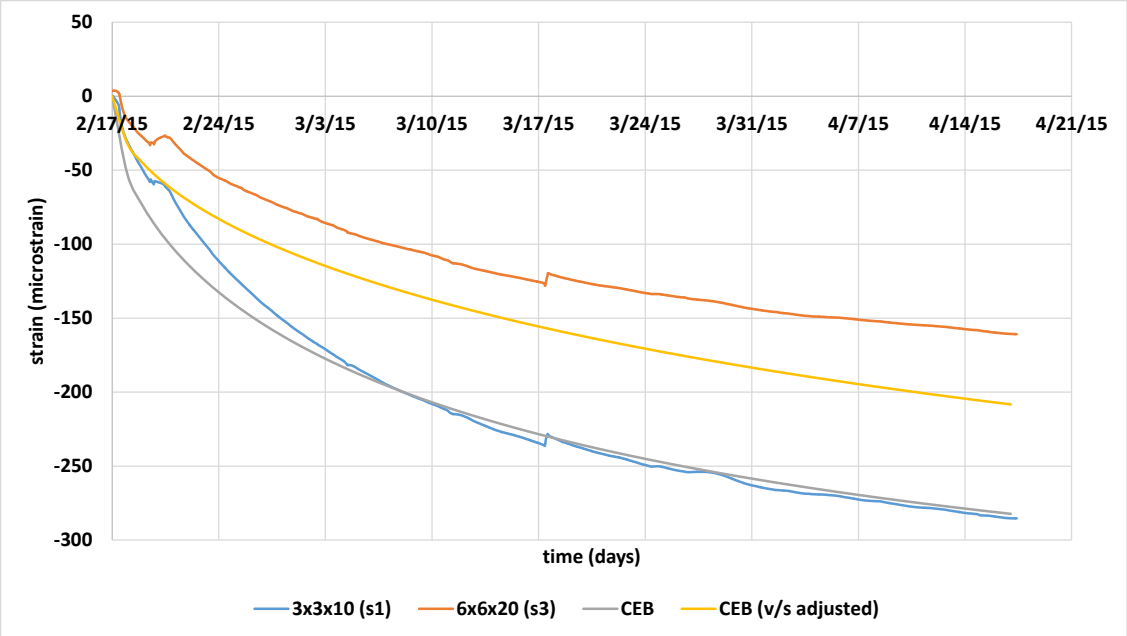

Figure 43: Adaptation of small sample shrinkage to larger sample

The CEB model was fit to the results gotten from the small sample as shown in the figure above. The value of the ultimate shrinkage was taken to be 390 microstrains to match the experimental results. Afterwards, while maintaining the same ultimate shrinkage, the volume to surface ratio (v/s) of the sample was changed to reflect that of the larger sample and the CEB (v/s adjusted) curve was derived and plotted. This was then compared to the measured result from the 6 x 6 x 20(s3) sample. The comparison indicates that the use of the v/s ratio correctly reflects a reduction in shrinkage due to an increase in sample size, even with the same ultimate shrinkage. However, the parameter did not produce a reduction commensurate to the measured result from the large sample. Additional samples were taken from a paper by Bryant and Vadhanavikkit (1987) to further investigate the use of v/s ratio for the adaptation of shrinkage to different sample sizes.

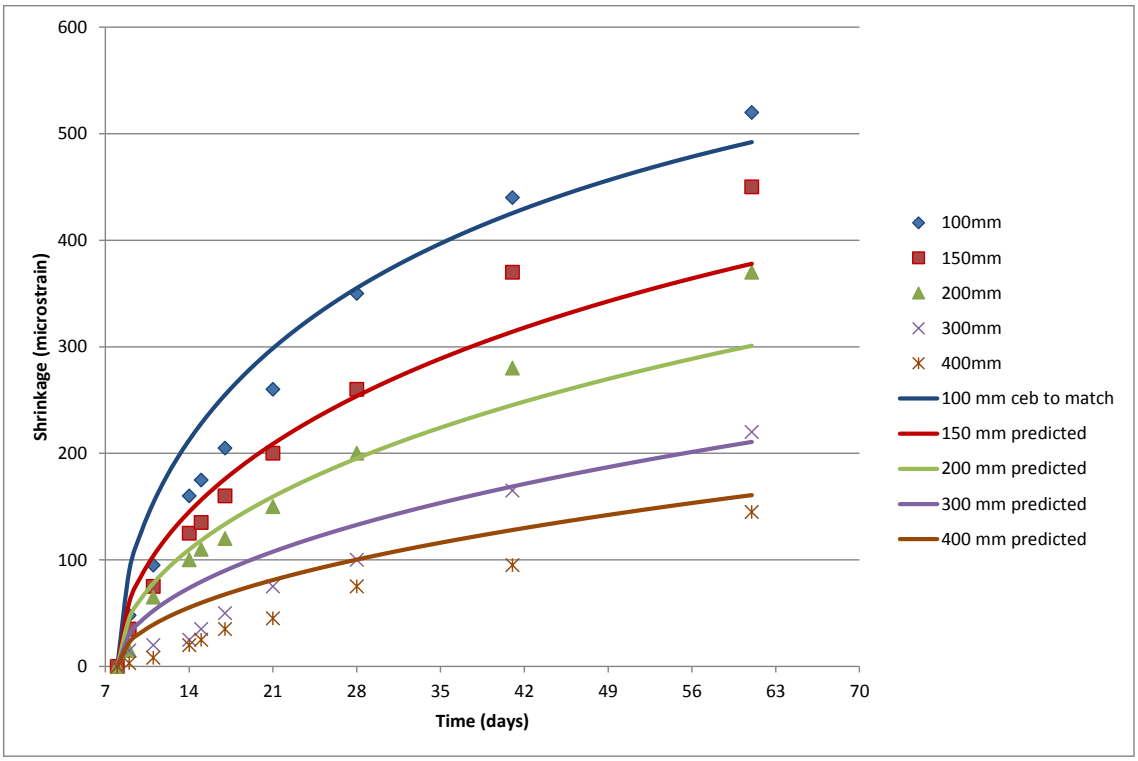

Figure 44: Investigation of volume to surface ratio

It was found that the adjustment using v/s ratio produced a closer comparison between the prediction and the measured data as the value of shrinkage increased, generally after 28 days than during the days prior. The average error for all the prediction curves after the initial 28 day period was 3%. However, it was noted that the error increased with increase in size. The data was adjusted from a sample with a thickness of 3.9 inches (100mm) up to a sample with a thickness of 15.7 in (400 mm). The typical thickness of a bridge deck is between 7 and 9 inches (200 mm), and the error in this case was found to be 11%. It was noted that some variability in the accuracy of the use of v/s ratio to extrapolate shrinkage data from small samples to larger samples exists.

The results of this experimental setup were used to study the effect of changing temperature conditions on the behavior of shrinkage in small samples. The results

indicated that taking the average of the maximum and minimum data points approximately removed the temperature effect relative to the sample taken under constant conditions, provided that the average temperature of the two samples were equal. Otherwise, the difference in the average temperature of the two samples must also be accounted for and removed by calculating the thermal strain due to the difference in the average temperatures and adjusting the data accordingly. Furthermore, the results were used to study the effect of varying sizes on the shrinkage of the small samples. It was observed that the smaller samples exhibited a higher shrinkage than the larger samples. However, the rate of shrinkage of the larger samples reduced slower than that of the smaller sample. Hence the ultimate shrinkage for the two samples was assumed to be approximately equal and the size effect was accounted for on the rate of shrinkage only.

5.2.4. Experiment 4 results

Finally, free shrinkage samples were cast and stored under external environmental conditions as discussed in experiment four of the laboratory setup section. Reinforcement bars were also embedded in half of the samples. Control samples were stored in an environmental chamber to facilitate comparison. In this setup, the effect of ambient conditions and reinforcement were combined to create conditions representative of field conditions. The results are shown and discussed below.

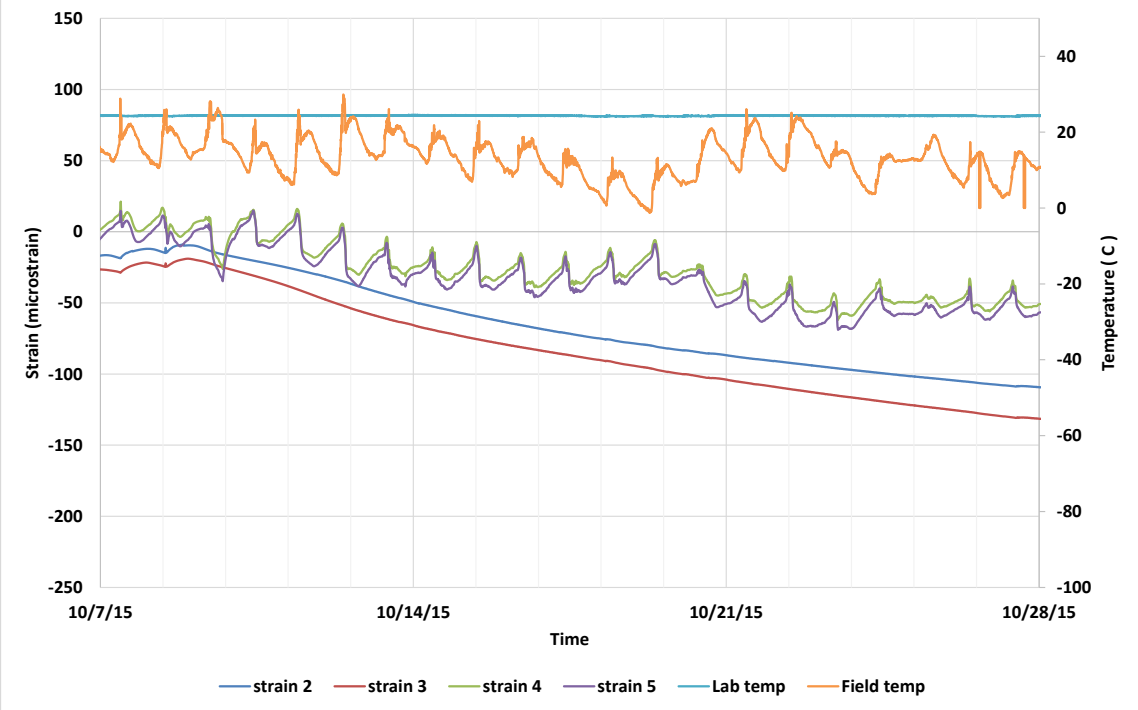

Figure 45: Results of experimental setup 4

The data was plotted from the period after the initial 14 days of curing during which shrinkage was minimal. Strain 2 and strain 3 are readings derived from samples stored under constant conditions in the environmental chamber. This can be observed in the plot above as the readings are steady which indicate that there is no daily temperature

fluctuation. Furthermore, strain 2 is derived from the sample containing embedded reinforcement while strain 3 is derived from a sample without reinforcement. The reading from strain 2 shows a reduced shrinkage compared to the reading from strain 3 due to the restraint introduced by the embedded reinforcement. This reconfirms the results from laboratory setup 2 whereby reinforcement was embedded into the free shrinkage samples and reduced values were measured. Furthermore, it was shown that the FE model was capable of accounting for a reduction in shrinkage due to the addition of reinforcement.

Strain 4 and strain 5 are readings derived from samples stored outdoors under external environmental conditions. This was observed in the plot above as the readings from these samples showed daily fluctuations indicative of temperature changes. Strain 4 was derived from a sample with embedded reinforcement while strain 5 was derived from a sample without reinforcement. Consequently, the readings from strain 4 were slightly less than strain 5 due to the restrain introduced by the reinforcement. It was observed that the reduction in strain due to the addition of reinforcement was more pronounced in the samples stored under constant conditions (strain 2 and 3) than in the samples exposed to ambient conditions (strain 4 and 5). It could be that the combination of environmental effects makes the addition of reinforcement less effective as the embedded rebar also responds to the changes in temperature and expands and contracts along with the concrete, thereby providing less resistance.

The temperatures under which the samples were stored are also shown in the figure above. The environmental chamber was kept at a constant temperature of 25°C while the external temperature ranged between 0°C and 32°C. The average external temperature over the measured time period was 13.3°C however, the variability during this period was

large. The procedure presented earlier for the removal of the temperature effect in the section on experiment three was once again applied to the results and is shown in the figure below.

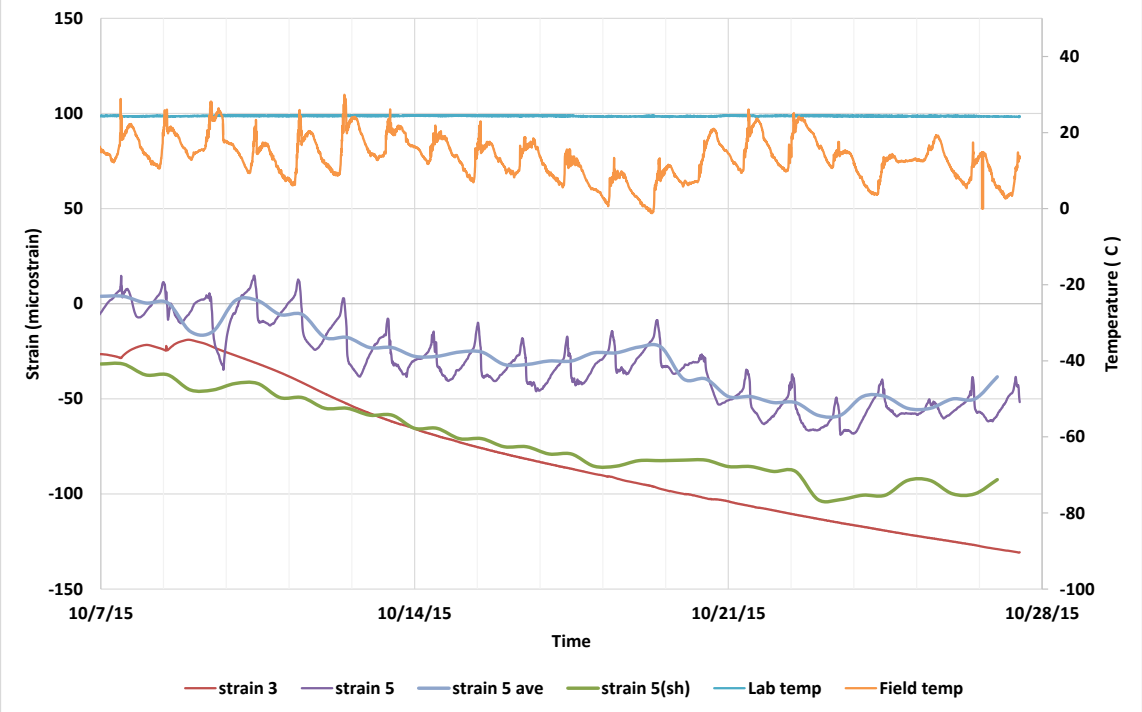

As discussed previously, the daily temperature fluctuation was first removed by taking the average of the daily maximum and minimum strain readings. This produced the curve labeled strain 5 ave. Moreover, the average temperature for each day still differed from the temperature at which the control samples were stored. This difference was observed in the plot as the strain 5 ave curve still differed significantly from the strain 3 curve. Therefore the average curve needed to be adjusted for this difference in average temperatures. The thermal strain due to the difference in temperature between the lab samples and the daily average temperature of the samples stored outdoors was derived and is shown in the figure below.

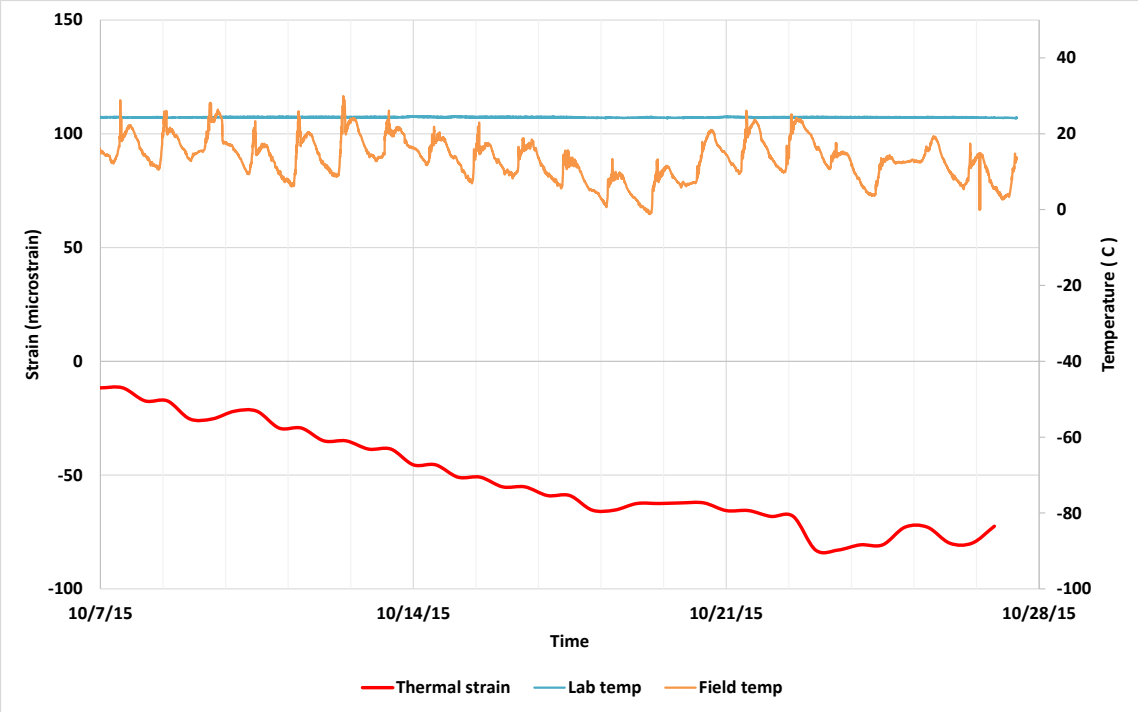

Figure 46: Thermal strain due to temperature difference in experiment 4

The coefficient of thermal expansion was taken as 2 °C/microstrain as the difference between the concrete and steel coefficients of thermal expansion. This thermal strain was then subtracted from the strain 5 ave curve to produce the strain 5(sh). Strain 5(sh) is the final result gotten after the temperature removal procedure was performed. The strain 5(sh) curve closely matches the result of the control sample stored under constant conditions.

The findings from the laboratory setup using small free shrinkage prisms were considered satisfactory. The procedure was transferred to a larger sample and is discussed in the following sections.

5.3. Laboratory slab experiment

As discussed in the laboratory setup section, data from experimental testing performed on a larger sample as documented by Frosch et. al (2006) in a controlled laboratory environment was collected. The sample was a scaled section of a bridge deck. This section discusses the results of the FE analysis of the sample.

The FE model was built using C3D8 brick elements for the slab. The slab was divided into three layers to derive more refined results. The girders were modeled using B32 beam elements. Connections were made using beam type Multi Point Constraints (MPC) to simulate full composite behavior between the concrete slab and steel beams. Reinforcement was applied as rebar layers within embedded surface elements. Since the slab contained four layers of reinforcement, four layers of embedded surfaces were included in the model to represent each reinforcement layer. The FE model is shown in Figure 47.

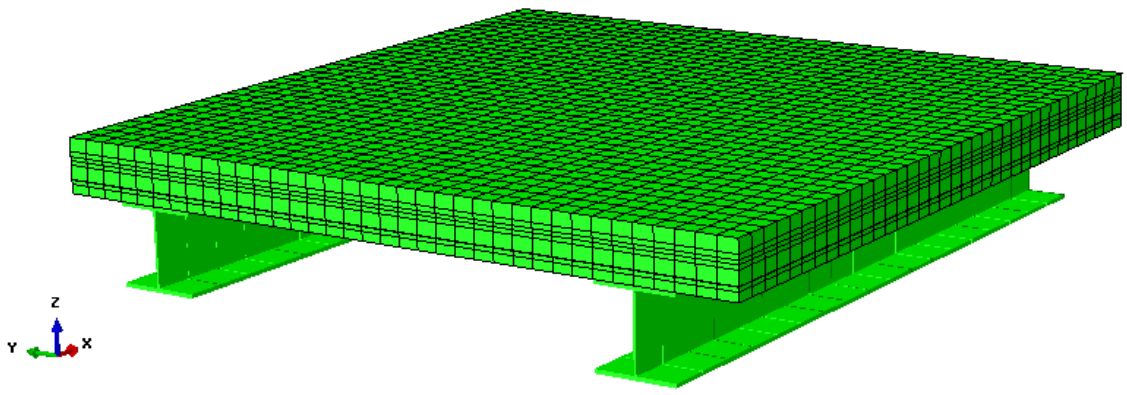

Figure 47: Finite element model of laboratory slab

The analysis was ran for a period of 21 days. However, the specimen was cured for four days, during which the shrinkage was taken to be zero as observed in the small free

shrinkage samples. The slab had a pin-roller boundary condition for the girders. The locations at which results were compared are shown in the figure below.

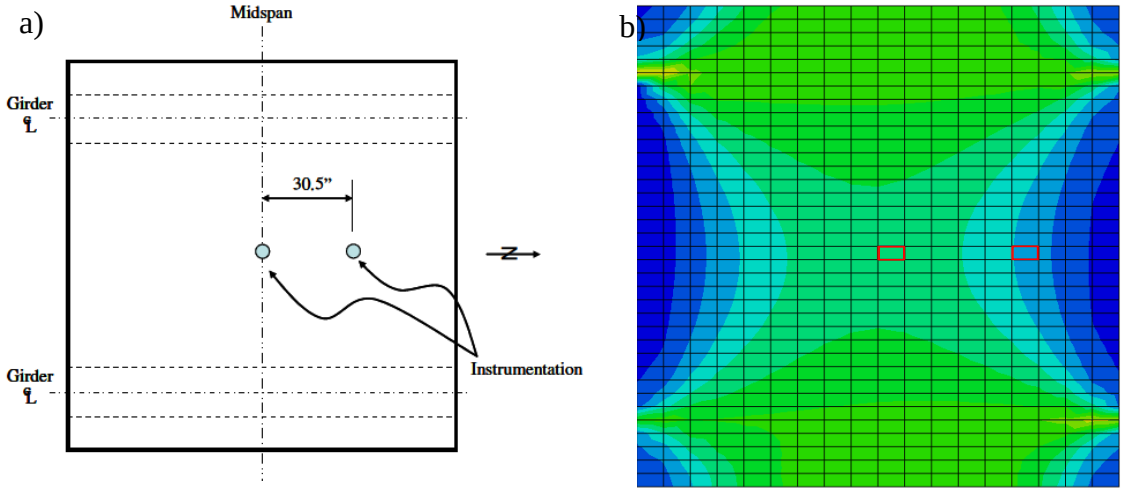

Figure 48: Corresponding sensor locations on a) experimental slab (Frosch, 2006) and b) FE model

There were a total of three functioning sensors in the slab. One sensor was installed in the center of the slab on the bottom rebar. The other two sensors were installed at 30.5 in north from the center as indicated in the Figure 48a above on the left, with one on the top rebar and another on the bottom rebar. The top reinforcement was a distance of 2.5 in from the top of the slab while the bottom reinforcement was a distance of 1 in from the bottom of the slab. The measured reinforcement strain results were compared to those from the finite element model and are shown in the charts below for each of the three measured locations.

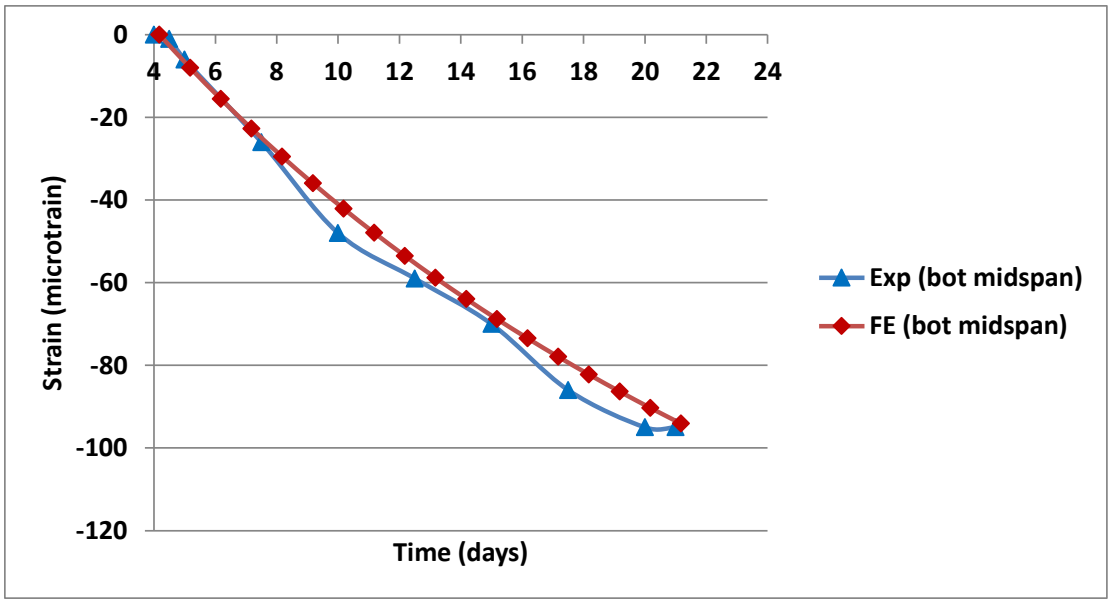

Figure 49: Comparison of experimental and FE results at bottom midspan

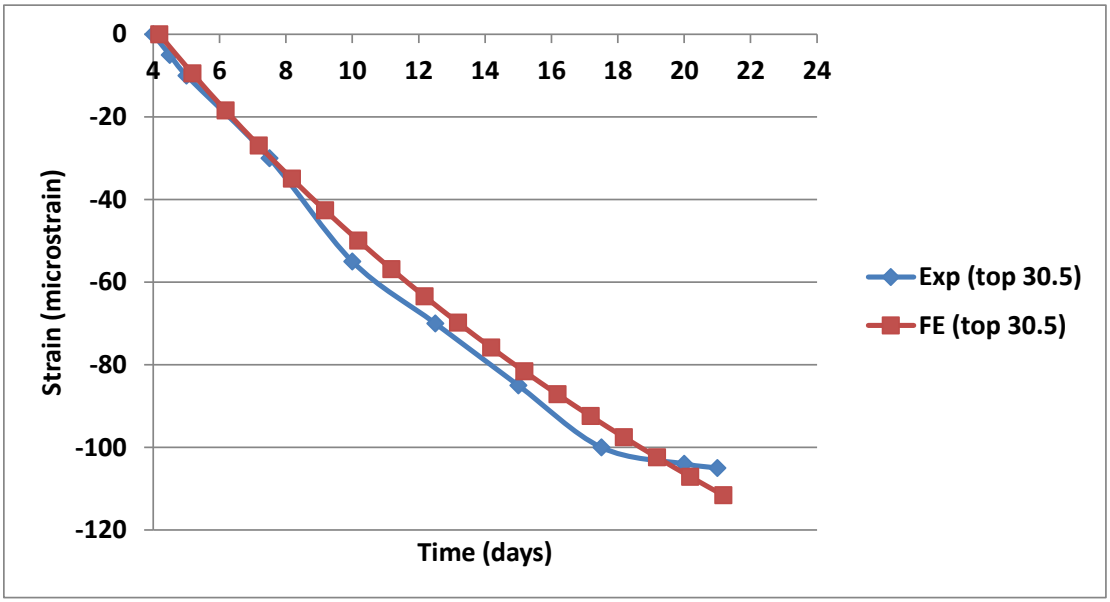

Figure 50: Comparison of experimental and FE results at top 30.5 in

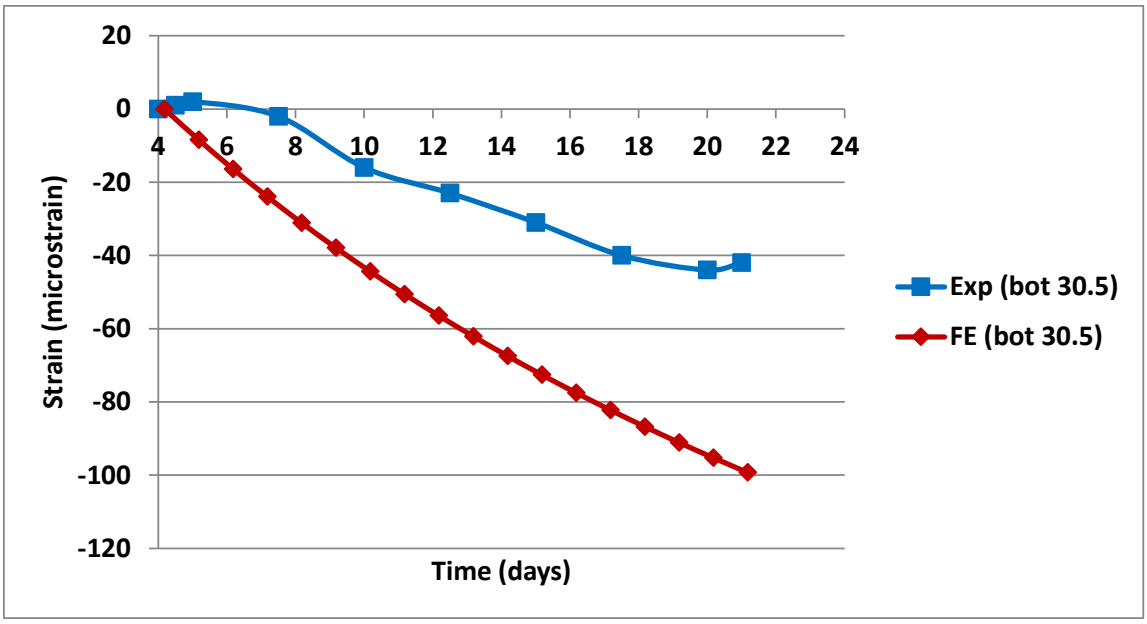

Figure 51: Comparison of experimental and FE results at bottom 30.5 in

The results for the locations at the bottom sensor at midspan and the top sensor at 30.5 in give reasonable results. The average error for each location respectively is 1% and 5.7%. However, it was observed that the result for the bottom location at 30.5 in did not agree as closely.

The above analysis was performed to verify the validity of the developed shrinkage model in a larger scale model which presented more challenges than the previously analyzed small scale model. The results showed that the shrinkage model produced similar behavior to the experimental results.

Although no results were measured in which the slab deck was restrained externally by elements such as abutments, a FE analyses was run with this case to observe the cracking behavior of the deck. The strain input in the model was increased to facilitate cracking as shown in the figure below.

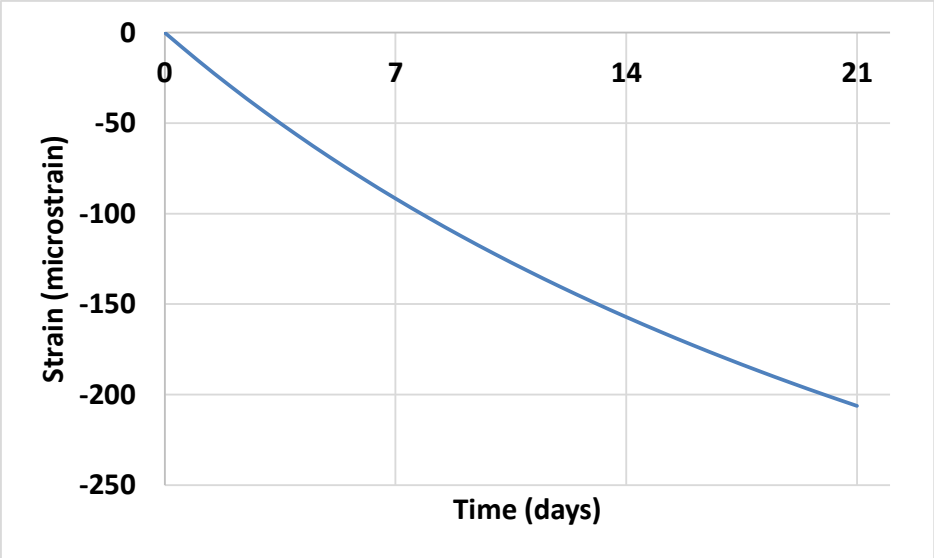

Figure 52: Strain input in laboratory slab specimen for cracking

The strain was increased to reach a value of 200 microstrains at about 20 days. The concrete strength was 5.8 ksi and the tensile strength was 0.531 ksi which was measured from a tensile splitting test performed on a small specimen of the concrete used. This value was gotten at 21 days and used as a conservative value for the 28 day tensile strength of the concrete. The modulus of elasticity was measured as 3550 ksi. Consequently, the cracking strain was calculated to be approximately 150 με. The boundary conditions on the slab specimen were modified in the model to prevent motion of the slab in the direction of the applied shrinkage. The results from the analysis are shown in the figure below.

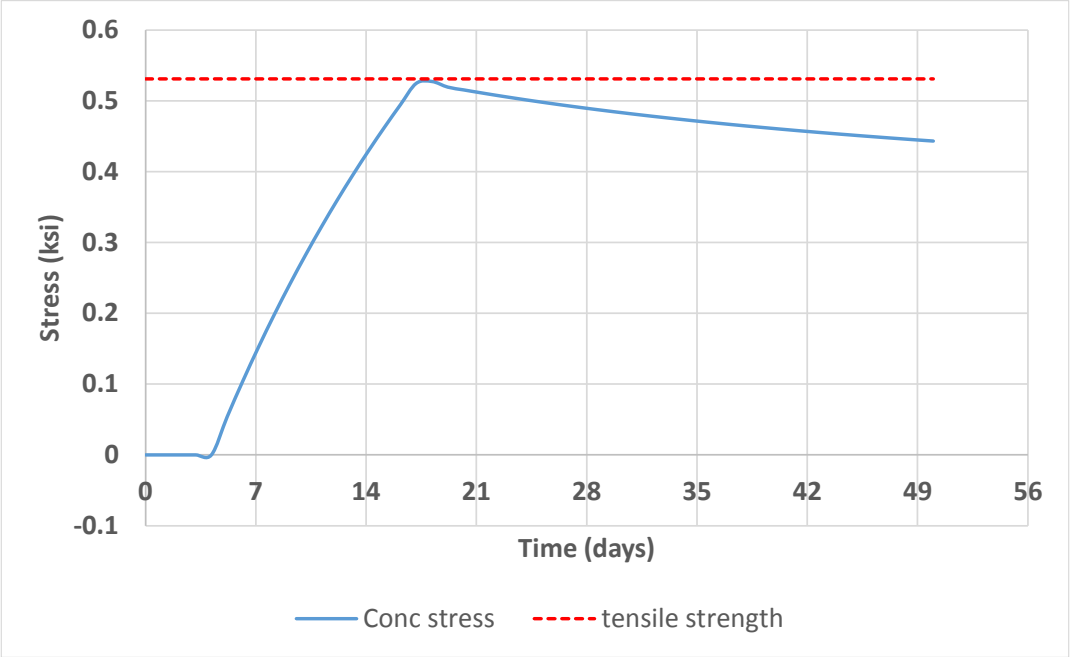

Figure 53: Strain output of restrained laboratory slab specimen

It was observed that the concrete cracked when the stress reached the maximum tensile capacity. This occurred after a period of 18 days when the applied strain was 155 microstrains. This value corresponds closely with the calculated cracking strain of 150 με.

The model was considered to be capable of simulating restrained behavior and the analyses was transferred to the full scale models bridge model sunder field conditions.

5.4. Bridge database

This section discusses the results of the FE analysis of the bridges in the database discussed in the section titled field setup.

5.4.1. Patcong Creek Bridge

A FE model of the Patcong Creek Bridge was developed to perform a shrinkage analysis using the free shrinkage data measured from a standard free shrinkage mold. The process of adapting the data measured from a small sample for use in this larger sample is detailed in this section. Consequently, a comparison is made between the experimentally measured data and the results of the FE analysis. The finite element models for the segments of the bridge are shown below in Figure 54.

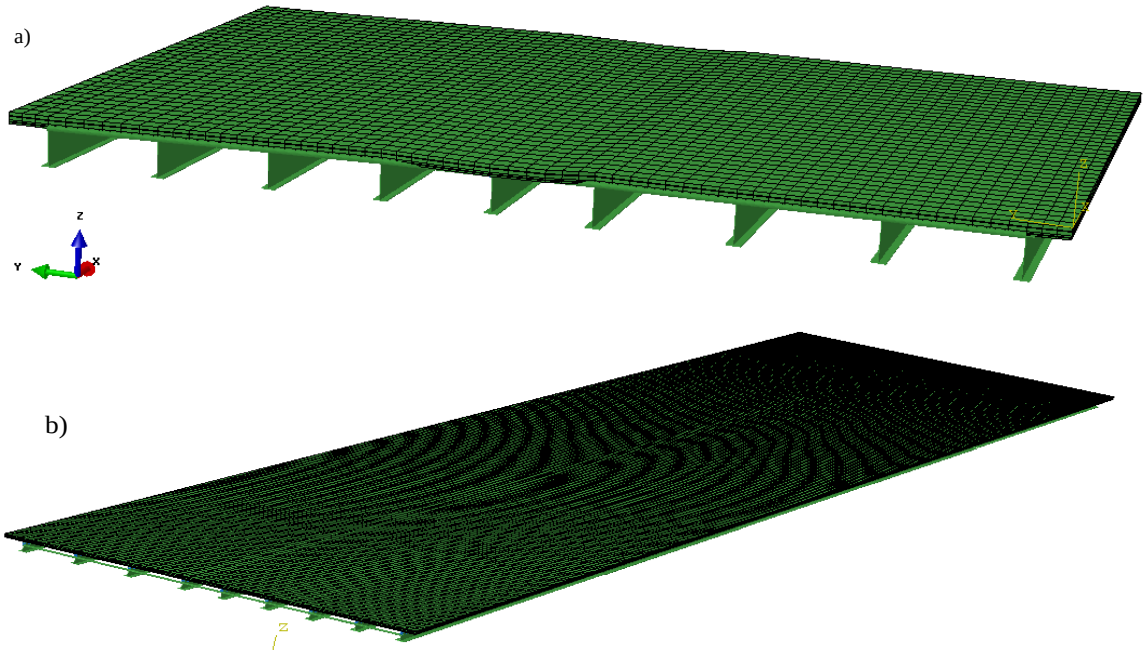

Figure 54: Finite element model of Patcong Creek Bridge (a) simply supported span (b) 3 span continuous

The model consists of solid C3D8 elements used for the concrete slab and B32 beam elements used for the girders. The slab is connected to the girder using beam type multi point constraints (MPC) which restrain the movement of the slab to the girders. Pin-roller boundary conditions are applied to the girders.

The input data to be used for the shrinkage analysis of the bridge was derived from smaller free shrinkage prism samples cast from the same batch of concrete. These samples were stored under constant temperature and pressure. These results were adapted for size and relative humidity before they were used in the FE analysis. This process is detailed in the sections following.

5.4.1.1. Free shrinkage data adaptation

The free shrinkage of a prism sample taken from the same concrete batch as a full scale bridge in the field was measured. The prism was cured for 14 days during which the sample swelled. Shrinkage was taken to begin at the end of curing. To adapt the CEB curve to the experimental measurements, a more accurate value for the ultimate shrinkage of the sample was derived from the experimental measurements. The CEB code suggests using a value of 480 microstrains if experimental data is unavailable, however, better results were achieved when the CEB equation was calibrated to measured data.

The ultimate shrinkage used in the shrinkage analysis was derived from the measured free shrinkage. This also eliminated the need for material correction factors since the shrinkage prism and the larger samples were gotten from the same batch and therefore had the same material composition. Hence, the material effects were the same and were already included in the experimental measurements.

The rate of shrinkage was plotted against the shrinkage as done by Hobbs and Mears (1971). Over time, the rate of shrinkage slowed down until it reached the point of ultimate shrinkage. Theoretically, at this point the rate of shrinkage was assumed to be zero.

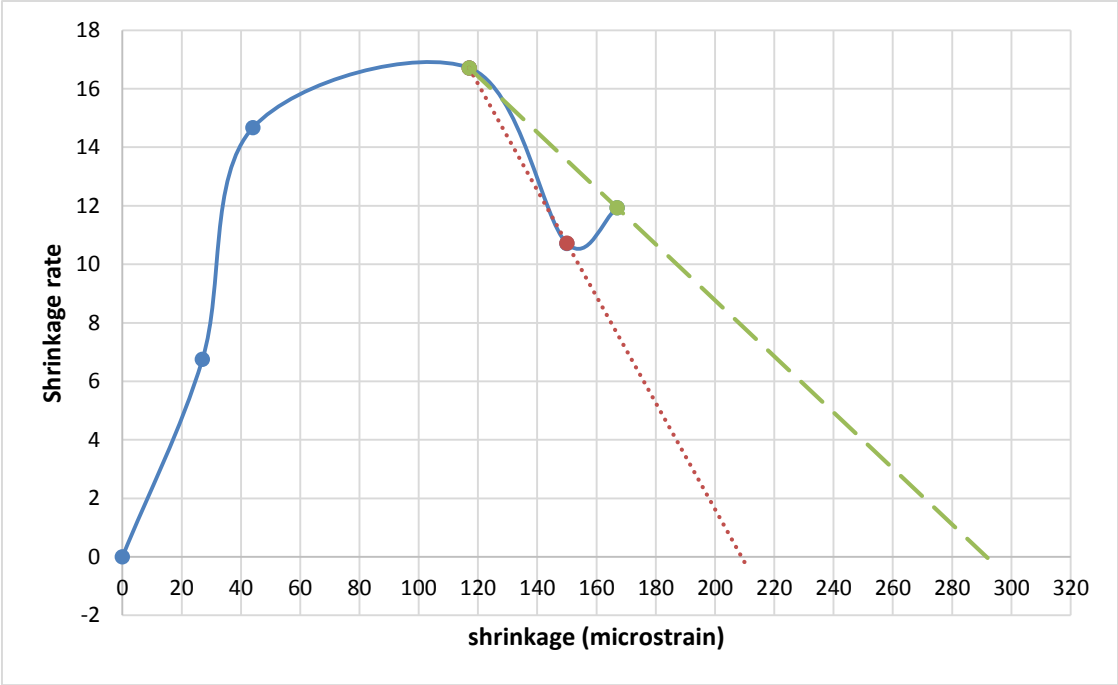

Figure 55: Derivation of ultimate shrinkage for PCB span 1

The linear portion of the curve is extrapolated to give the ultimate shrinkage. However, only 2 points were measured during which the period in which the rate of shrinkage began to decrease. These points give different trends for the ultimate shrinkage as shown in the figure above. An average value was taken between the two points and a value of 250 microstrains was used as the ultimate shrinkage for the sample. Using this derived value, the CEB prediction model was calibrated to the data for the collected sample. The original data and the CEB curve are shown in the figure below.

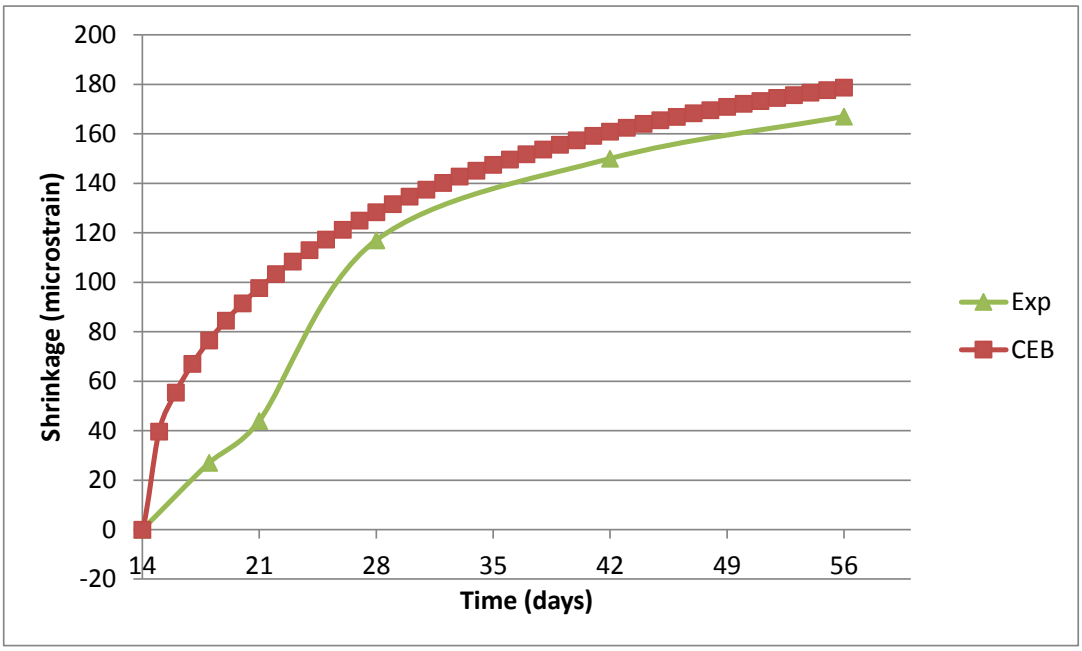

Figure 56: Free shrinkage and CEB calibration for PCB span 1

Afterwards, the effect of relative humidity was taken into account. Weather records for the applicable period were collected for the full scale bridge. It was observed from the plot that the ambient and sensor temperatures followed a seasonal trend.

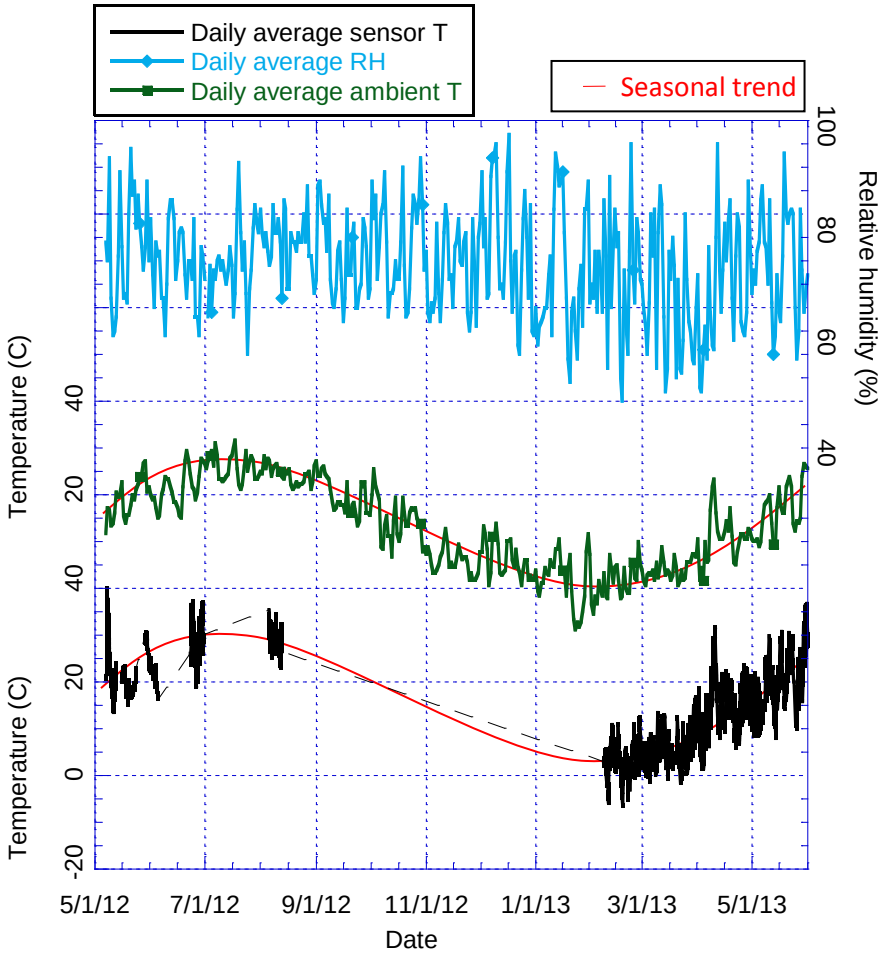

Figure 57: Temperature and relative humidity for Patcong Creek Bridge

Sensor temperatures did not differ significantly from one VWSG to another. Hence the average of all the sensor temperatures was plotted in the figure as the temperature inside the concrete. The daily average ambient temperature and relative humidity were also plotted in the figure. The sensor temperature closely followed the ambient temperature. The average sensor temperature was 23.8°C (74.8°F). The average sensor temperature over the six month period was less reliable due to multiple periods of data loss indicated by the broken line in the plot above. The average relative humidity was 71.1%.

The free shrinkage samples were stored at a relative humidity of 50% as mentioned previously. The data was then adjusted for relative humidity using multipliers specified by the CEB model. The CEB equation provides an adjustment to the predicted notional (ultimate) shrinkage based on relative humidity. The code considers the effect of relative humidity on shrinkage development with time to be negligible between 50 and 75%. Therefore, the effect of relative humidity on time development was disregarded since both the small sample and the full scale bridge fell within this range. The average relative humidity in the field was taken to be 70%. The relative humidity factor βrh was calculated at 50% and at 70%, and the difference was applied to the predicted free shrinkage strains. This was done because the effect of the 50% humidity was already included in the measured results and so only the difference was further accounted for.

Table 9: Relative humidity multiplier

Relative Humidity	βrh (h)
50	1.356
70	1.018

An increase in relative humidity from 50% to 70% reduced the notional shrinkage by .338 based on the CEB equation. Consequently, the ultimate shrinkage for the full scale bridge was reduced from 250με to 188με.

Finally, the free shrinkage data was modified for sample size to that of the full scale bridge. As previously discussed, the CEB code does not account for the effect of sample size on the ultimate shrinkage of a sample. The rate of shrinkage was adapted using the

CEB equation by modifying the volume to surface ratio (v/s) to that of a full scale bridge. The initial v/s ratio for the prism was calculated to be 0.652 while that of a full scale bridge was found to be 9 assuming that the bridge lost moisture primarily from the exposed top surface. This effectively altered the shape of the FS curve and the results are shown in the figure below.

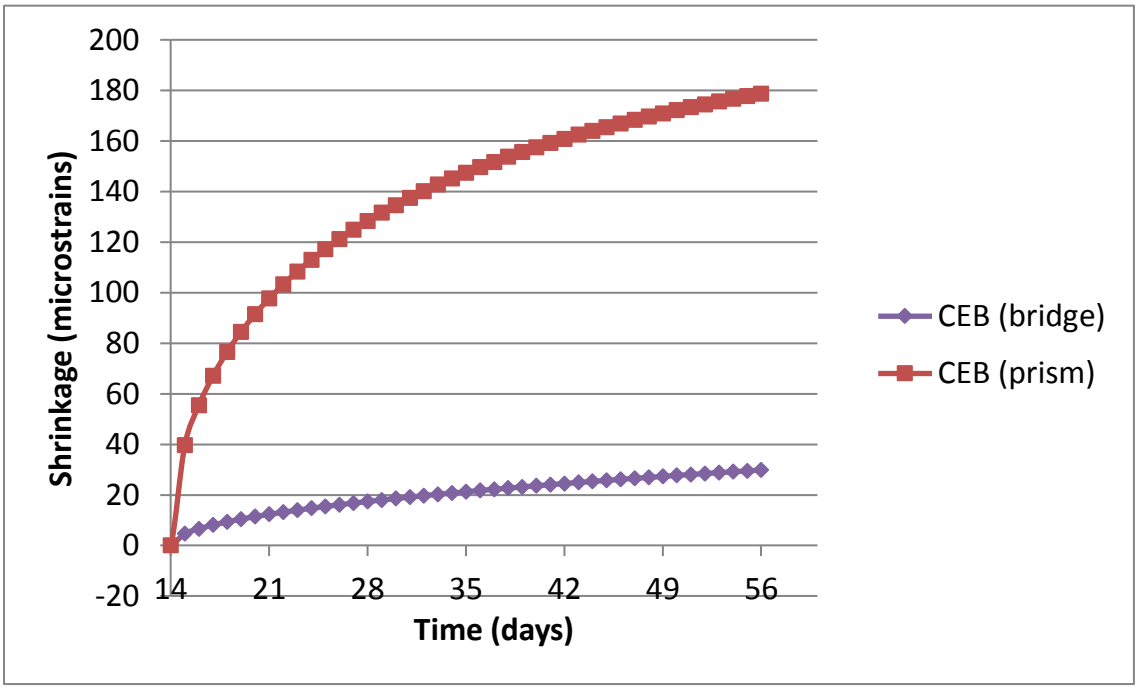

Figure 58: Adjusted free shrinkage curve for full scale bridge

This new curve was taken to be the effective free shrinkage curve for the full scale bridge. This new curve was then used to perform a shrinkage analyses on the full scale bridge using the developed finite element model.

5.4.1.2. Temperature removal

To allow for a better comparison between the measured field data and the FE results, the field data was filtered to remove the effect of temperature and isolate the shrinkage strain.

This was achieved using the same averaging process used on the laboratory free shrinkage prism experiments performed under fluctuating temperature, as discussed in an earlier section. Readings from a sensor installed on PCB span 1 as well as temperature and relative humidity data are shown in the figure below, prior to any adjustments.

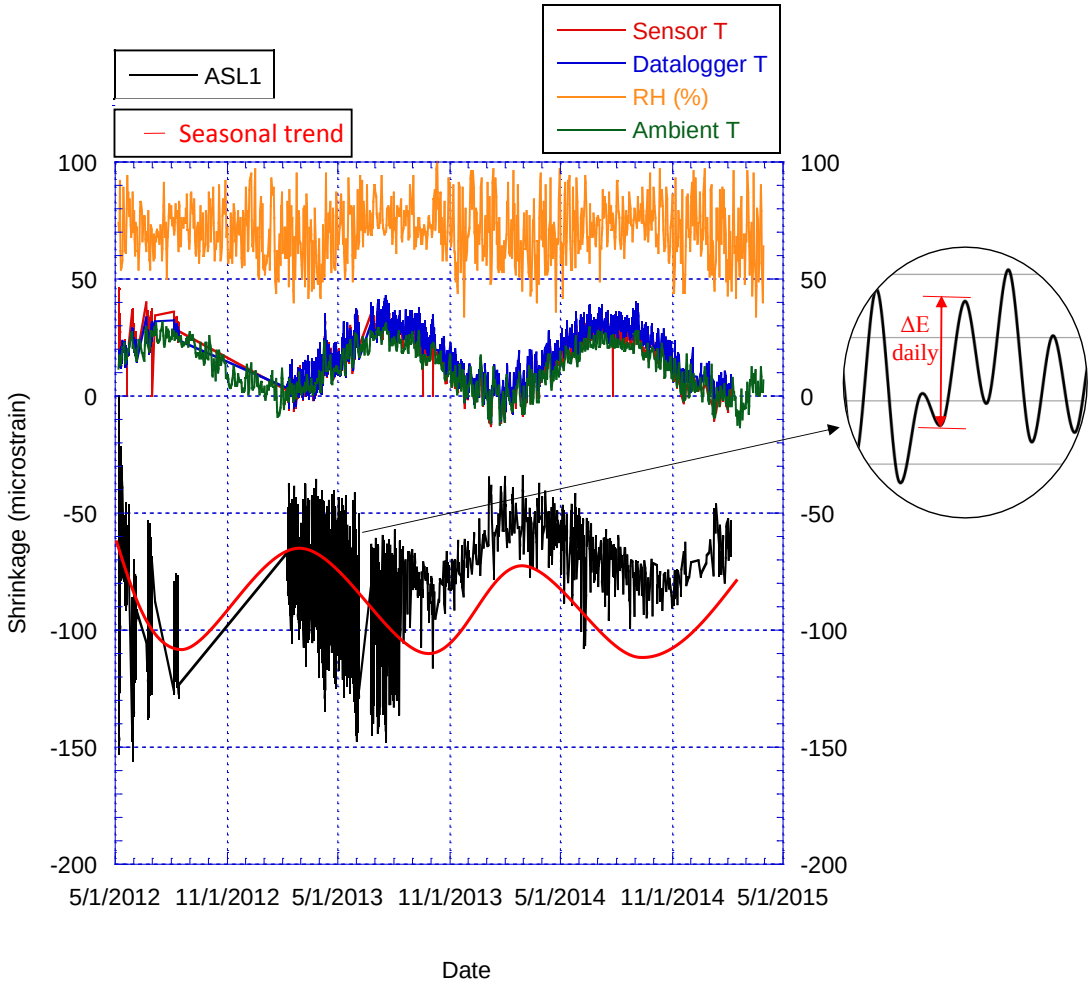

Figure 59: Unfiltered strain data for PCB sensor ASL1

It was observed that the strain measurement captured temperature data as well as shrinkage data. A daily fluctuation in the readings was caused by daily changes in

temperature. A seasonal trend was also observed caused by cyclical changes in average temperature with the change in seasons. These are highlighted in the figure above.

As performed in the smaller samples discussed previously, daily temperature effects were removed by averaging the daily peak and valley strain readings. The table below shows this procedure for a period spanning one week.

Table 10: Average daily strain

Date	E (Peak)	E (Valley)	E (average)
5/16/2012	-84.8	-55.4	-70.1
5/17/2012	-88.2	-55.4	-69.9
5/18/2012	-91.3	-49.2	-70.2
5/19/2012	-88.4	-47.5	-67.9
5/20/2012	-75.7	-58.2	-66.9
5/21/2012	-72.7	-60.9	-66.8
5/22/2012	-74.1	-58.7	-66.4

A plot of this data in the figure below shows that taking the average of the daily peak and valley strain values produced a smooth curve. This indicates that the daily effect of temperature had been removed from the readings.

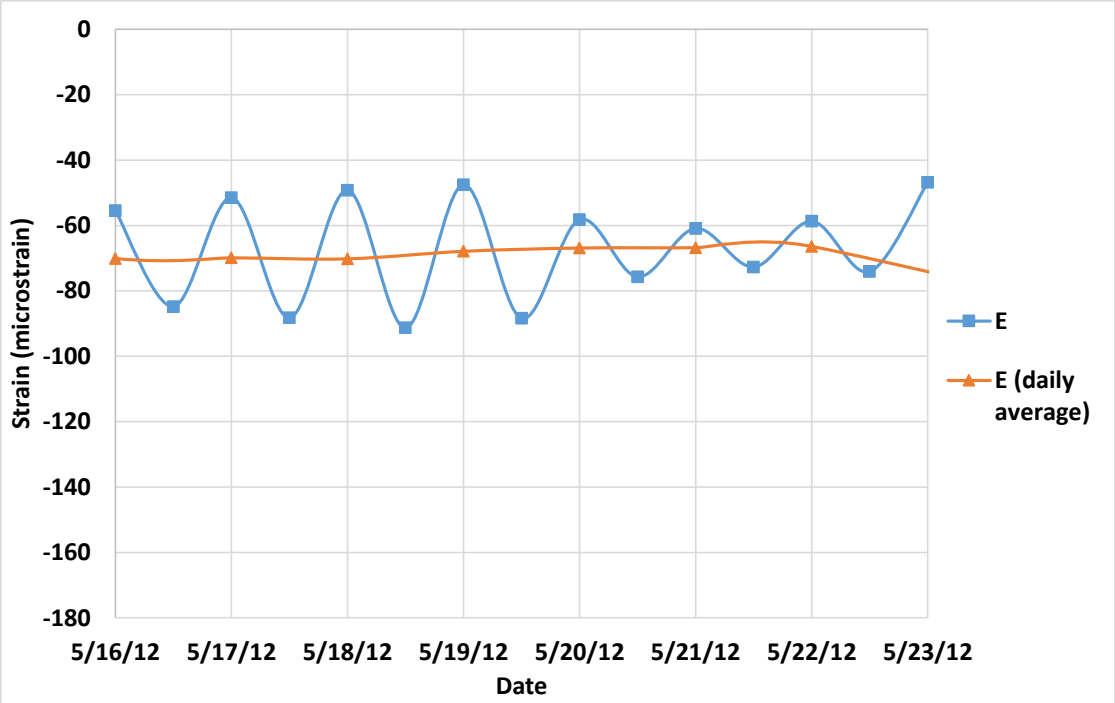

Figure 60: Removal of daily temperature effect from PCB span 1

The plot of the daily average curve was extended to a one year period as shown in Figure 61 below. From this plot, it was observed that the curve still followed a seasonal trend. This was because the average daily temperature for the bridge under field conditions still differed from the average temperature of the small sample collected and stored in the laboratory under controlled conditions.

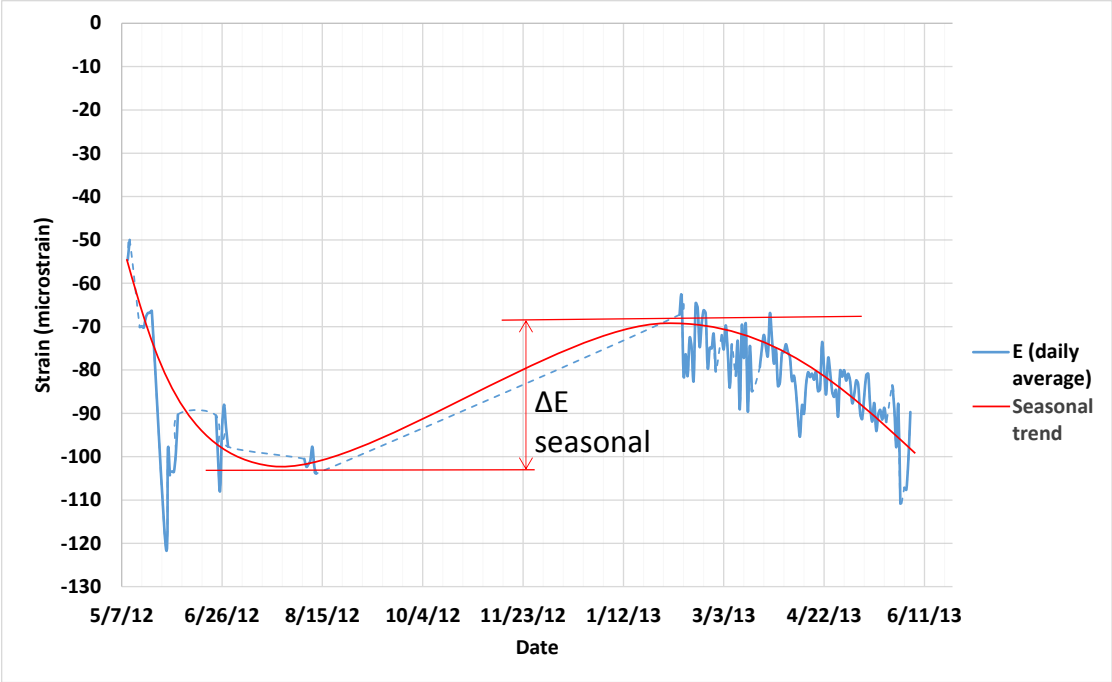

Figure 61: Seasonal variation of strain in PCB span 1

This seasonal effect was quantified by taking the average of the seasonal peak and valley strain readings. This was found to be 105 με and 75 με respectively. The difference in these values is 30 με which indicates a seasonal temperature variation of ±15 με from the average value during peak and valley months. The peak and valley strain readings were modified by 15 με respectively to 90 με. These values were then used as markers from which a new approximate curve for shrinkage was plotted. The approximate shrinkage curve makes use of five points as detailed in the table below.

Table 11: Data point description for shrinkage curve

Point	Description	Value

number		
1	First data point recorded	0
2	Data point at end of heat of hydration reaction (~2 days)	-50
3	Adjusted peak data point	-90
4	Midpoint of adjusted points	-90
5	Adjusted valley data point	-90

Using this procedure, a new plot was derived for the isolated shrinkage strain as shown in Figure 62 below. The new strain plot serves as a guideline for the isolated shrinkage over time. It was observed that the current adaptation appears flat. Shrinkage is expected to increase over time although this process occurs very gradually due to the large size of the specimen and the increased average relative humidity. Furthermore, the number of data points collected after the initial one year period was reduced significantly. As a result, the valley data points were excluded during collection which compounded the difficulty of observing the downward trend.

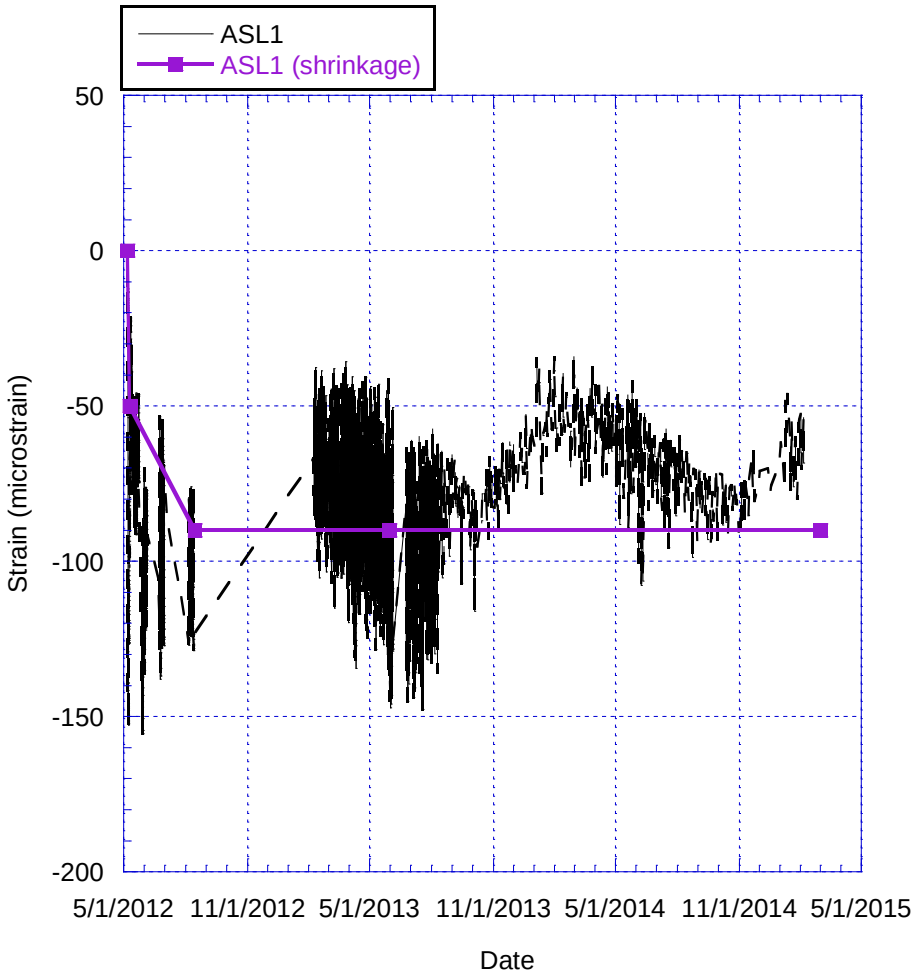

Figure 62: Typical strain reading showing isolated shrinkage effect

The filtered strain data shows a rapid rise in shrinkage within the first few months after which the shrinkage effect becomes more gradual. Hereafter, the isolated shrinkage strain data was then used for comparison with the analysis data.

5.4.1.3. Data comparison

The modified free shrinkage data taken from small samples was used as strain input to perform a shrinkage analyses of the FE model of the Patcong Creek Bridge. Additionally, the measured strain data was filtered according to the procedure above to isolate the

shrinkage component of the strain. Comparisons between the filtered experimental strain data and the FE analysis results are shown in the figures below. A total of five VWSGs were installed on span 1 in the longitudinal direction to capture transverse strains however data for the last sensor was corrupted and unused.

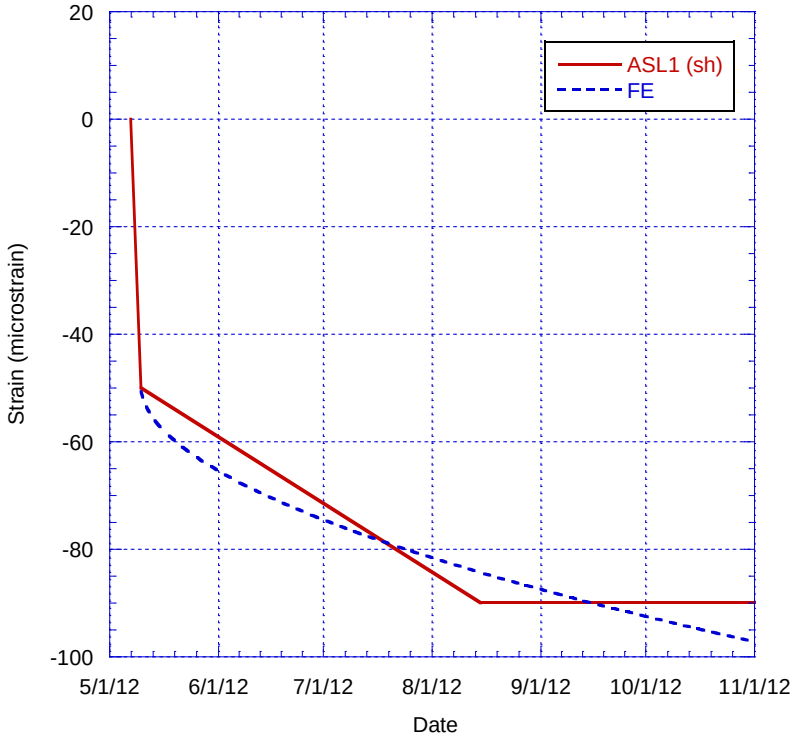

Figure 63: Comparison of PCB sensor ASL1

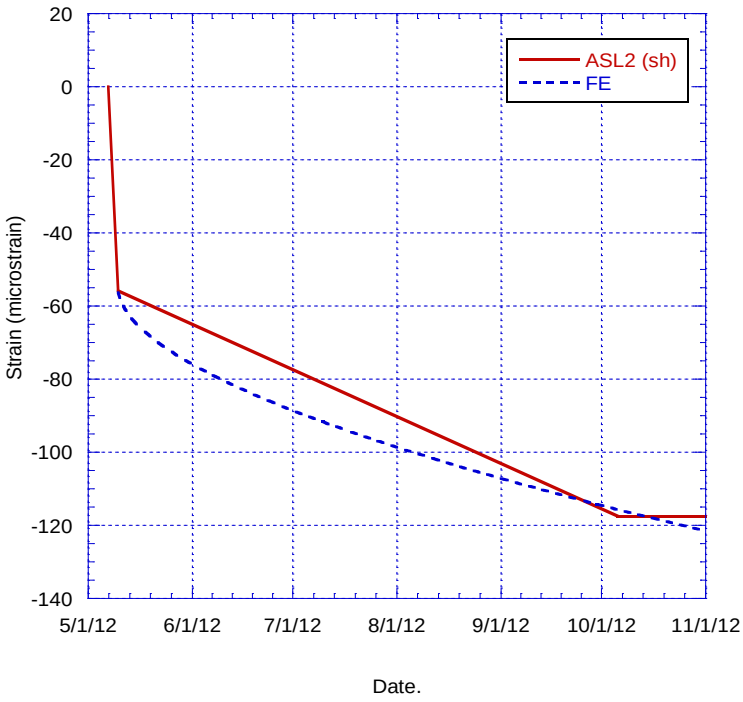

Figure 64: Comparison of PCB sensor ASL2

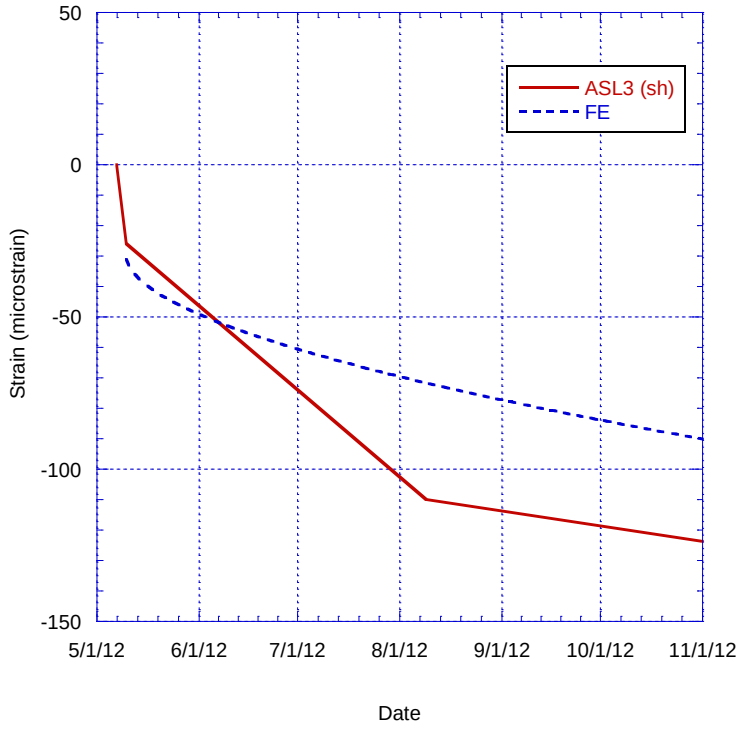

Figure 65: Comparison of PCB sensor ASL3

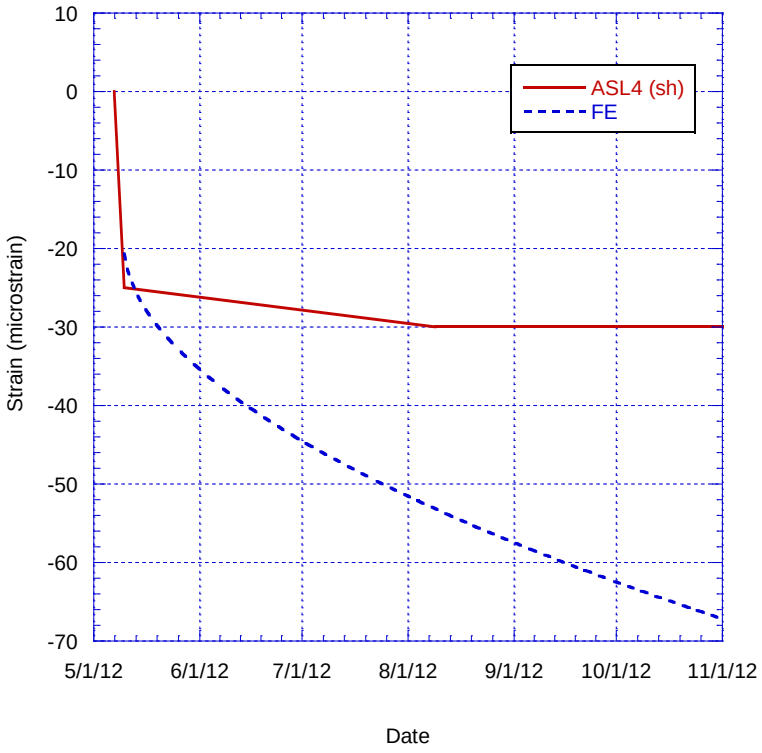

Figure 66: Comparison of PCB sensor ASL4

The comparison between the FE results and the measured data began after the initial heat of hydration reaction as this process was not accounted for in the FE model. This was approximately 2-3 days after pouring as a retarder was used in the concrete mix. The comparison showed better correlation between the measured results and the FE analysis during the earlier time period. However, as the time increased, the results gradually deviated. This is because the FE input makes use of extrapolated data which reduces in accuracy the further the data is extrapolated. Furthermore, shrinkage in the measured results slowed down significantly within the first three to six months after pouring. Conversely, the FE results continue to increase albeit at a more gradual rate, as determined by the prediction model based on a smaller sample.

The comparison for sensor ASL3 produced a less satisfactory match. This was due to a jump in the unfiltered measured strain which occurred after a period where data was lost. This jump caused a larger strain average to be derived during the data filtering process. It is likely that the sensor or the connection for this sensor was affected and the result therefore, altered. ASL4 is the sensor located at the bottom of the concrete deck. This location takes the longest to feel the effect of shrinkage due to the shrinkage gradient and loses moisture much slower than sections closer to the top of the deck. It is also located directly above a girder which makes this region stiffer. As a result, the recorded shrinkage for this location was low and showed a relatively flat trend.

The analysis procedure detailed above was also performed for the three span continuous segment of the Patcong Creek Bridge. Two sections of concrete were poured separately as previously described. The ultimate shrinkage based on measurements taken from the segments was found to be 260 and 230 microstrains. The comparison is shown in the figures below.

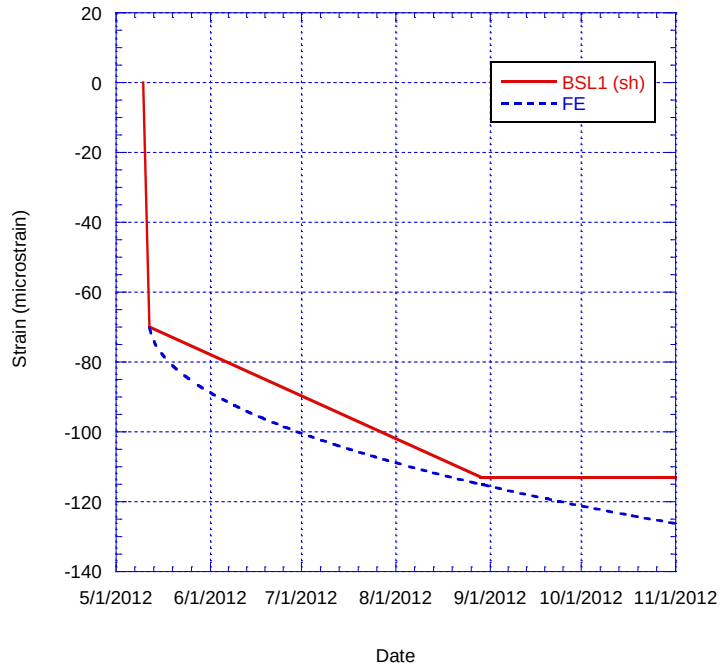

Figure 67: Comparison of PCB sensor BSL1

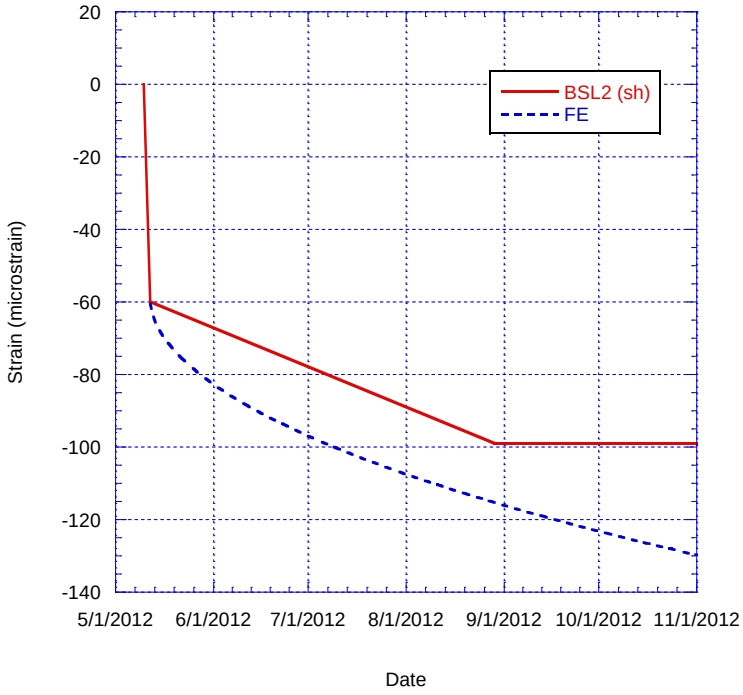

Figure 68: Comparison of PCB sensor BSL2

Figure 69: Comparison of PCB sensor BSL3

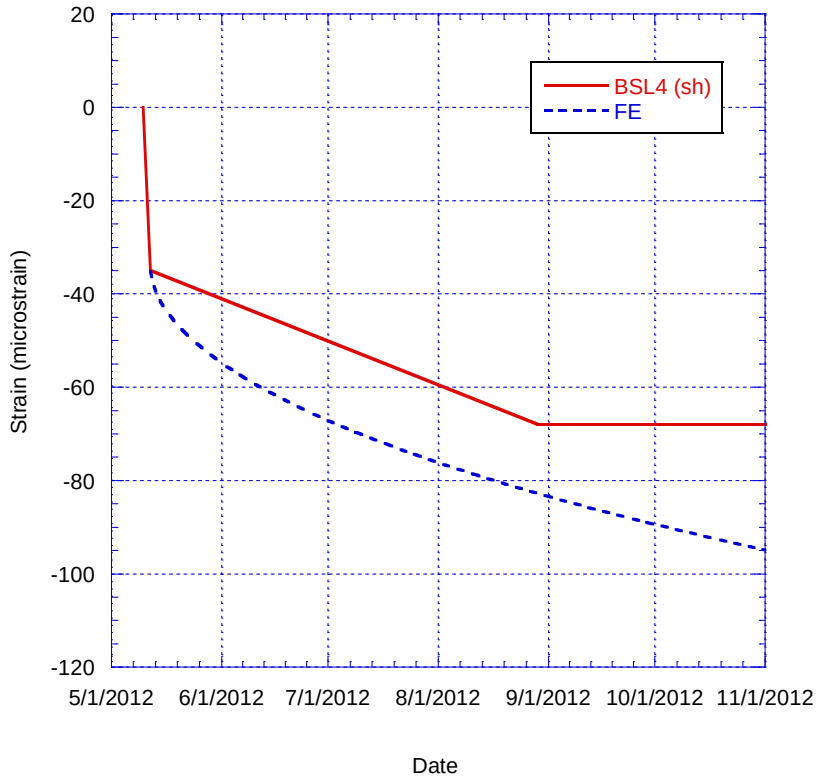

Figure 70: Comparison of PCB sensor BSL4

A correlation can be observed between the FE results and the filtered measured data. The comparison also produced better results earlier on and deviated as time increased due to the absence of longer term input data. The measured results stabilized within the first four months and showed a slower rate of shrinkage then the FE results.

5.4.2. Garden State Parkway Interchange 67

A FE model of the Garden State Parkway Interchange 67 was used to perform a shrinkage analysis using the free shrinkage data measured from a standard free shrinkage mold. The finite element model of the bridge is shown in the figure below.

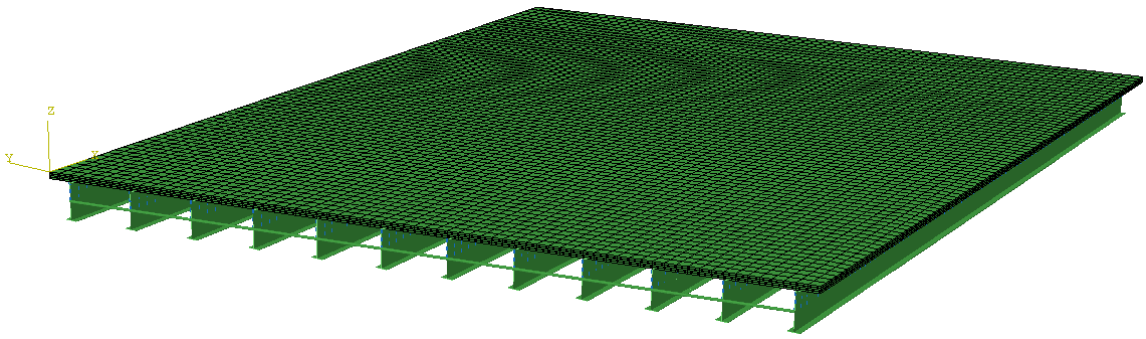

Figure 71: FE model of GSP I-67

This model consists of two layers of C3D8 solid elements used for the concrete slab and B32 beam elements used for the stringers. Reinforcement was embedded in surface elements. The slab was connected to the girder using beam type multi point constraints (MPC) which restrain the movement of the slab to the girders. Pin-roller boundary conditions were applied to the girders. The procedure outlined in the earlier section for the preparation of input data for use in the shrinkage analysis was also performed for this bridge. The ultimate shrinkage of the small sample was found to be 454 microstrains. The temperature and relative humidity under field conditions at the location of the bridge are shown in the figure below.

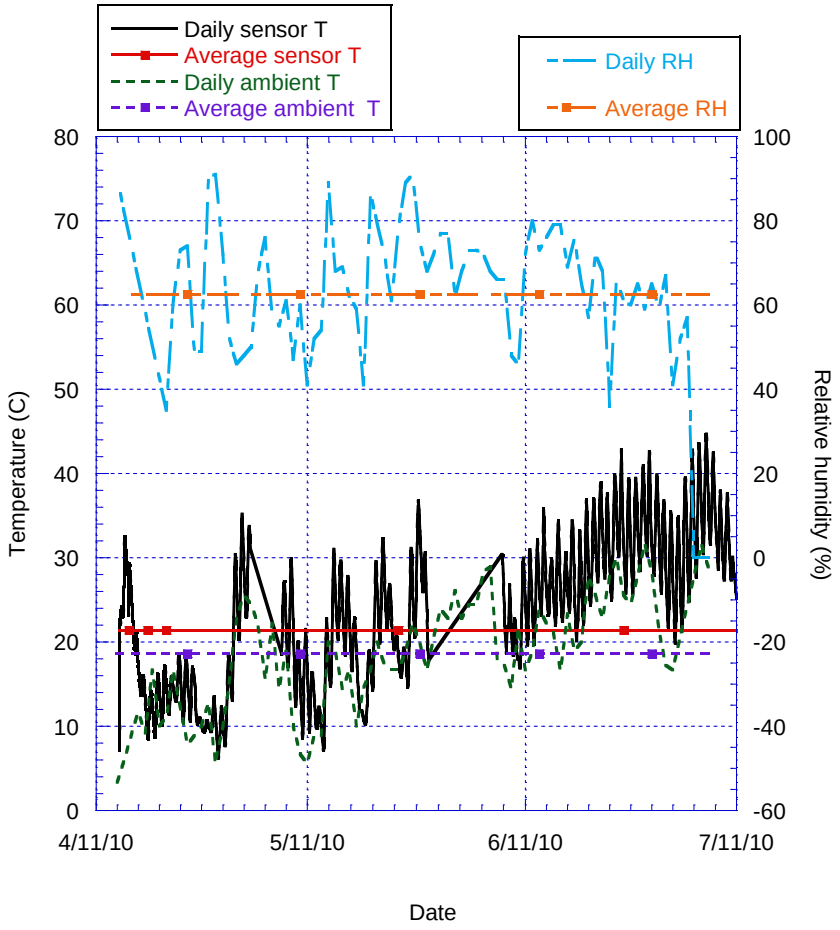

Figure 72: Temperature and relative humidity for Garden State Parkway Interchange 67

The strain data collected for the bridge was also filtered to isolate the shrinkage component following the procedure outlined above. A comparison was made between the measured data and the finite element model analysis results and is discussed in the next section.

5.4.2.1. Data comparison

The same procedure used in the previous sections was repeated for this bridge to facilitate the shrinkage analysis. Comparisons between the filtered experimental strain data and the FE analysis results are shown in the figures below.

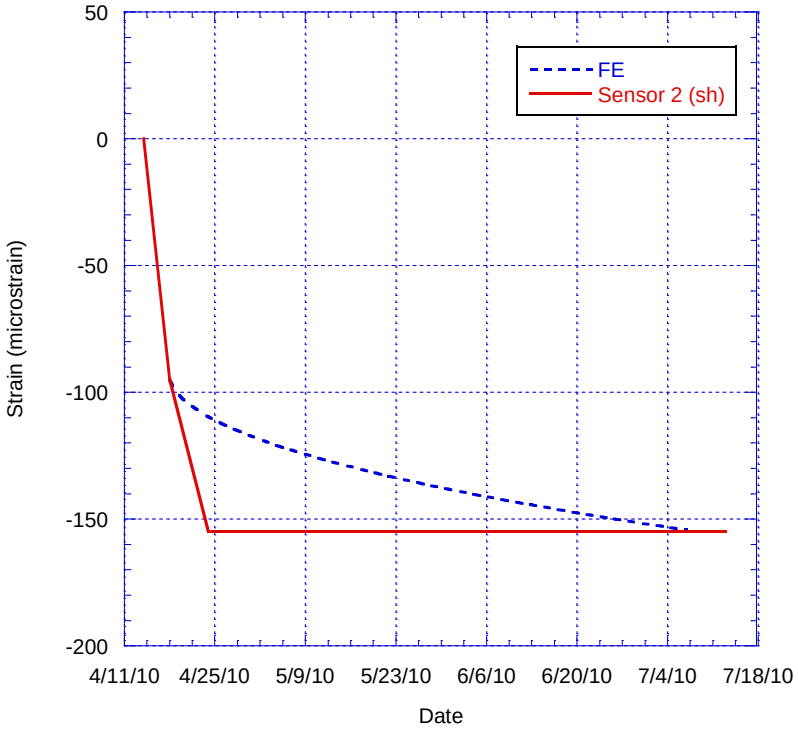

Figure 73: Comparison of GSP I-67 Sensor 2

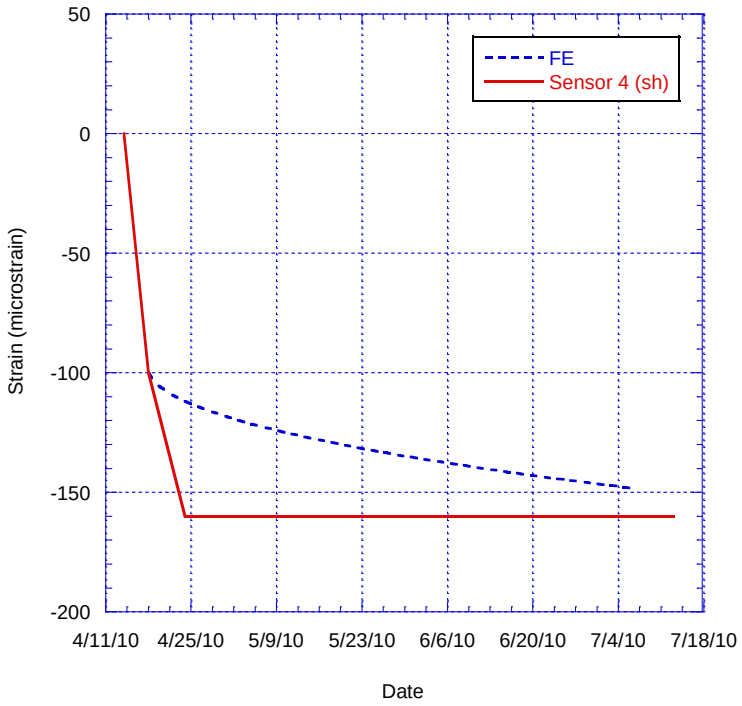

Figure 74: Comparison of GSP I-67 Sensor 4

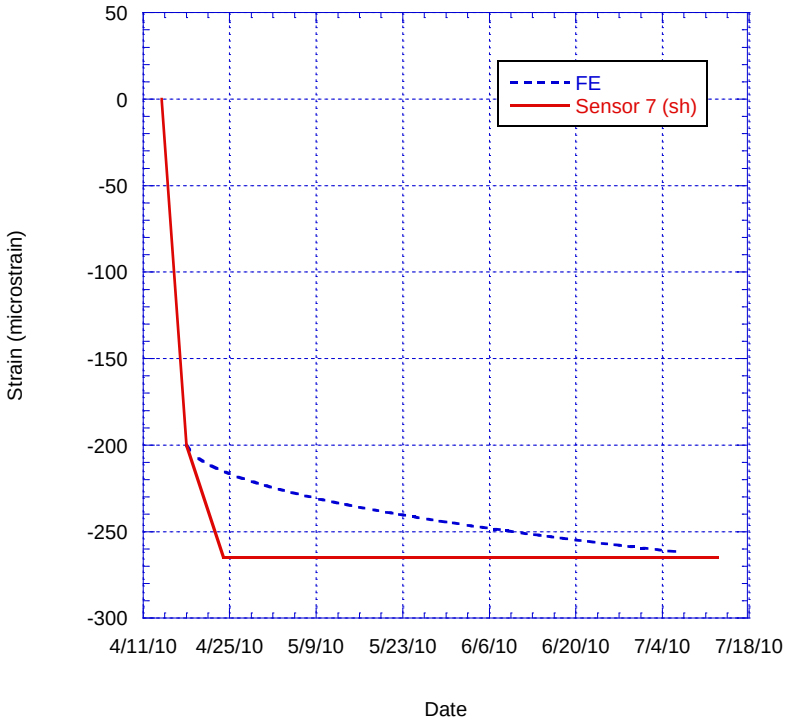

Figure 75: Comparison of GSP I-67 Sensor 7

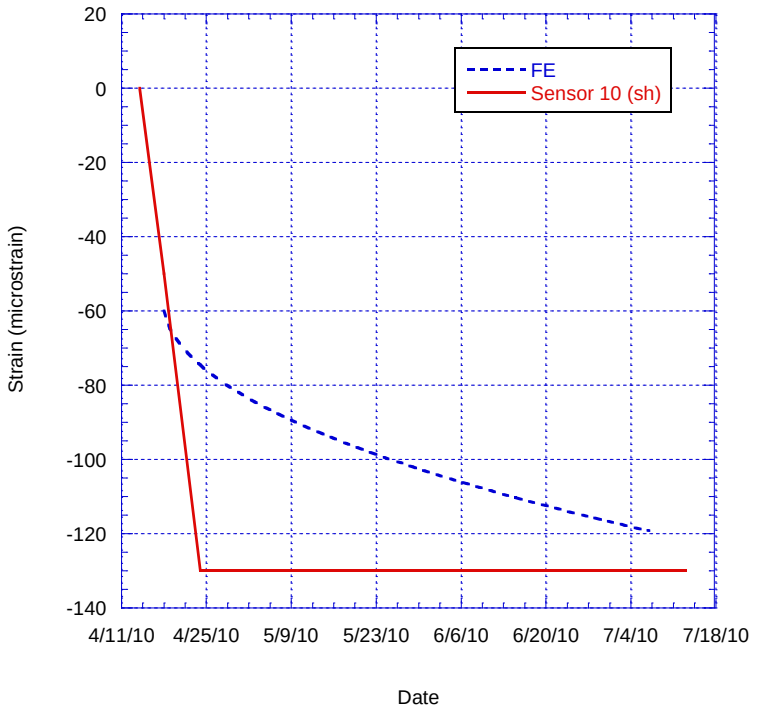

Figure 76: Comparison of GSP I-67 Sensor 10

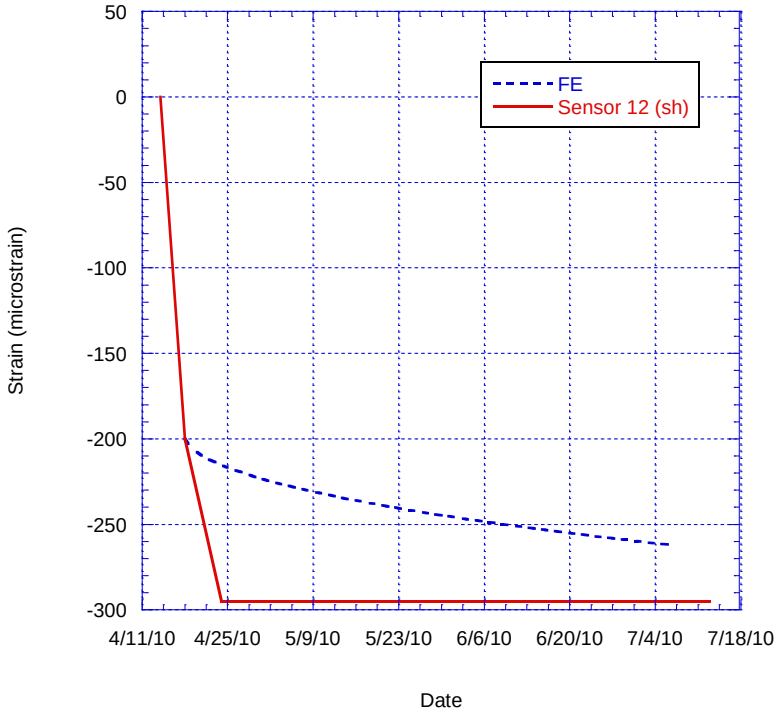

Figure 77: Comparison of GSP I-67 Sensor 12

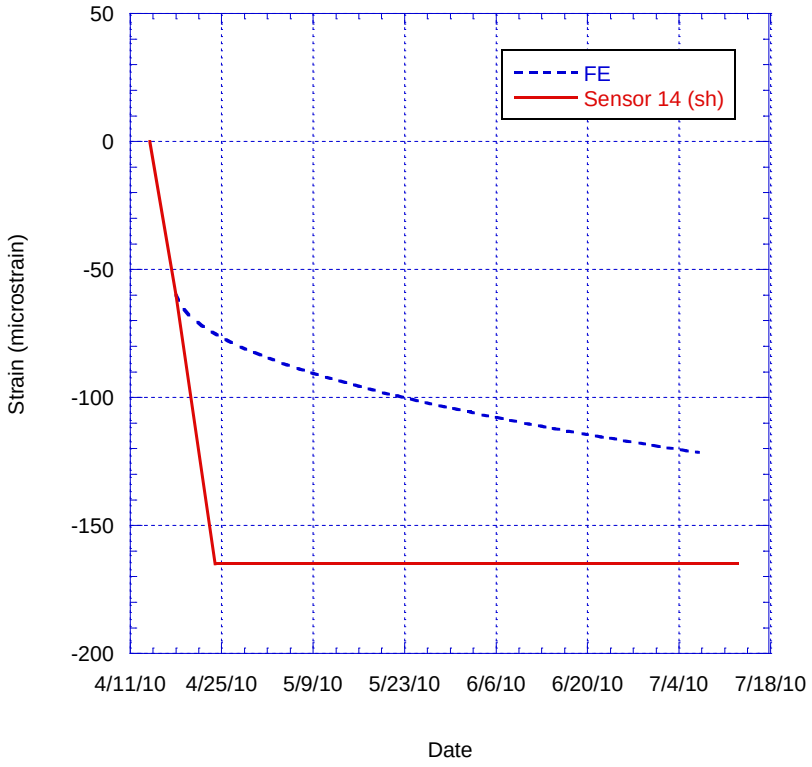

Figure 78: Comparison of GSP I-67 Sensor 14

The comparison between the measured and the FE results produced a reasonable match. From the plots above, the measured shrinkage steadied within the first month. The available data for the GSP I-67 bridge consisted of a three month time period spanning April to July. As discussed previously, this time period excluded the coldest and hottest months of the year which affected the performance of the averaging method since the seasonal high and low are unknown. However, the majority of the time period during which data was collected occurred during months with more moderate temperatures and as such, the seasonal temperature effect was minimized. The data from sensor 14 showed the greatest disparity as there was a slight dip in the data which caused the averaging process to reflect a greater value. In the absence of longer term data, such anomalies in the data have a greater effect on the filtered results.

5.5. Summary

The incorporation of shrinkage analysis into FE modelling described in the chapter produced acceptable results although some limitations were observed. The comparison between field and FE results showed greater agreement during the first months and gradually deviated afterwards. This indicates that the accuracy of extrapolation of short term data is limited and the further the data is extrapolated, the less accurate the results. Additionally, results based on measured data from small samples were observed to continue increasing after the measured data from larger samples had otherwise stabilized. Since larger samples undergo shrinkage slower than smaller samples, it is expected that data adapted from smaller samples would exhibit an increasing trend beyond data measured from a larger sample. Furthermore, longer measurement periods enabled the removal of thermal strain better than shorter measurement periods as the seasonal effect in short time periods was more difficult to observe.

CHAPTER 6

PARAMETRIC ANALYSIS

A parametric analysis was performed using the models previously developed to observe the impact of design variables on the shrinkage behavior of the modeled bridges. During the development of a bridge, designers have greatest impact on the design factors rather than the environmental conditions or construction factors. Therefore, a greater understanding of these design factors in relation to concrete shrinkage can improve the impact of shrinkage strain on a bridge from a design perspective. The developed shrinkage models were used to make relative comparisons between several design factors and the impact was observed and discussed in greater detail in the sections following. All models made use of 4000 psi concrete which is a common design strength for concrete bridge decks. The associated tensile strength was taken as 0.08 to 0.09 of the concrete compressive strength. This gave a tensile strength between 320 and 360 psi.

6.1. Variables

Previous studies have been performed to determine which variables affect the shrinkage behavior of a bridge therefore no new analysis was performed towards this end. Additionally, variables were chosen such that designers have control over the decision making during the design process. The variables chosen for use in the parametric study such are reinforcement, boundary conditions and deck thickness.

6.2. Influence of reinforcement

The reinforcement of the developed bridge models was varied to study its impact. The bridges were designed with #5 rebars spaced at 12 in. The spacing of the rebars was held constant. The results are compiled in the plots below for the available bridge models. A high shrinkage strain was applied to the models to encourage cracking so that the behavior under this condition could be observed.

6.2.1. Reinforcement size

The stress and strain in the concrete for the change in reinforcement size are shown in the plots below.

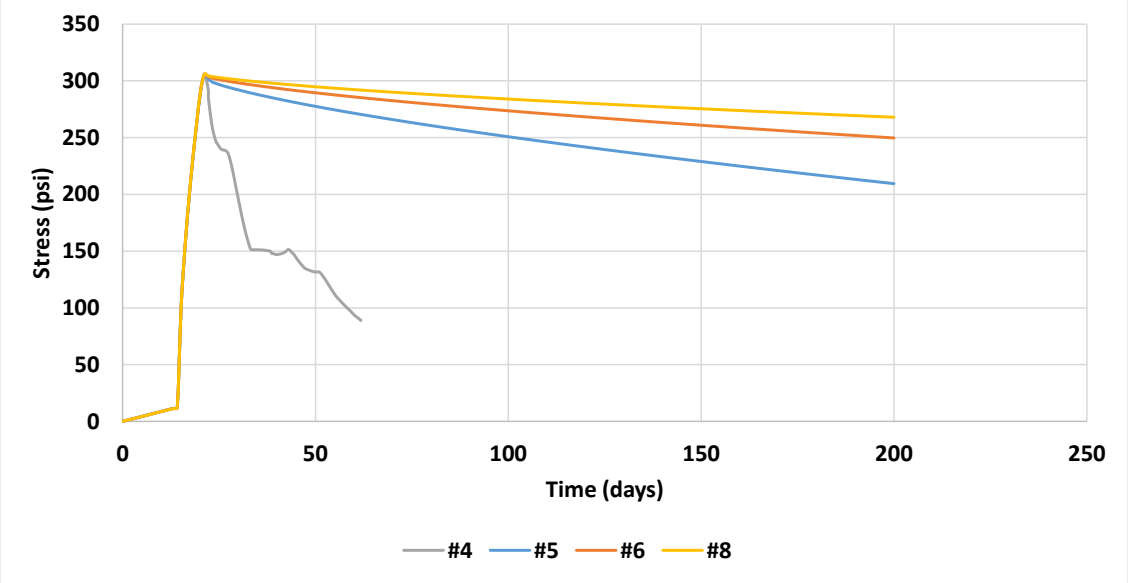

Figure 79**:** Stress in PCB simply supported span reinforcement analysis

The plot above shows the stress in the PCB simply supported span. The stress results above indicate that the concrete cracks when the tensile capacity is reached. This occurred at a tensile strength of approximately 306 microstrains. All the analysis cases

cracked at this capacity regardless of the rebar size, indicating that cracking in concrete is mainly a result of the concrete stress and the concrete tensile capacity. However, the post cracking behavior differed between the bridges. The #4 rebar provided little resistance after cracking and the tensile capacity of the bridge deck reduced greatly. The #8 rebar provided the greatest post cracking resistance.

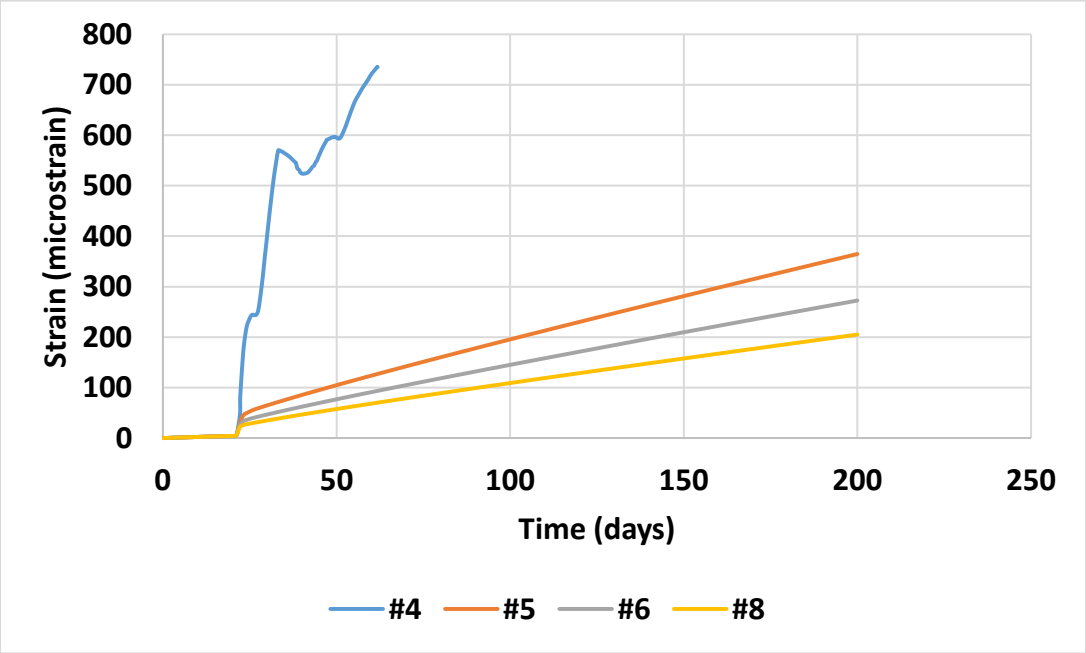

Figure 80: Strain in PCB simply supported span reinforcement analysis

The strain in the concrete reflects the results of the stress shown in the plot above. Upon cracking, the bridge deck with the #4 rebar experienced a very high strain as the cracks continued to open. This reinforcement performed less satisfactorily than the #5, #6 and #8 rebars to control the crack after cracking began.

The result of the influence of reinforcement on the continuous span are shown in the figure below.

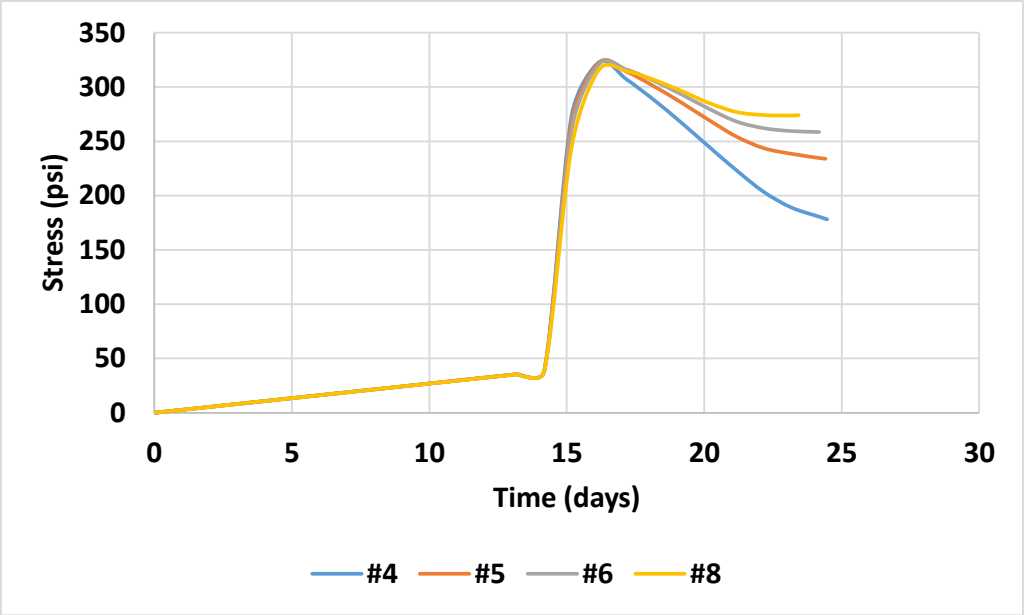

Figure 81: Stress in PCB continuous span reinforcement analysis

The concrete cracked at a tensile stress of 316 microstrains. Again, the larger rebars provided better resistance after cracking than the smaller rebars. This agrees with the results derived above for the simply supported span.

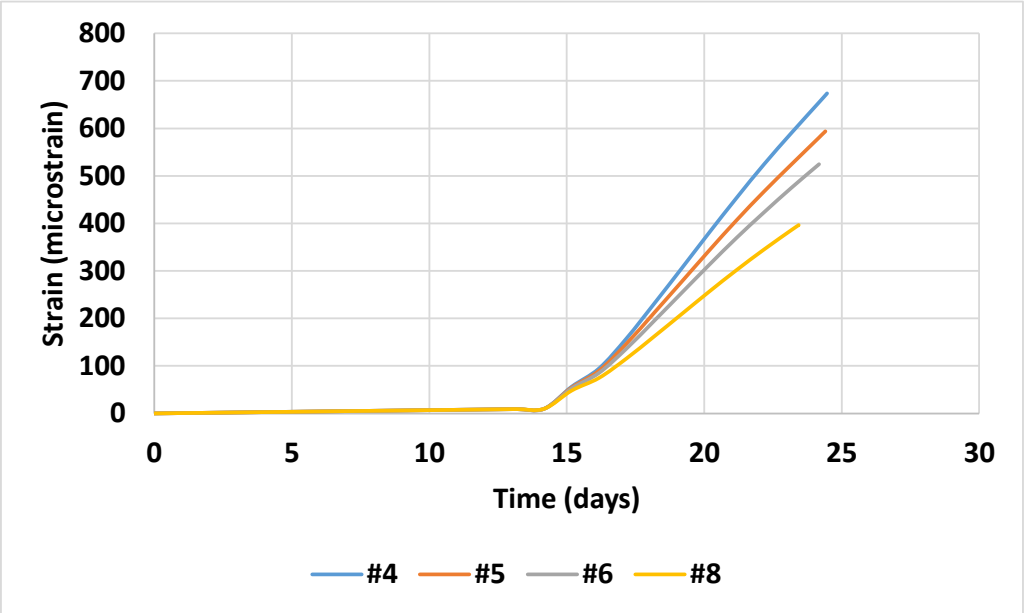

Figure 82: Strain in PCB continuous span reinforcement analysis

The strain in the continuous span also indicated that larger rebars provided a better response after the concrete undergoes cracking.

The results for the Garden State Parkway Interchange 67 are shown in the plots below.

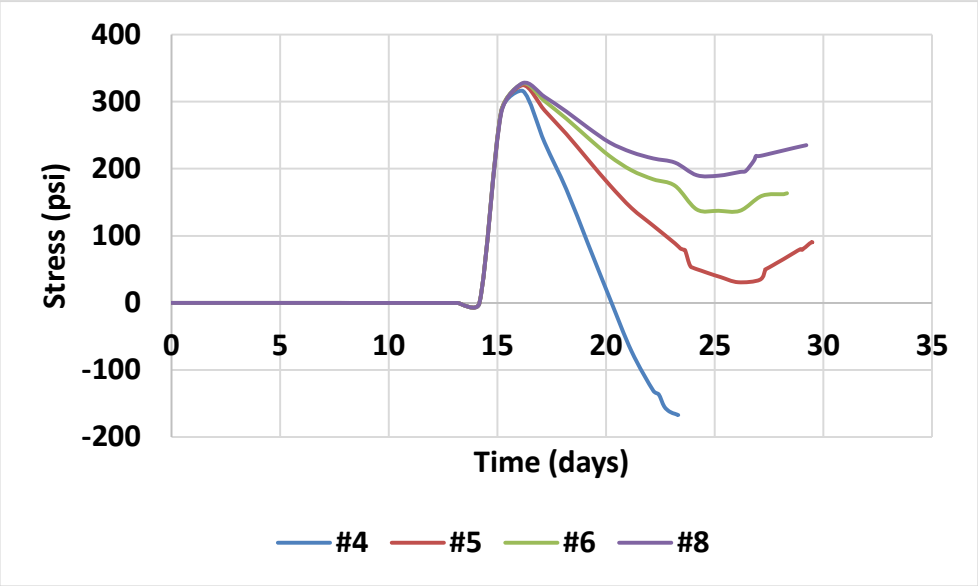

Figure 83: Stress in GSP I67 reinforcement analysis

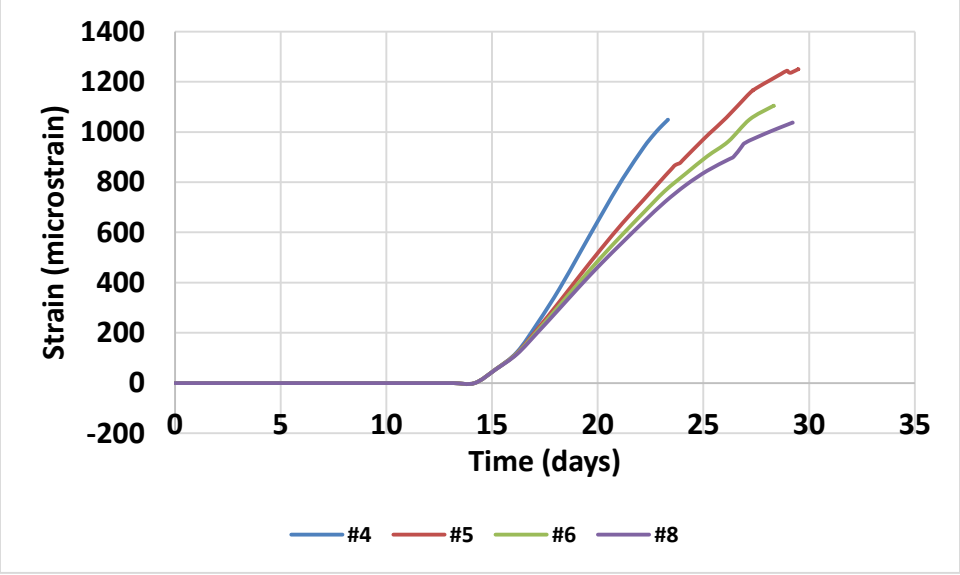

Figure 84: Strain in GSP I67 reinforcement analysis

The behavior of the reinforcement in the GSP I67 Bridge mirrored the behavior of the Patcong Creek Bridge. The use of a #4 rebar showed continued material failure after the concrete exceeded its tensile capacity. Larger rebars however provided some post cracking resistance. The increasing strain in the concrete deck was due to a widening of the cracks in the concrete deck as the tensile strain continued to increase even after initial cracking. Larger rebars also provided a greater resistance to the growth of cracks.

6.3. Influence of boundary conditions

The boundary conditions of the developed bridge models were varied to study its impact. The results were compiled in the plots below for the available bridge models. The influence of boundary conditions on the simply support PCB span is shown in the plot below.

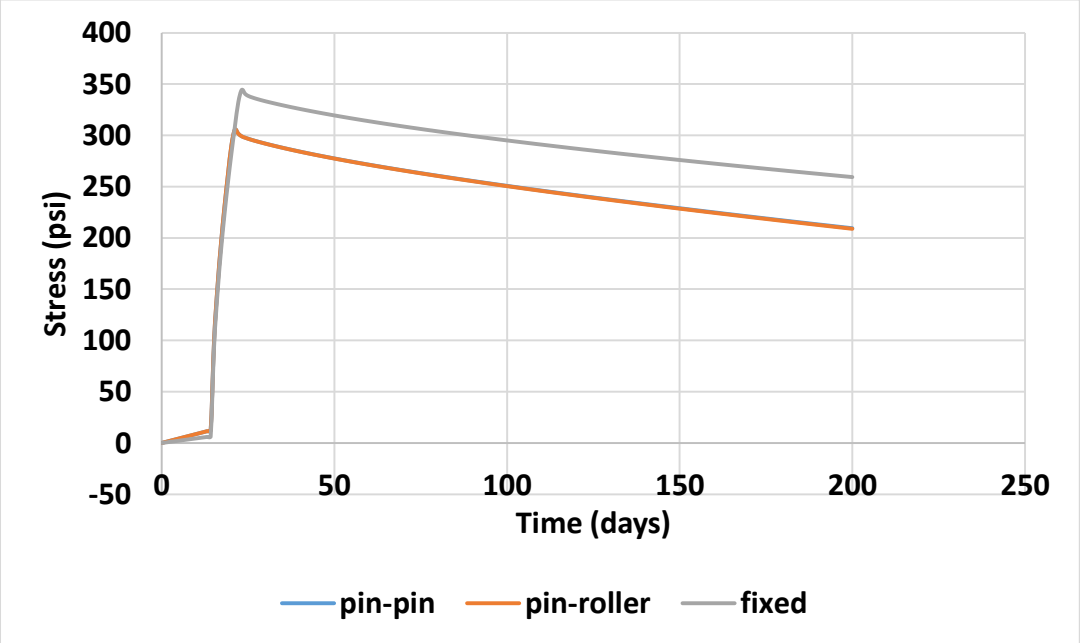

Figure 85: Stress in PCB simply supported span boundary condition analysis

The behavior of the bridge deck was similar when the ends were pinned and when a pin-roller connection was used. Greater stress was observed in the model when the deck was fixed as a fixed boundary condition resists strain more than a pinned or roller boundary condition. The concrete deck withstood a greater stress when the ends were fixed before a reduction in capacity occurred.

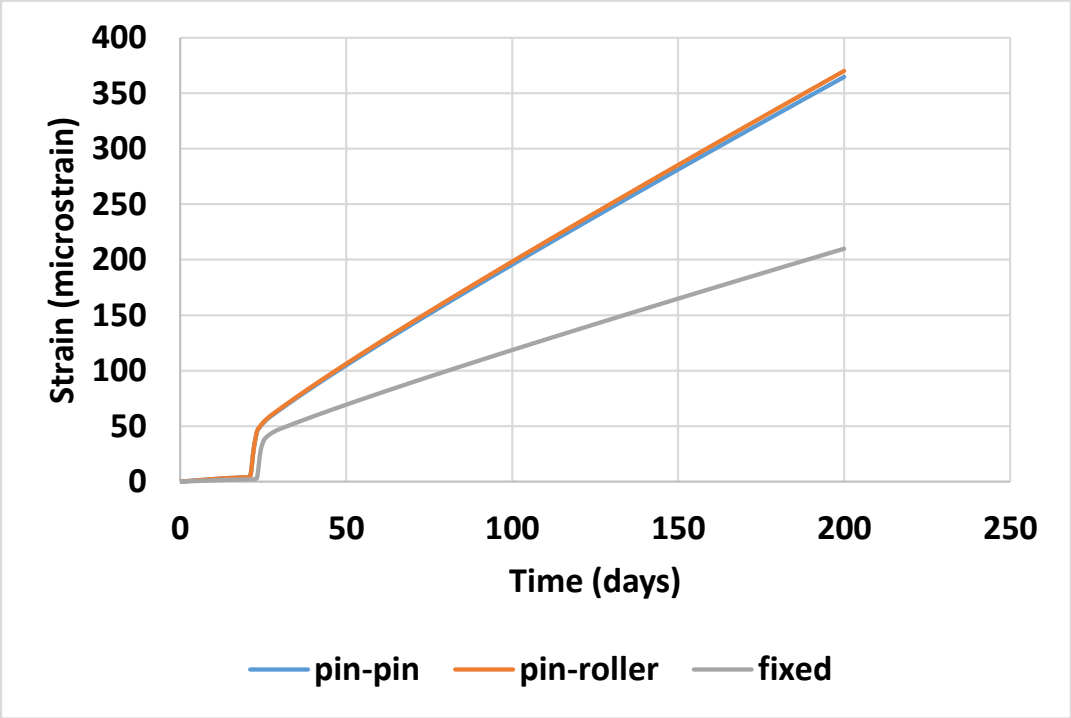

Figure 86: Strain in PCB simply supported span boundary condition analysis

The strain results also showed that the behavior of a pinned end and a rollered end were similar. However, the when the end was fixed, the shrinkage strain was significantly reduced as the bridge was not free to move as freely. The results for the continuous span segment of the Patcong Creek Bridge is shown in the plot below.

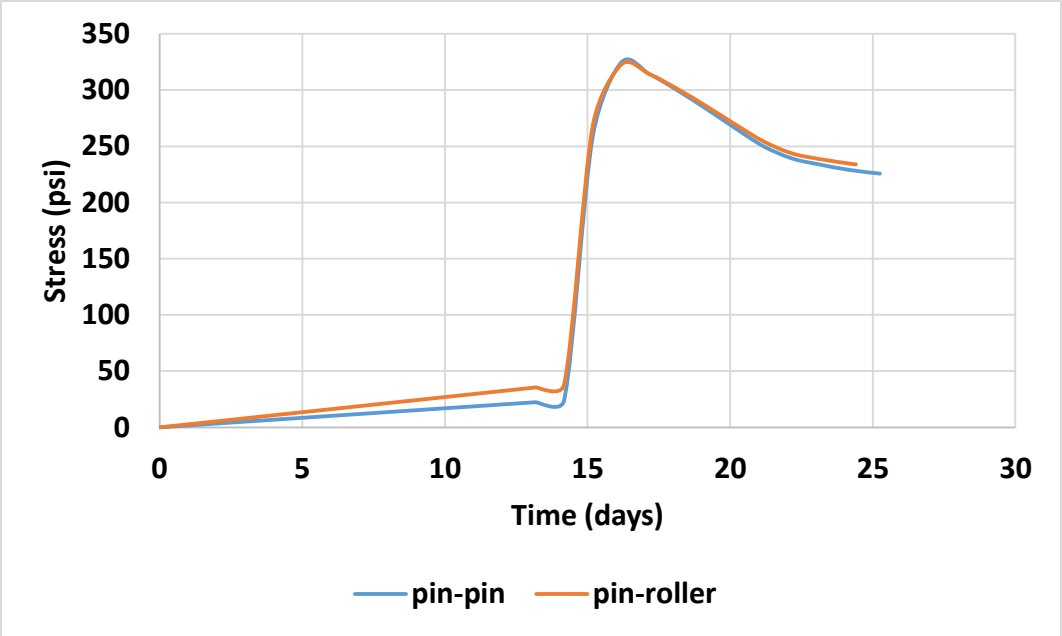

Figure 87: Stress in PCB continuous span boundary condition analysis

In the case of the continuous span, the difference in the use of a pinned boundary condition over a rollered boundary condition was also less distinguishable. The strain results given in the figure below also indicated that the difference in the use of a pin connection over a rollered connection was marginal. This effect was not influenced by the type of span used.

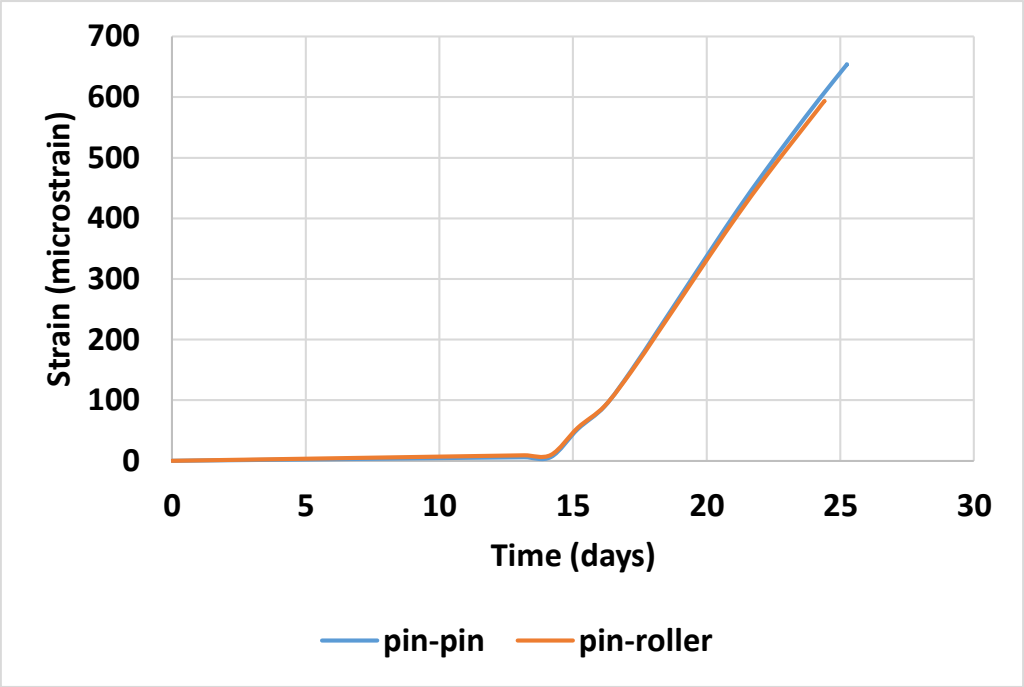

Figure 88: Strain in PCB continuous span boundary condition analysis

The results of the change in boundary condition for the GSP I67 Bridge are shown in the plots below.

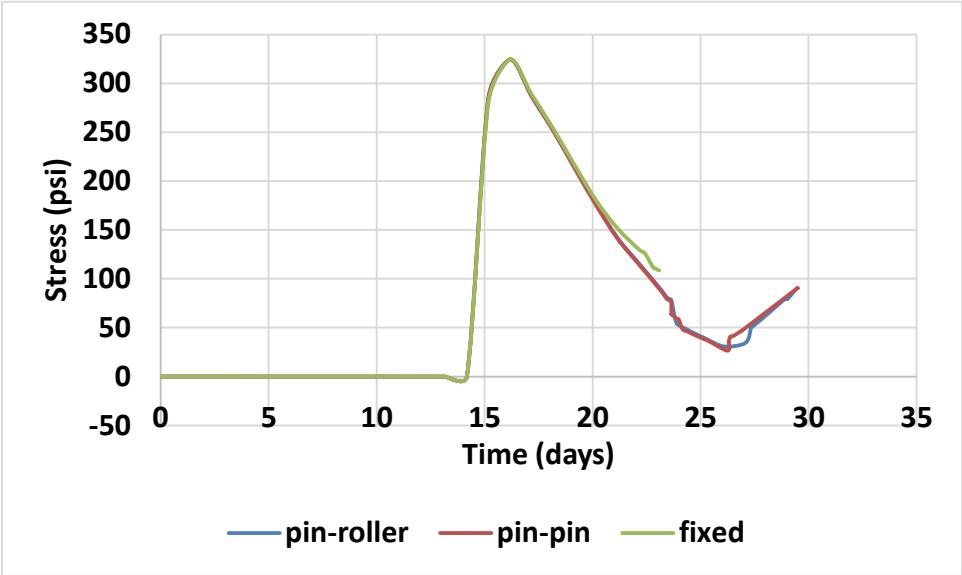

Figure 89**:** Stress in GSP I67 span boundary condition analysis

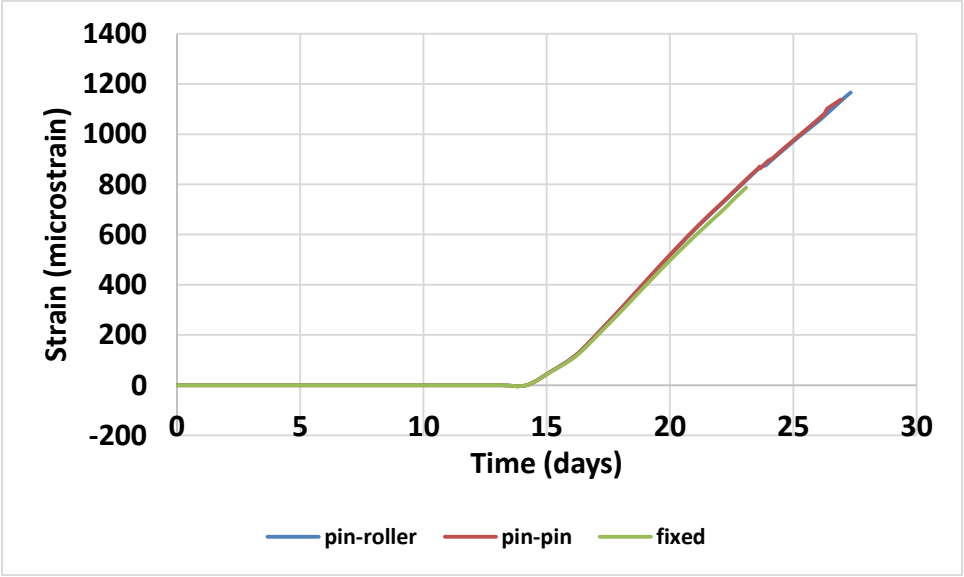

Figure 90: Strain in GSP I67 span boundary condition analysis

The results of the stress and strain in GSP I67 indicated that the fixed end analysis terminated early which can be attributed to excessive cracking. However, there was no significant difference observed in this case due to a change in boundary conditions.

6.4. Influence of deck

The deck thicknesses of the developed bridge models were varied to study its impact. The results were compiled in the plots below for the available bridge models. The Patcong Creek Bridge was designed with a deck thickness of 9 in whereas the Garden State Parkway Interchange 67 was designed with a deck thickness of 8.5 in.

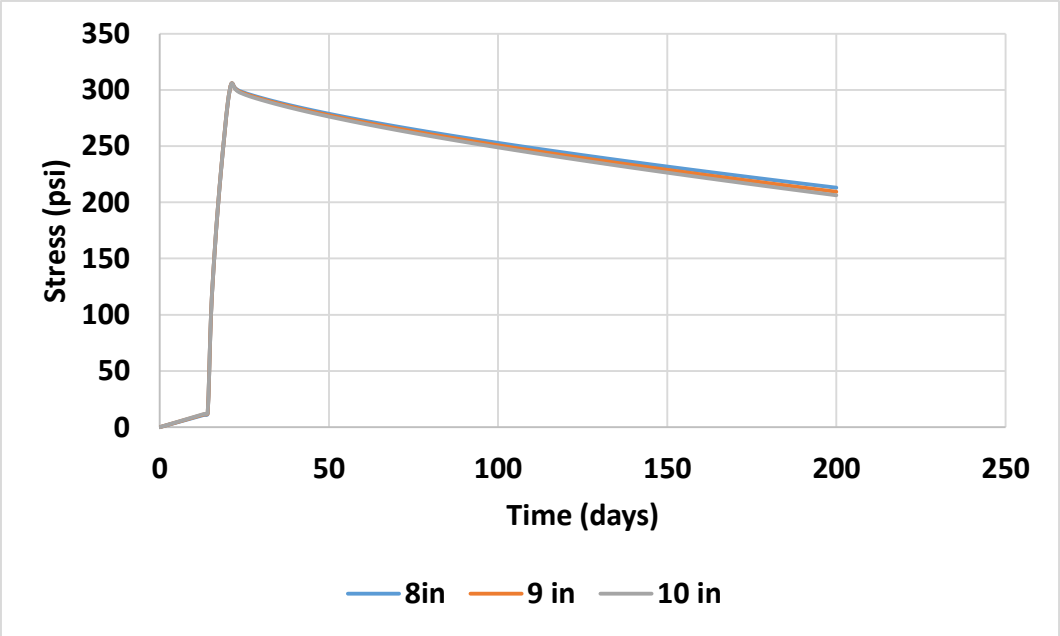

Figure 91**:** Stress in PCB simply supported span deck thickness analysis

In the PCB simply supported span, no significant differences in the stress were observed when the thickness of the deck was altered during the parametric analysis.

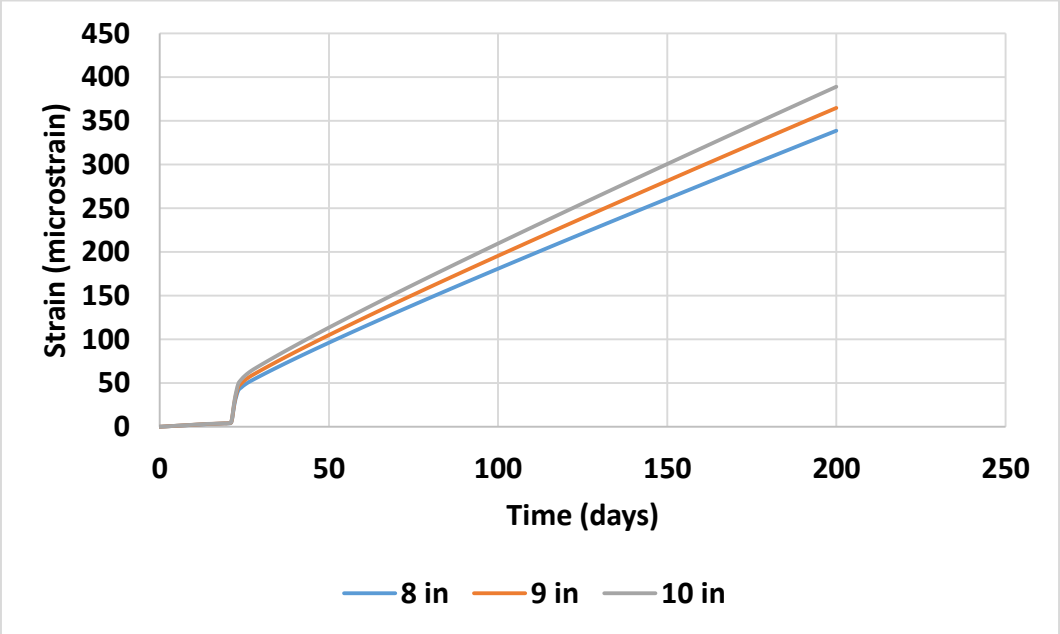

Figure 92: Strain in PCB simply supported span deck thickness analysis

From the strain results, it was observed that a reduction in the deck thickness showed a reduced shrinkage strain, however an increase in the thickness of the deck indicated an increase in shrinkage strain. The results for the PCB continuous span are continued below.

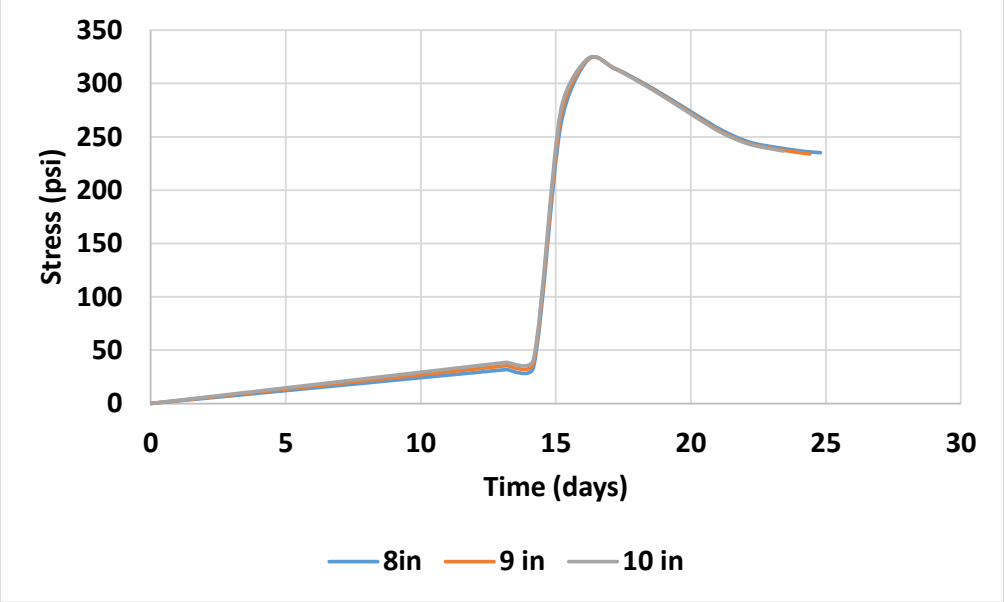

Figure 93: Stress in PCB continuous span deck thickness analysis

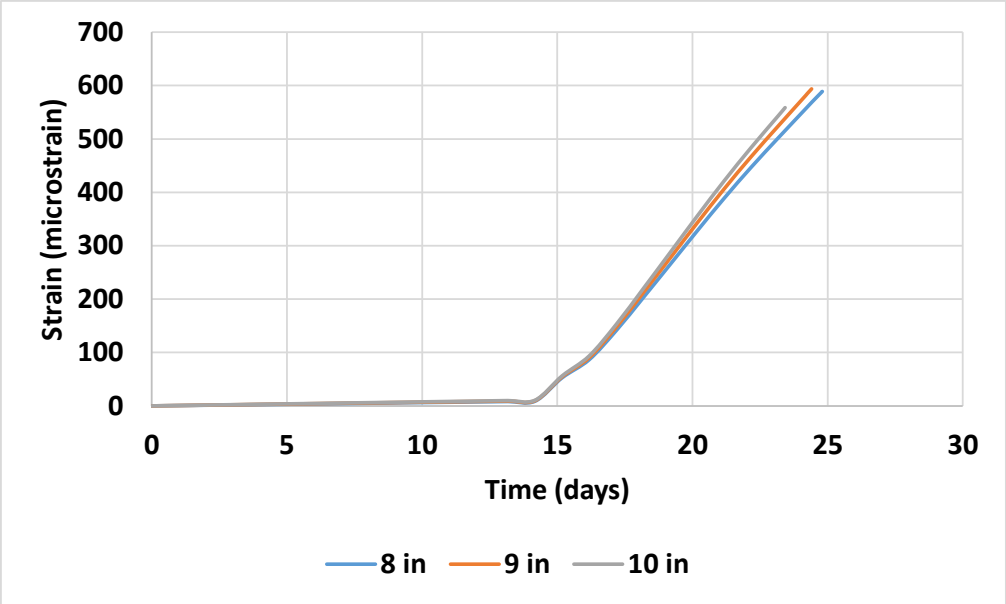

Figure 94: Strain in PCB continuous span deck thickness analysis

The results of the continuous span did not show a significant difference in the stress or strain in response to the change in the thickness of the deck. The results for the influence of deck thickness on the GSP I67 Bridge are shown in the figures below.

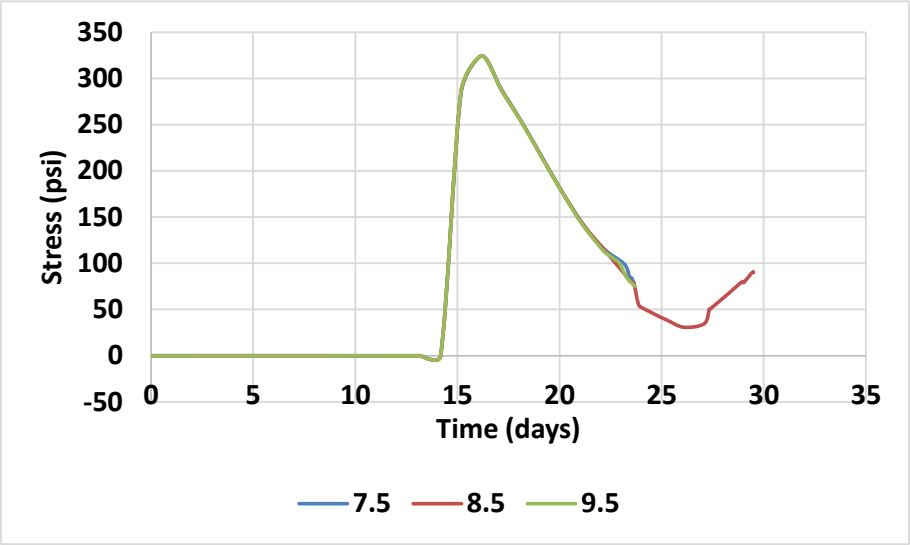

Figure 95**:** Stress in GSP I67 span boundary condition analysis

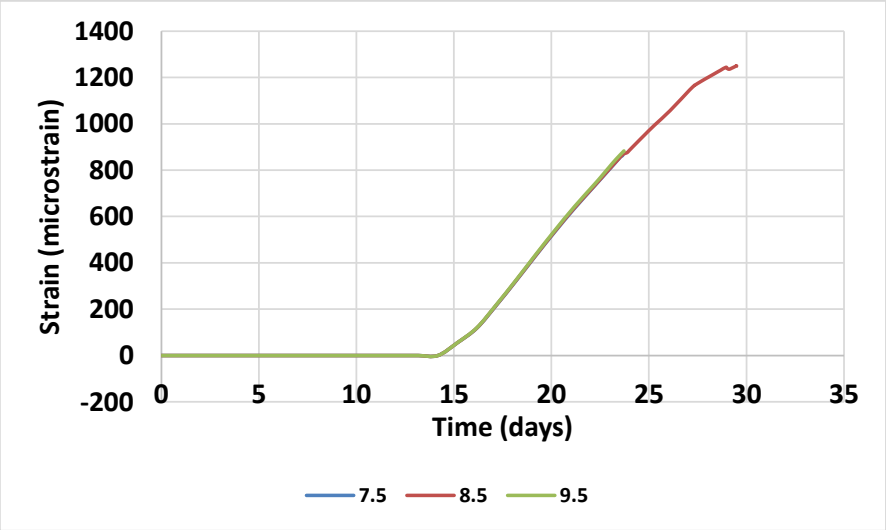

Figure 96: Strain in GSP I67 span boundary condition analysis

Similar to the behavior of the PCB, the stress and strain in the GSP I-67 Bridge showed no significant response to the change in deck thickness.

From the results above, the plots for reinforcement size from PCB and GSP I67 all indicated that less reinforcement produced greater strain and more reinforcement produced less strain. The #4 rebar provided insufficient resistance after the onset of cracking. The amount of reinforcement in the bridge deck did not affect the stress at which the concrete cracked but influenced the post cracking behavior. The response of a simply supported bridge to shrinkage strains did not differ significantly from a bridge with pinned supports on both ends. However, a bridge which was fixed on one end showed greater resistance to shrinkage strain due to an increase in stiffness. Finally, the reduction in deck thickness did not produce any significant effect on the stress or the strain of the concrete.

The findings from the parametric analysis were used to discuss the guidelines provided by the code for the control of shrinkage cracking in the following section.

6.5. Code impact

The analysis above indicated that the use of reinforcement was the most effective way to deal with shrinkage cracking in concrete bridge decks. The stipulations from the code were revisited to compare the guidelines on shrinkage with the performance of the parametric analysis of the full scale bridges.

As discussed previously, the code provides two methods for the design of bridge decks which are, the empirical and traditional method.

The empirical method in the AASHTO LRFD code specified a minimum of 0.27 in^2/ft of reinforcement in each bottom layer of steel and 0.18 in^2/ft of reinforcement in the top layer. A maximum spacing of 18 in was also specified. The commentary on the code states that 0.27 in^2/ft corresponds to 0.3 % reinforcement ratio for a deck with a thickness of 7.5 in. This value was specified for the purposes of better crack control since a 0.2 % reinforcement ratio was seen to be sufficient to satisfy strength requirements. Furthermore, a reduced amount of reinforcement of 0.18 in^2/ft is specified in the top layer to prevent spalling of the concrete caused by corrosion of the rebar. It is of note that shrinkage in bridge decks is higher at the exposed surface of the deck than at the bottom surface bounded by a deck pan. No specific layer of reinforcement was designated as shrinkage reinforcement.

The traditional method provides four layers of rebar provided that the slab meets certain design requirements. Specifications for the design of the top transverse and longitudinal as well as the bottom longitudinal reinforcement are outlined in the code. However, the top longitudinal reinforcement is designed as temperature and shrinkage reinforcement as specified in section

5.10.8 of the AASHTO LRFD code (AASHTO, 2010) since no other specific reference is made for the design of top distribution reinforcement.

The guidelines from the code are shown in the table below. Furthermore, the minimum requirements for the Patcong Creek Bridge and the Garden State Parkway Interchange 67 based on these guidelines are shown in the table as well.

Table 12: AASHTO code reinforcement requirements for selected bridges

	Required reinforcement per face per direction (in^2/ft)	PCB	GSP I67
Empirical method (AASHTO 9.7.2.5)	0.18 top layer (0.2% reinforcement ratio) 0.27 bottom layer (0.3% reinforcement ratio)	0.18 (0.216) 0.27 (0.324)	0.18 (0.204) 0.27 (0.306)
Traditional method (AASHTO 9.7.3.2/5.10.8)	$A_s \geq \frac{1.30bh}{2(b+h)f_y}$ $0.11 \leq A_s \leq 0.60$	0.0557 0.11	0.0539 0.11
As built		0.31	0.31

As mentioned in the literature review section, transverse shrinkage cracking is the most prominent type of cracking in bridge decks as documented by reports over the years. As such, this was the focus of this study. Furthermore, shrinkage is more severe at the top surface of a bridge deck than at the lower surface where the concrete is less exposed. It follows that the top longitudinal reinforcement is the primary reinforcement responsible for the control of shrinkage cracks in the bridge decks.

In the table above, the minimum reinforcement for the Patcong Creek Bridge and the Garden State Parkway Interchange 67 Bridge derived based on the guidelines given in code are

calculated and compared with the actual reinforcement used in the bridge as designed. Both bridges make use of #5 rebars spaced at 12 in for the temperature and shrinkage reinforcement to give a reinforcement ratio of 0.287 % and 0.304 % respectively. These values are greater than the 0.2% reinforcement minimum specified for the top layer of reinforcement. However, the reinforcement ratio for the Patcong Creek Bridge is less than the 0.3% which the code states is preferable for improved crack control. Both bridges have greater reinforcement than the values specified by the shrinkage and temperature reinforcement requirements used in the traditional method. In the case of the PCB, The empirical method is more conservative than the design and while for the GSP I67, it is less conservative. This difference in the outcome is due to the difference in the thicknesses of the bridge decks. The empirical method is also more conservative than the traditional method in the specification of top longitudinal reinforcement to mitigate the effect of transverse shrinkage cracking.

The parametric analysis indicates that satisfactory post cracking behavior is better achieved with a reinforcement of 0.31 in^2/ft in the bridges used above, with an average reinforcement ratio of 0.296 %. This value is close to the minimum values specified by the empirical method using a guideline of 0.3 %. However, this value differs significantly from the minimum for the traditional method which at 0.11 in^2/ft would give an average reinforcement ratio of 0.105 %. According to the parametric analysis performed above, a reinforcement amount producing less than satisfactory post cracking behavior could be chosen based on the minimum guidelines given by shrinkage and temperature reinforcement guidelines used in the traditional method.

Furthermore, when the equation given by the shrinkage and temperature requirement is used in the traditional method for a 12 in width of bridge deck, a thickness of at least 66 in is required to meet the minimum reinforcement of 0.11 in^2/ft. This thickness value is unlikely with regards to

bridge deck design and the chosen design value would simply default to the minimum of 0.11 in^2/ft. This again indicates that the use of the temperature and shrinkage guidelines when using the traditional method falls short in ensuring adequate post cracking behavior.

6.6. Discussion

In this section, a parametric analysis was performed to see the effect of various design parameters on the performance of the concrete deck of several bridges under restrained conditions. The post cracking behavior was compared as the design parameters were varied. It was observed that the post cracking behavior of the bridge decks responded most significantly to the change in reinforcement. This is also the parameter used by the code to address shrinkage and temperature cracking. It was observed that higher reinforcement sizes provided better post cracking resistance than smaller bars, especially when a #4 rebar was used. Furthermore, the temperature and shrinkage reinforcement requirements given by the AASHTO code were discussed.

It was found that the empirical method provided guidelines that encouraged better post cracking performance of bridge decks based on the results of the parametric analysis. However, the code stipulates a reduced reinforcement ratio for the top reinforcement layer of the deck than the bottom layer of the deck, whereas shrinkage stresses are higher at the top of the deck than at the bottom of the deck. It was noted that the code does this to prevent spalling of concrete at the top layer of the deck. Further analysis is needed to optimize the reinforcement in the top layer of the deck between optimal resistance to shrinkage strains after cracking and prevention of spalling of concrete to prevent reinforcement corrosion.

The guidelines for temperature and shrinkage used in the traditional method allowed for very low reinforcement ratios, which could cause have less than satisfactory post cracking behavior, to be used. Additionally, bridge decks designed today typically have a

thickness between 7 in and 9 in. However, the equation given by the AASHTO code for temperature and shrinkage reinforcement consistently produces a reinforcement ratio below the stipulated minimum of 0.11 in^2/ft. This makes the equation given by the code impractical for use in bridge decks as the minimum reinforcement chosen by the designer will always default to the minimum value. This minimum value of 0.11 in^2/ft would not encourage good post cracking resistance based on the results of the parametric analysis. It is recommended that this minimum reinforcement ratio be increased.

CHAPTER VII

SUMMARY AND CONCLUSIONS

7.1. Summary

In this study, shrinkage under restrained conditions and field conditions was investigated. Laboratory experiments were performed and information was gathered on small prism samples, a scaled down slab section and full scale bridges under field conditions. Finite element models for the experiments were developed and the models were validated using measured data. Shrinkage analyses were also performed using the developed models. A comparison was made between the measured data from the laboratory experiments and the finite element model results. Finally, a parametric analysis was performed on the full scale bridge models to observe the shrinkage response of the bridges to changes in variables. These variables included reinforcement size, boundary conditions and deck thickness. From this analysis, observations were made to aid in the understanding of shrinkage under field conditions. Finally, the results were compared to the AASHTO LRFD guidelines on reinforcement in bridge decks as relates to shrinkage. Key findings from the study are itemized below.

7.2. Findings

(1) The use of short term data from small samples to predict long term field behavior is limited in accuracy and the further out data is extrapolated, the less accurate the results.

(2) Shrinkage in larger samples stabilizes significantly quicker than smaller samples from the same concrete. Shrinkage in the field samples was found to have slowed down significantly within the first two months of data collection. Subsequent increases in shrinkage also occur at a much slower pace than smaller samples.

(3) The use of volume to surface ratios to estimate the shrinkage of larger samples based on smaller samples accurately predicts a reduction in shrinkage strain. However, the modification is less accurate as the size of the sample being predicted increases.

(4) There is a significant reduction due to size in the shrinkage of a full scale bridge deck. Strains due to shrinkage alone are unlikely to cause cracking in bridge decks. However, when combined with strain due to thermal and live loading, cracks are likely to occur.

(5) There is a significant strain due to the hydration reaction within the first few days of the pouring of the concrete locked into the bridge deck.

(6) It was observed that the reduction in strain due to the addition of reinforcement was more pronounced in the samples stored under constant conditions than in the samples exposed to ambient conditions possibly due to expansion and contraction of reinforcement.

(7) The average of the strain of a sample stored under fluctuating temperature conditions is comparable to the strain of a sample stored under constant temperature conditions, provided that the average temperature under fluctuating conditions equals the temperature under constant conditions.

(8) The parametric analysis indicated that less reinforcement produced greater strain and vice versa. The #4 rebar performed poorly in post cracking behavior and offered less resistance than the #5, #6 and #8 rebar.

(9) The stress in the concrete and the onset of cracking was not greatly affected by the size of the reinforcement used. Instead, it was determined by the tensile strength of the concrete.

(10) The bridges produced a similar response when both roller supports and pinned supports were investigated. However, there was a reduction in shrinkage strain when the ends were fixed due to increased stiffness

(11) The reduction in deck thickness resulted in a marginal response in stress and strain in the concrete bridge deck.

(12) The results indicated that the modification of reinforcement provides the greatest influence on the stress and strain in the deck particularly in the post cracking behavior of the deck.

(13) It was found that the empirical method produced more conservative reinforcement specifications than the traditional method for shrinkage and temperature reinforcement in the top longitudinal layer of a bridge deck.

(14) It is recommended that the reinforcement ratio for the top layer of reinforcement in the empirical method be increased to match the bottom layer of reinforcement given that shrinkage is higher in the top layer of a concrete deck, subject to the adverse effect of concrete spalling.

(15) It is recommended that the minimum reinforcement ration in the shrinkage and temperature guidelines in section 5.10.8.2 of the AASHTO LRFD code be

increased to prevent the use of too little reinforcement to ensure adequate resistance after the onset of cracking in decks.

7.3. Conclusions

The following conclusions were drawn from the analysis performed in this study.

(1) Short term data from small samples can be used to the behavior of larger samples in the field with limited accuracy. The use of longer term data from larger samples is recommended.

(2) Finite element models can be used to simulate and study the behavior of shrinkage of large samples which would otherwise be challenging and resource intensive.

(3) It is necessary to filter out temperature strains from the total strain measured under field conditions to derive an accurate representation of shrinkage strain in the field. These can be approximately averaged out using long term data covering several seasonal cycles.

(4) Reinforcement is a more effective parameter in the control of post cracking behavior than deck thickness or boundary conditions.

REFERENCES

Grand Challenges: A strategic Plan for Bridge Engineering. AASHTO Highway Subcommittee on Bridges and Structures. (2005)

AASHTO (2008). "LRFD bridge design specifications", American Society of State Highway and Transportation Officials (AASHTO), Washington, D.C.

Acarcan, M., (2004). Volumetric Deformations and Crack Control in Reinforced Concrete Structures. Master's Thesis, Ryerson University, Toronto, Ontario, Canada.

ACI committee 207. *Effect of Restraint, Volume Change and Reinforcement on Cracking of Mass Concrete* (ACI 207.2R-95). American Concrete Institute, Detroit, Michigan, 1995.

ACI committee 209. *Prediction of Creep, Shrinkage and Temperature Effects in Concrete Structures* (ACI 209R-92), American Concrete Institute, Detroit, Michigan, 1997.

ACI Committee 318, *Building Code Requirements for Reinforced Concrete (ACI 318-08),* American Concrete Institute, Detroit, Michigan, 2008.

American Society for Testing and Materials Standard (2008). "C157/C157M Standard Test Method for Length Change of Hardened Hydraulic-Cement Mortar and Concrete"

Al-Saleh, S. A., & Al-Zaid, R. Z. (2006). *Effects of drying conditions, admixtures and specimen size on shrinkage strains.* Cement and concrete research, 36(10), 1985-1991.

Almudaiheem, J. A., & Hansen, W. (1987). Effect of specimen size and shape on drying shrinkage of concrete. *ACI Materials Journal*, *84*(2).

Babaei, K., & Purvis, R. L. (1995). *Prevention of Cracks in Concrete Bridge Decks: Report on Laboratory Investigations of Concrete Shrinkage* (No. PA-FHWA-95-004+ 89-01).

Banks, R. K. (1986). Bridge Decks: Their Problems and Solutions. *Public Works*, *117*(12), 26.

Bazant, Z. P., & Baweja, S. (2000). Creep and shrinkage prediction model for analysis and design of concrete structures: Model B3. *ACI SPECIAL PUBLICATIONS*, *194*, 1-84.

Blackman, D. (2002) Evaluation of Design Methods for the Control of Early Age Bridge Deck Cracking (Master's Thesis, Purdue University)

Bissonnette, B., Pierre, P., & Pigeon, M. (1999). Influence of key parameters on drying shrinkage of cementitious materials. *Cement and Concrete Research*, 29(10), 1655-1662.

Branson, D. E., and Christiason, M. L. (1971). Time dependent concrete properties related to design-strength and elastic properties, creep and shrinkage. SP-27, American Concrete Institute, Farmington Hills, MI. pp 257-277.

Byard, B. E., Schindler, A. K., Barnes, R. W., & Rao, A. (2010). Cracking tendency of bridge deck concrete. *Transportation Research Record: Journal of the Transportation Research Board*, *2164*(1), 122-131.

Campbell-Allen, D., & Rogers, *D. F. (1975).* Shrinkage of concrete as affected by size. *Matériaux et Construction*, 8(3), 193-202.

CEB,1991. Evaluation of time dependent properties of concrete.Bulletin d'information No.199. Comite Euro-Internationale du Beton/Federation Internationale de la Precontrainte, Lausanne, Switzerland, 201 pp.

Chaunsali, P., Lim, S., Mondal, P., Foutch, D., Richardson, D., Tung, Y., & Hindi, R. (2013). *Bridge Decks: Mitigation of Cracking and Increased Durability*. Illinois Center for Transportation (ICT).

Curtis, R. H. (2007). NYSDOT Bridge Deck Task Force Evaluation of Bridge Deck Cracking on NYSDOT Bridges.

Darwin, D., Browning, J., Lindquist, W., McLeod, H. A., Yuan, J., Toledo, M., & Reynolds, D. (2010). *Low-Cracking, High-Performance Concrete Bridge Decks: Case Studies over First 6 Years* (No. 7IBEC-0014).

Deshpande, S., Darwin, D., & Browning, J. (2007). Evaluating Free Shrinkage of Concrete for Control of Cracking in Bridge Decks.

Eldhose, S. (2006). Simulation of the Long Term Behavior of Precast/Prestressed Concrete Bridge. Master's thesis, University of Cincinnati. Cincinnati, OH.

ElSafty, A., & Jackson, N. M. (2012). *Sealing of Cracks on Florida Bridge Decks with Steel Girders* (No. BDK82 977-02).

Folliard, K., Smith, C., Sellers, G., Brown, M., & Breen, J. E. (2003). *Evaluation of Alternative Materials to Control Drying-Shrinkage Cracking in Concrete Bridge Decks* (No. FHWA/TX-04/0-4098-4,).

French, C. E., Eppers, L. J., Le, Q. T., & Hajjar, J. F. (1999). Transverse Cracking in Concrete Bridge Decks.

Frosch, R. J., Bice, J. K., & Erickson, J. B. (2006). Design Methods for the Control of Restrained Shrinkage Cracking.

Frosch, R. J., Blackman, D. T., & Radabaugh, R. D. (2003). Investigation of bridge deck cracking in various bridge superstructure systems.

Gardner, N. J., & Lockman, M. J. (2001). Design provisions for drying shrinkage and creep of normal-strength concrete. ACI Materials Journal, 98(2).

Ganapuram, S., Adams, M., & Patnaik, A. (2012). *Quantification of Cracks in Concrete Bridge Decks in Ohio District 3* (No. FHWA/OH-2012/3). Ohio Department of Transportation, Office of Research and Development.

Hansen, T. C., & Mattock, A. H. (1966, February). Influence of Size and Shape of Member on the Shrinkage and Creep of Concrete. In *ACI Journal Proceedings* (Vol. 63, No. 2). ACI.

Hadidi, R., & Saadeghvaziri, M. A. (2005). Transverse cracking of concrete bridge decks: state-of-the-art. *Journal of Bridge Engineering*, *10*(5), 503-510.

Hornby, I. W., & Noltingk, B. E. (1974). The application of the vibrating-wire principle for the measurement of strain in concrete. *Experimental Mechanics*,*14*(3), 123-128.

HOVER, K. (2005). Much ado about shrinkage. *Concrete Construction*, *50*, 42-46.

Instruction Manual (n.d). *Model 4200 Series Vibrating Wire Strain Gages*. Geokon, Lebanon, New Hampshire.

Krauss, P. D., & Rogalla, E. A. (1996). *Transverse cracking in newly constructed bridge decks* (No. Project 12-37 FY'92).

Laman, J.A., Sellers, J.B. and Schulz, J.L. *Influence of Temperature on Highway Bridge Strain Measurements Using Vibrating Wire Gages.*

Lange, D. A., Roesler, J. R., DAmbrosia, M. D., Grasley, Z. C., Cowen, D., & Lee, C. J. (2003). *High performance concrete for transportation structures* (No. UILU-ENG-2006-2006).

Li, Q., Ni, F., & Li, Z. (2009). Experimental Tests and Finite Element Modeling of Shrinkage Behavior in Cement Stabilized Aggregate Base. In *Critical Issues in Transportation Systems Planning, Development, and Management. Ninth International Conference Chinese Transportation Professionals* (pp. 2754-2760).

Minnetyan, L., & Janoyan, K. D. (2011). *Tool for Analysis of Early Age Transverse Cracking of Composite Bridge Decks* (No. C-06-37).

Mokarem, D. W., Weyers, R. E., & Lane, D. S. (2005). Development of a shrinkage performance specifications and prediction model analysis for supplemental cementitious material concrete mixtures. *Cement and Concrete Research*, *35*(5), 918-925.

Nassif, H., Aktas, K., Najm, H., & Suksawang, N. (2007). *Concrete Shrinkage Analysis of Bridge Deck Concrete* (No. FHWA NJ-2007-007).

Nielson, R., Schmeckpeper, E.R., Shiner, C. and Blandford, M. (2010). *The Effect of Bridge Deck Design Methodology on Crack Control.* Report RP184.

Qiao, P., McLean, D. I., & Zhuang, J. (2010). *Mitigation strategies for early-age shrinkage cracking in bridge decks* (No. WA-RD 747.1).

Radabaugh, R. D. (2001). *Investigation of Early Age Bridge Deck Cracking*, Master's Thesis, Purdue University, West Lafayette, IN.

Rahim, A. M., Jansen, D. C., & Abo-Shadi, N. A. (2006). *Concrete Bridge Deck Crack Sealing: An Overview of Research*. California Polytechnic State University, Civil and Environmental Engineering.

Ramey, G. E., Wolff, A. R. and Wright, R. L. (1997). Structural Design Actions to Mitigate Bridge Deck Cracking. *Practice Periodical on Structural Design and Construction, 2*(3).

Ray, I., Gong, Z., Davalos, J. F. and Kar, A. (2012). Shrinkage and Cracking Studies of High Performance Concrete for Bridge Decks. *Construction and Building Materials, 28*, 244 – 254.

Saadeghvaziri, M. A., & Hadidi, R. (2002). *Cause and control of transverse cracking in concrete bridge decks* (No. FHWA-NJ-2002-019,).

Saadeghvaziri, M. A. & Hadidi, R. (2005). Transverse cracking of concrete bridge decks: effects of design factors. *Journal of Bridge Engineering, 10*(5), 511 – 519.

Sakata, K. (1993). Prediction of concrete creep and shrinkage. In RILEM PROCEEDINGS (pp. 649-649). CHAPMAN & HALL.

Schmitt, T. R., & Darwin, D. (1995). *Cracking in Concrete Bridge Decks. Final report* (No. K-TRAN: KU-94-1).

SENER, S., SENER, H. D., & Varol, K. O. Ç. (2009). Drying Effect of Normal and High Strength Concrete Cylinders with Different Sizes. *Gazi University Journal of Science, 22(4), 333-340.*

Subramaniam, K. V., & Agrawal, A. K. (2009). *Concrete Deck Material Properties* (No. C-02-03).

Tam, K.S.S and Scanlon, A. (1984). Effect of restrained shrinkage on concrete slabs

Tarr, Scott M., and Farny, James A.; *Concrete Floors on Ground*, EB075, http://members.cement.org/ebiz50/ProductCatalog/Product.aspx?ID=263 Fourth Edition, Portland Cement Association, Skokie, Illinois, USA, 2008, 256 pages.

Tang, F. (2000). Overlay for concrete segmental box-girder bridges. *Journal of Bridge Engineering, 5*(4), 311 – 321.

Tia, M., Subramanian, R., Brown, D., & Broward, C. (2005). *Evaluation of shrinkage cracking potential of concrete used in bridge decks in Florida* (No. UF Project No. 4910-4504-797-12).

Walkowich, T. (2011). Field Monitoring of Shrinkage Cracking Potential in a High Performance Concrete Bridge Deck. Master's thesis, Rutgers University. New Brunswick, NJ.

Wang, K., Schlorholtz, S. M., Sritharan, S., Seneviratne, H., Wang, X., & Hou, Q. (2013). *Investigation into Shrinkage of High-Performance Concrete Used for Iowa Bridge Decks and Overlays* (No. IHRB Project TR-633).

Wiliam, G. W., Shourkry, S. N. and Riad, M. Y. (2005). Early Age Cracking of Reinforced Concrete Bridge Decks. *Bridge Structures*, *1*(4), 379-396.

Xi, Y., Shing, B., Abu-Hejleh, N., Asiz, A., Suwito, A., Xie, Z., & Ababneh, A. (2003). *Assessment of the Cracking Problem in Newly Constructed Bridge Decks*